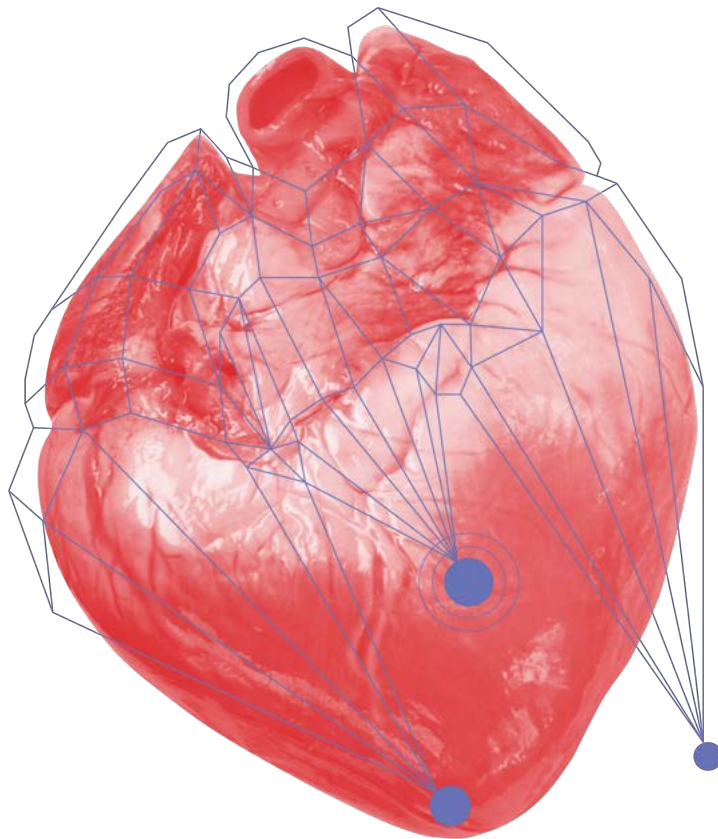


Department of Precision and Microsystems Engineering

Energy Harvesting for Pacemakers: Combining Cardiac Measurement Techniques to Improve Testing

R. Bastiaanse

Report no : 2021.007
Coach : Dr. N. Tolou & Ir. T.W.A. Blad
Professor : Ir. J.W. Spronck
Specialisation : MSD
Type of report : Master Thesis
Date : 26 January 2021



Energy Harvesting for Pacemakers

Combining Cardiac Measurement Techniques to Improve Testing

by

R. Bastiaanse

to obtain the degree of Master of Science
at the Delft University of Technology,
to be defended publicly on 26 January 2021 at 13:30.

Student number: 4299493
Report number: 2021.007
Project duration: November 4, 2019 – January 26, 2021
Thesis committee: Ir. J. W. Spronck, TU Delft, Committee chair
Dr. N. Tolou, Flexous Mechanisms B.V., Supervisor
Ir. T. W. A. Blad, TU Delft, Daily supervisor
Dr.ir. G. J. Verbiest, TU Delft, Extern member

An electronic version of this thesis is available at <http://repository.tudelft.nl/>.

Preface

As a kid, if someone asked me what I wanted to become, 'engineer' would not be the answer. At primary school I answered this question with: dolphin trainer. Later, in high school I answered it with: pilot. Even during my studies I had not yet thought that I would eventually become a mechanical engineer. The interest in technology and the fascinating possibilities that it brings are slowly grown. Which has now led me to observing the latest technologies with full admiration and the urge to work on them myself.

During my master I thought a lot about what kind of mechanical engineer I would like to become. This resulted in, eventually, that I want to help others. Engineering for medicine falls within this goal, in which technology makes life more comfortable for patients and can assist doctors during surgery. With the help of many technical developments, medicine has grown into what it is today.

With this thought the direction of this thesis was chosen. It is still a long way off, but energy harvesting for pacemakers is such a technical development. The patients comfort increases, since a pacemaker replacement would no longer be required. I enjoyed working on this research, bearing in mind that this will hopefully bring energy harvesting for pacemakers a step closer to reality. And that, in my own way, I have been able to contribute to the improvement of the medical world. Even if it is only a small contribution. I hope you enjoy reading my thesis.

R. Bastiaanse
Delft, January 2021

Summary

A pacemaker runs on a conventional battery that lasts for approximately 6-12 years, after which the pacemaker must be replaced. Converting the heart wall vibrations into electricity through a vibration energy harvester has been considered a promising solution to this problem. However, the complexity of the heart signals on which the energy harvester has to operate is a challenge. The human heart signal is a broadband signal, consisting of a varying acceleration amplitude at low frequencies. Most of the testing signals used in the labs are harmonic signals, Gaussian white noise or Gaussian coloured noise. These signals do not have the same characteristics as a human heart signal. In addition, the dynamical behaviour of an energy harvester differs per input signal. Therefore, it is important to test energy harvesters on the operation signal, in this case human heart acceleration signals. A heart signal differs per person depending on, for instance, someone's age, sex and health. This means that multiple human heart input signals are needed. Ethical requirements make the measurement of these signals with the necessary details a challenge in itself.

In order to meet this demand and to avoid this ethical issue, a heart signal generator is developed as a first step towards the testing of energy harvesters on an approximation of human heart signals. Three different sources of heart signals are combined in order to obtain a new source of heart signals, an approximation of reality, which can be used for the testing. Speckle Tracking Echocardiography signals, open-chest pig heart acceleration signals and human chest motion acceleration signals are analysed and their characteristics are used as the source for the heart signal generator. This heart signal generator is able to mimic multiple heartbeats and the influence of the heart rate on the amplitude and signal duration. The disadvantages of accelerometer measurements are compensated with the advantages of Speckle Tracking Echocardiography measurements, and vice versa, in order to obtain an accurate and detailed heart signal.

The output of the heart signal generator is a one-dimensional acceleration signal. An energy harvester is tested on multiple generated heart signals for a heart rate range of 120-200 bpm. It was observed that the mean power output and the efficiency of the energy harvester differs per heart signal. This shows that testing on multiple heart signals is crucial in order to validate that enough power is generated for charging the battery.

Contents

1	Introduction	1
1.1	Background	2
1.2	Energy Harvester Testing	2
1.3	Problem Statement	3
1.4	Thesis Outline	3
2	The Human Heart	5
2.1	Anatomy	6
2.2	Heart Contraction Activation	6
2.3	Heart Motion	8
2.4	Arrhythmia	8
2.5	Pacemakers	9
3	Discussing the Current Development Status of Energy Harvesting for Powering a Pacemaker	11
3.1	Introduction	12
3.2	Energy Harvesters for Pacemakers	13
3.3	Heart Signal Measurements	14
3.4	Energy Harvester Overview	16
3.5	Testing Signals	19
3.6	Discussion	21
3.7	Conclusion	23
4	Combining Cardiac Measurement Techniques to Improve Testing for Energy Harvesting Pacemakers	25
4.1	Introduction	26
4.2	Background	27
4.3	Methods	28
4.4	Results	33
4.5	Discussion	33
4.6	Conclusion	36
4.7	Acknowledgments	36
5	Discussion, Conclusion and Recommendations	37
5.1	Project Reflection Discussion	38
5.2	Conclusion	38
5.3	Recommendations	39
A	Leadless Pacemaker Requirements	43
A.1	Technical Requirements	44
A.2	Testing Requirements	45
B	Heart Signal Measurement Method	49
B.1	Heart Signal Requirements	50
B.2	Measurement Method	50
B.3	Method Decision	53
C	STE and TDI Measurements	55
C.1	Measurement Method	56
C.2	Signal Processing	58
C.3	Comparison STE and TDI Measurements	60
C.4	Acceleration Amplitude	62

D Accelerometer Measurements	65
D.1 Measurement Method	66
D.2 Heart Comparison	67
D.3 Signal Processing	69
D.4 Comparison STE and Accelerometer Measurements	72
D.5 Trajectory Analysis	75
D.6 Influence Heart Rate	81
E Orientation	85
E.1 PCA Pig Heart	86
E.2 Comparison Three Dimensions	87
E.3 Generator Orientation	88
F Heart Signal Generator	91
F.1 Code	92
F.2 Results	94
G Energy Harvester	97
G.1 Energy Harvester for Experiments	98
G.2 Design Process of the unused Energy Harvester	99
H Heart Wall Imitation	103
H.1 Material	104
Bibliography	107

1

Introduction

This chapter introduces the concept of energy harvesting for powering pacemakers. It discusses what is needed for further developments. This is translated into a problem statement and research question. Finally, the thesis structure is outlined.

1.1. Background

Each year 600.000 new pacemakers are implanted [1]. A pacemaker ensures that the heart of a patient with cardiac arrhythmia keeps beating in the right rhythm. The activity of the pacemaker necessary to combat the arrhythmia determines the battery life. Nowadays, a pacemaker runs on a conventional battery that lasts for approximately 6-12 years, after which the pacemaker must be replaced [2]. This means that a new pacemaker implantation is needed, accounting for approximately 25% of all pacemaker implantation procedures. As these procedures come with complications, such as infections or bleeding [3], powering the pacemaker through an energy harvester has been considered to be a promising alternative. Energy can be harvested by heat, wind or vibration, for example. Vibration energy harvesting refers to the method in which ambient vibrations are converted to electricity [4]. These vibrations can be anything in the environment, from machines that vibrate, the oscillations of a bridge and, in this case, the pulsation of the human heart wall. By converting these vibrations into electricity, a battery can be recharged. A method of converting these vibrations to electricity is by the use of piezoelectric material, which starts to vibrate due to the heart wall vibrations. The continuous movement causes the material to stretch and compress. A characteristic of this material is that when it experiences stretch, this stretch generates electrical energy. This energy can be used to recharge a battery. This example can be seen in a schematic overview in Figure 1.1. The ventricular wall motion caused by a contraction of the heart would be a reliable power source, since it is continuous with an average heart rate of 70 beats per minute [2].

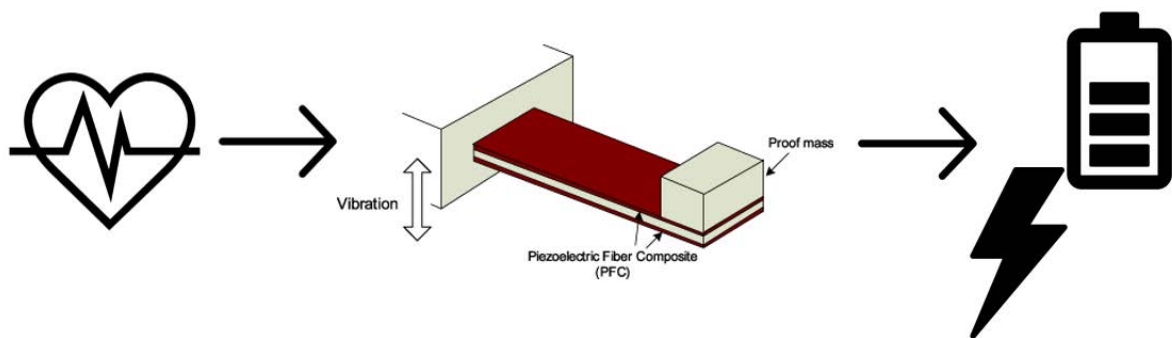


Figure 1.1: Schematic overview of vibration energy harvesting via heart wall motion. Figure of energy harvester obtained from [5].

1.2. Energy Harvester Testing

Previous research has shown that the dynamical behaviour of a harvester could differ for various input signals [6]. This changing behaviour influences the performance of the harvester and could slow the charging of the battery. Neri et al. [7] experimented with a nonlinear energy harvester, and observed that the design to obtain a maximum power output depends on the shape and intensity of the used input signal. This shows that an energy harvester designed for a certain application should be tested on the input signal of that application to accurately estimate the performance. An energy harvester intended for powering a pacemaker should be tested on a heart signal in order to obtain the matching dynamic behaviour. However, the majority of the energy harvesters are tested on a harmonic signal. The characteristics of a harmonic signal do not match the characteristics of the human heart signal. The heart signal is a broadband signal, consisting of a varying acceleration at low frequencies. An example of a human heart signal measured by Kanai et al. [8] is shown in Figure 1.2a and Figure 1.2b, the time and frequency domain, respectively. The signal has a high power at low frequencies, which decreases for higher frequencies. Several researchers tested their designed energy harvesters on a heart signal of a single human, giving information of the behaviour of the energy harvester on the needed operation signal. However, this operation signal can differ per person, since it also depends on a subjects age or health and the time of measuring [8, 9]. Furthermore, it is questionable whether the measurement methods used give a signal that is representative enough for the testing of energy harvesters. According to the Food and Drug Administration are for the implementation of new implantable pacemakers bench tests needed to verify the mechanical and electrical working principle. This shall be tested under

conditions in the operational environment [10]. During the clinical trial of a new device, the pilot phase, consisting of 10-30 subjects, the preliminary safety and performance in humans is investigated [11]. Since the dynamical behaviour of an energy harvester depends on the input signal, it is likely that the bench tests should also be validated on 10-30 different heart signals.

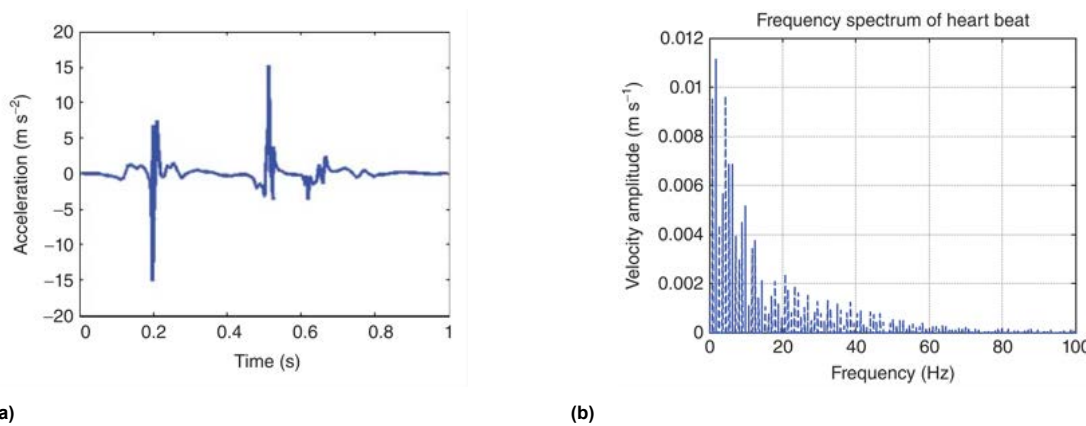


Figure 1.2: The heart signal measured with ultrasonic measurements. (a) The time signal of the acceleration of the heart wall. (b) The frequency response of the same signal. Both obtained from [4].

1.3. Problem Statement

More heartbeat signals measurements are needed to verify the performance of energy harvesters for different input conditions, such that it could be widely used in pacemakers. The aim is to approximate the human heart signal, containing the required information for the testing of energy harvesters. In addition to the heartbeat frequency, the signal should also contain the input acceleration information during the cardiac cycle. The database of heartbeat signals is expanded, helping researchers with the verification of the performance of the energy harvester in a realistic manner. This leads to the following research objective for this thesis:

To obtain and verify signals to approximate the human heart wall motion to perform experiments for energy harvesters intended for powering pacemakers to improve the testing facilities.

For this objective the following research question is formulated:

On what signals should the testing for energy harvester intended for powering a pacemaker be performed in order to obtain sufficient information?

In order to answer this question, two sub questions are formulated:

- How accurate are measurements performed on the human heart wall in order to obtain acceleration information?
- How can different sources of heart signals be combined in order to obtain an approximation of the human heart acceleration signal?

1.4. Thesis Outline

This thesis aims to bring the research for powering pacemakers with an energy harvester one step closer to reality. The state of the art is discussed, in order to find what is needed to improve the testing facilities. To this end a tool is developed.

As some readers may be unfamiliar with the working principle of the human heart and the medical terms used in this thesis, Chapter 2 provides a short introduction. The general heart anatomy and properties are discussed. In addition, the chapter discusses the heart motion, heart arrhythmia and

how this can be treated with pacemakers.

Chapter 3 contains the literature research paper, discussing the current development status of energy harvesting for powering a pacemaker. Here, a first analysis of the heart signal measurement methods found in literature is performed. An overview of nonlinear techniques currently used in MEMS low frequency energy harvesters is given and the dynamical behaviour of energy harvesters is discussed. The testing signals used for testing in the lab are analysed and it is investigated if these signals are sufficient for the testing of energy harvesters for pacemakers. The signals are compared to a human heart signal, whose properties are explained.

This is followed by Chapter 4, presenting the experimental paper. Here heart signals were obtained from three different sources: open-chest pig heart acceleration signals, human heart ultrasound measurements and human chest motion signals. These signals are analysed in detail and the signal characteristics are described. The characteristics are processed in a heart signal generator, to approximate human heart wall acceleration signals. Various heart signals are generated with the generator and used for testing in the lab. An energy harvester with moving mid magnets is used and the power output and efficiency on the different signals is analysed.

The final chapter, Chapter 5, contains the discussion and conclusion. The discussion reflects briefly on the challenges and learning points during the project, followed by the conclusions of the entire project and recommendations for further research are given.

Appendices were added that substantiate the results obtained in this thesis, the analysis performed to obtain all the information for the heart signal generator and background information for energy harvesting for powering pacemakers. Appendix A argues whether energy harvesting could be used for powering a pacemaker. Different boundary conditions are discussed, intended to align the view on matters of energy harvesting for pacemakers. In this chapter also the testing conditions for medical implantable devices are discussed. Appendix B consists of a short description of the potential measurement methods to obtain the human heart signal. Positive and negative aspects of these methods are discussed and compared. Then, Appendix C explains the measurement methods used in this thesis in more detail. A signal analysis is performed and it is elaborated how the results are used in the heart signal generator. Appendix D discusses the acceleration signals, how the signals are processed and analyses how the signals can be used for the further analysis. Then, the discussion of the principle component that should be the output of the heart signal generator can be found in Appendix E. Appendix F elaborates on the heart signal generator design. It is explained how previous findings are processed in the code and the results are shown and discussed. The generated signals are compared to the human heart signals and the pig heart signals. For the testing of the signals in the lab an energy harvester was designed. However, eventually this energy harvester was not used during the testing. The design process is shown in Appendix G. Finally, Appendix H shows how the heart wall can be imitated with silicone. This was intended for tests in the lab, but this experiment was found to be out of the scope of the thesis. This information can be used for future research.

2

The Human Heart

This chapter describes several aspects of the human heart. First, the anatomy of the heart is discussed. Second, the working principle of the heart contraction is explained, answering the question: what ensures that the heart remains beating? This is followed by a description of the heart motion. Then different types of arrhythmia are discussed, as well as their influence on someone's health. Finally, a solution for arrhythmia is discussed: the pacemaker. This final section describes how the device solves heart failures and what kind of pacemakers there are.

2.1. Anatomy

The human heart, which can be thought of as a pump, is responsible for the circulation of the blood through the body. It actually consists of two pumps: the right side of the heart ensures the circulation of the blood through the lungs for the oxygen exchange, while the left side of the heart is responsible for pumping the oxygenated blood to the organs [12]. Each side has an output of approximately 5 L/min, which can be increased up to 25 L/min during exercise. The heart consists of two atria, which collect the blood that flows in through the veins. Via the tricuspid valve (TV) and the mitral valve (MV) the blood flows into the right and left ventricle, respectively. The ventricles pump the blood to the arteries via the pulmonary valve (PV) toward the lungs and the aortic valve (AV), and then to the rest of the organs [13, 14]. This is shown in Figure 2.1a. For the pumping of the blood, the heart makes translational motions during contraction and relaxation, but also twists: it twists during the contraction and untwists during the relaxation. Due to this twisting the ejection fraction of the human heart is increased. The heart has a longitudinal, radial and circumferential axis, which are indicated in Figure 2.1b. The heart twists around the longitudinal axis [15]. Furthermore, in Figure 2.1a the interventricular septum is shown, separating the left and right ventricles. The heart wall consists of three layers: the epicardium, the myocardium and the endocardium. The epicardium is the outer layer of the heart and protects the heart. The myocardium is the middle layer, the thickest layer, and consists of the cardiac muscle fibers [16]. Finally, the endocardium is the inner layer of the heart. For humans in rest, the heart rate lies between 60-100 beats per minute (bpm).

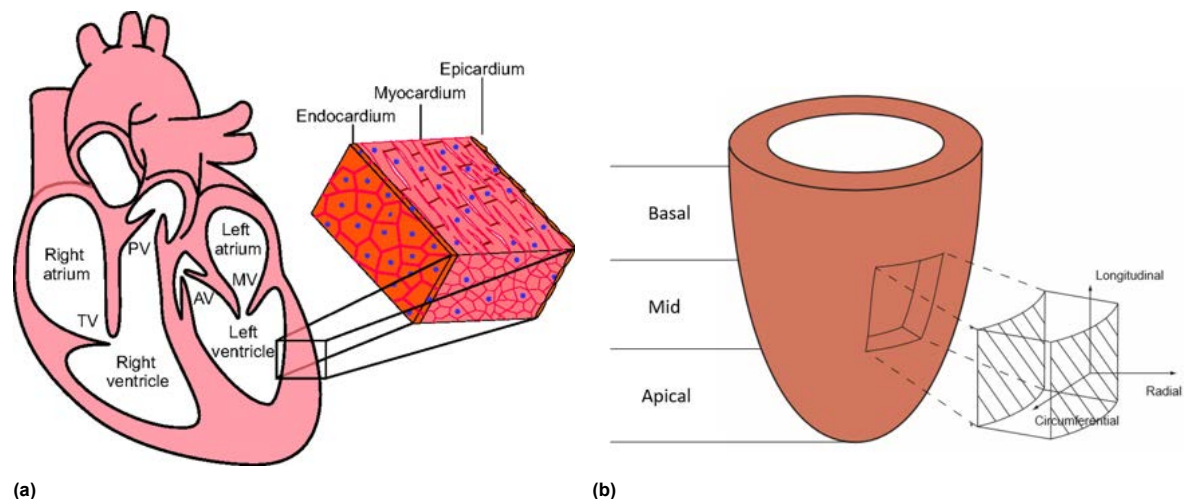


Figure 2.1: The human heart. **(a)** The anatomy of the heart, with the two atria and ventricles indicated. The four valves (pulmonary valve, PV; tricuspid valve, TV; atrial valve, AV; mitral valve, MV) and the three layers of the heart are also shown. Figure obtained from [14]. **(b)** The three directions of the axes in the heart: longitudinal, radial and circumferential, and the three regions of the ventricle are indicated: basal, mid and apical. Figure obtained from [17].

Figure 2.2 shows the Wiggers diagram. The Wiggers diagram is an overview of the whole cardiac cycle. Here the electrocardiogram (ECG), phonocardiogram, ventricle volume and pressure during the cardiac cycle are displayed. It shows that at the R-peak in the ECG the systole, or isovolumic contraction, starts. This results in an increasing pressure and decreasing volume in the ventricle: the ejection of the blood. At the end of the T-wave the diastole, or isovolumic relaxation, starts, resulting in a decreasing pressure and increasing volume in the ventricle: the blood flows back into the ventricles.

2.2. Heart Contraction Activation

To ensure that the blood circulation remains constantly flowing, the heart has to be activated continuously. To obtain an optimal output of the heart, the heart has to contract in a certain order [12]. This is done via action potentials. First, the ventricles depolarise, causing the heart muscle to repolarise and contract. When the contraction of the left and right ventricle are synchronized, the heart has an optimal output. In order to obtain this, the action potentials must be timed [12]. This is performed by three pacemaking tissues or heart muscle cells. These tissues are autorhythmic, meaning that with no input of the nerves these tissues still control the heartbeat [19].

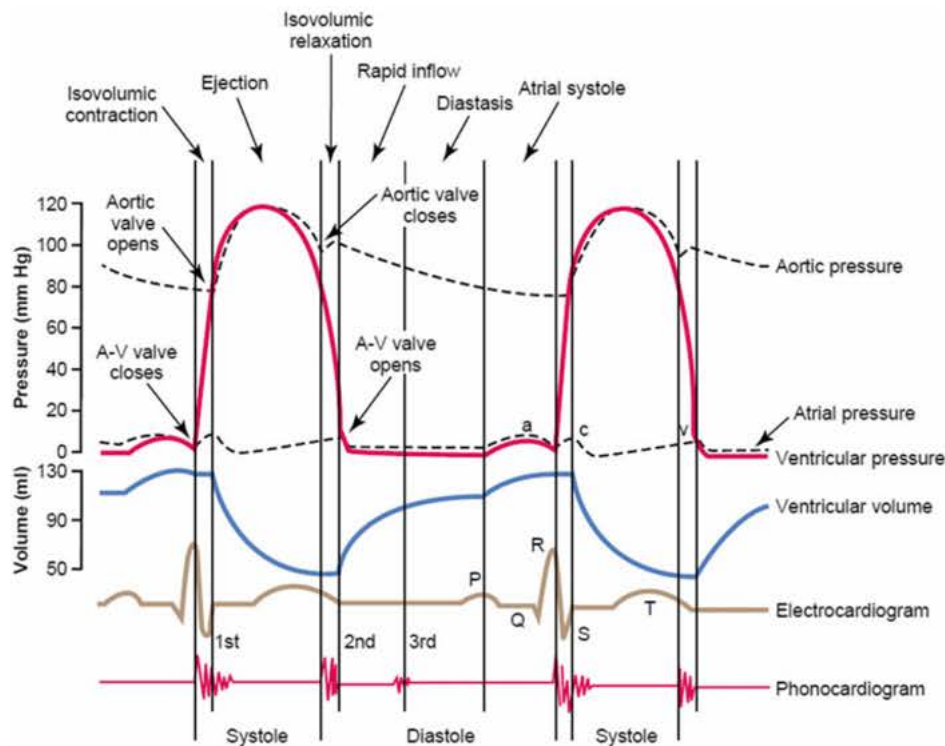


Figure 2.2: The Wiggers diagram, showing the electrocardiogram (ECG), phonocardiogram, ventricle volume and pressure. The contraction (systole) and relaxation (diastole) are shown. The change in volume and pressure in the heart during a heart cycle can be observed. Figure obtained from [18].

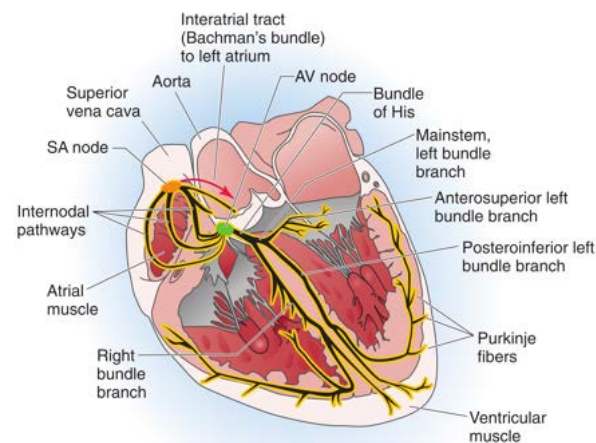


Figure 2.3: The working principle of the heart when electrically activated. This figure shows the action potential from the SA node, via the AV node, to the Purkinje fibers. Figure obtained from [12].

The action potential of the heart muscle cells can be divided into five phases. During these phases, the heart muscle cells depolarise and repolarise in order to activate the muscle [19]. The heart muscle has two types of cells, which are myocardial contractile cells and myocardial conducting cells. The conducting cells pass the signal to contract to the contractile cells [19]. The depolarisation of the heart travels through the heart wall in a specific order. It starts in the sinoatrial (SA) node, which is an area of specialised conductive cells. This SA node lies in the right atrium of the heart. When depolarising, it

also depolarises neighboring cells, providing a wave of depolarising cells in the right atrium, making the atrium contract. The second node, the atrioventricular (AV) node, lies close to the TV. This node transmits the depolarization of the atrium to both ventricles, which then travels via the right and left bundle branches to the Purkinje fibres. All this ensures a synchronized contraction [20]. Thus, the three pacemaker tissues are the SA node, the AV node, and the Purkinje fibers. How the depolarization travels through the heart and the nodes is shown in Figure 2.3. These nodes have a hierarchy among them, which depends on the frequency at which the depolarization signals are sent, and set the heart rate. Because the fastest node is the SA node, this node sets the heart rate. For a human at rest, the rate of this node is 60 bpm or higher [12]. The SA node can adjust the frequency in three ways. It can decrease the steepness of the depolarization during phase four (the resting phase), lower the maximum diastolic potential, or make the threshold for the action potential more positive, prolonging the time it takes to reach the threshold which causes the heart rate to drop [12]. Due to the action potentials and the order in which they travel through the heart, the cardiac cycle starts with atrial contraction, followed by isovolumetric contraction, rapid ejection, reduced ejection, isovolumetric relaxation, rapid filling and reduced filling [21]. Problems in the nodes, however, influence the heart rate and the heart contraction (see section 2.4).

2.3. Heart Motion

The sequence of action potentials and timing of the contraction and relaxation optimizes the output of the heart. Besides this, the heart motion can also positively influence the heart output. The heart motion during a contraction consists of translations and rotations, as previously described. Due to the combination of different motions the pumping is improved. The translational and rotational motions vary for different parts of the heart. The ventricles can be divided in the basal, mid and apical region. These segments are shown in Figure 2.1b. In the basal region the longitudinal translation is the dominant motion. In the apical region this is more of a combination of motions: besides the longitudinal translation, the circumferential rotation is also a dominant motion [22, 23]. During the contraction the apical region rotates in the anticlockwise direction and the basal region rotates in the clockwise direction. Due to this opposite movement the ejection of the blood is improved. During the relaxation the untwisting of the heart encourages the early filling of the left ventricle. For the right ventricle, according to Grymyr [23], the motion is "a combination of longitudinal shortening, inward movement of the free wall and bulging of the interventricular septum into the right ventricle during left ventricular contraction". The described motions, however, are different for the endocardium and epicardium layers. As explained, these layers contain muscle fibers, which are differently orientated for the different layers. As described by Bansal and Kasliwal [24] the fibers on the endocardium are oriented parallel to the longitudinal axis and have a dominant longitudinal motion. The fibers on the epicardium, on the other hand, are more parallel to the circumferential axis, resulting in the radial, circumferential and rotational motion being more dominant.

Heart motion is an important topic in this report and previous sections show that the heart motion is complex. The motion is not the same for different parts of the heart - and even for these different parts, the heart motion appears to be varying on the outer or inner heart wall. This should be kept in mind during this research.

2.4. Arrhythmia

Cardiac arrhythmia can influence the electrical activity of the heart, resulting in a non-optimized heart contraction and relaxation. Problems can arise with a heart rate that is too fast, too slow or when the action potential does not start in the SA node [25]. For example, this could lead to the amount of blood pumped through the body to be too low, resulting in an inability to meet the demands of the organs [20]. When the heart rate is below 60 bpm the arrhythmia is defined as a bradycardia. When the heart rate is higher than 100 bpm, it is called a tachycardia. Below some forms of arrhythmia are described:

- **Sinus bradycardia** With this arrhythmia the heart rate is slower than normal, but the travel pattern is the same. Due to this slower heart rate a person could feel tired, light-headed or dizzy, since not enough oxygen is available in their body [25].
- **Sinus tachycardia** This arrhythmia is the opposite of previous one. With this arrhythmia the heart rate is faster than normal, however, the rate rarely exceeds 180 bpm [20]. Symptoms

of this arrhythmia are, for instance, difficulty with breathing, dizziness, fainting, chest pain and anxiety [26].

- **Atrioventricular (AV) blocks** With this arrhythmia the SA node works fine, but the impulses do not travel through the AV node to the ventricles, with the result that the ventricles do not contract. Spontaneous activity in the Purkinje fibers can contract the ventricles, but this happens at a very low heart rate [20]. The symptoms are similar to the other arrhythmia and include dizziness, fainting, fatigue, chest pain, lightheadedness or shortness of breath [27].
- **Ventricular tachycardia (monomorphic VT)** This arrhythmia is caused by repeating circuits within the ventricles, resulting in a ventricle that beats three or more consecutive times at a higher rate than 120/min. This arrhythmia can cause syncope or cardiac arrest [20].
- **Asynchrony** The heart can also beat irregular. As a result, the right and left side of the heart may not contract at the same time, leading to congestive heart failure due to congestion of the blood [25].
- **Atrial Fibrillation** Lastly, with this arrhythmia the atria are quivering and the impulses sent to the ventricles are irregular and erratic. This arrhythmia is a form of tachycardia. This is the most common arrhythmia for older people [25].

As mentioned above, a slow or different heart rate can make a person feel tired, dizzy, shortness of breath, palpitations, or result in a loss of consciousness. When this is the case a pacemaker is needed. A pacemaker detects the arrhythmia and sends an electrical pulse to obtain a normal heartbeat [25].

2.5. Pacemakers

Pacemakers are mostly implanted to solve problems caused by SA node dysfunction, AV conduction block or tachyarrhythmias [28]. They detect a problem with the heart rhythm and send out a pulse in order to make sure the action potentials travel through the heart wall as they should be. The first pacemaker was implanted in 1950: it had the size of a hockey puck and the battery was empty in less than a year [25]. Nowadays pacemakers are smaller and the batteries last longer. A pacemaker consists of a battery, a sensing part, an impulse sending part and leads [25]. An original pacemaker consists of one to three leads, attached to different places on the heart. These places depend on the electrical activity needed to improve the rhythm of the heart. The simplest pacemakers, single-chamber pacemakers, have one lead usually connected to the right ventricle, see Figure 2.4a. A pacemaker with two leads is called a dual-chamber pacemaker and is attached to the right atrium and right ventricle. Pacemakers with three leads have their leads in the right atrium, right ventricle and in the left ventricle. This helps to synchronize the contraction of the right and left ventricle [25]. Aside from the differences in the number of leads, pacemakers can have different program settings in order to normalize the heart rate. Different settings are for instance a fixed-rate pacemaker, which sends an impulse at a steady state independent of the heart's own activity. Another setting is sending on demand: the pacemaker measures the heart rhythm and when detecting an arrhythmia, for instance a heart rate that is too slow, the pacemaker sends an impulse. The third setting is called a rate-responsive pacemaker. With this pacemaker, a sensor detects a person's activity and the heart rate is sped up or slowed down depending on the person's activity [28]. Depending on the arrhythmia, the number of leads and program settings are chosen. Other specifications of the pacemaker are shown in Table 2.1.

Further developments have been made to improve pacemakers. Problems can arise during the placement of the leads, as they can dislodge or cause infections. Some studies argued that the weakest component of lead pacemakers are the leads [30], which is why leadless pacemakers have been developed. Leadless pacemakers have the same pace characteristics as a single chamber lead pacemaker, but the leadless pacemaker is placed in the right ventricle so it doesn't provide any leads, see Figure 2.4b. A leadless pacemaker paces in the ventricle, detects the heartbeat in the ventricle and inhibits itself. An example of a leadless pacemaker is the Mirra from Medtronic. In this leadless pacemaker the detection in the ventricle is executed by an accelerometer. The accelerometer in the leadless pacemaker senses the activity and the pacing frequency is adjusted to that activity. These accelerometers include a mass and piezoelectric material, of which the voltage is changed when it

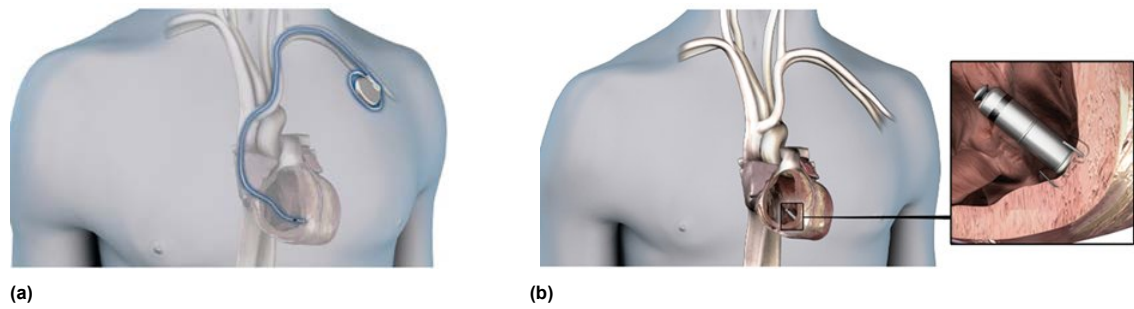


Figure 2.4: The two pacing systems. (a) The single chamber lead pacemaker. (b) The leadless pacemaker. Both figures obtained from [29].

moves or accelerates [23]. This is interesting, because such accelerometers work with the same principle as energy harvesters, but here the voltage change is used for sensing instead of powering the battery. The newest development of Medtronic is a Micra AV leadless pacemaker. This pacemaker can also sense in the atrium [31]. The implementation procedure of a leadless pacemaker differs from a lead pacemaker, as it is implanted via a catheter into the right ventricle [32]. The comparison of the specifications of the lead and leadless pacemaker are shown in Table 2.1.

Table 2.1: Comparing the specifications of a lead and leadless pacemaker [33, 34].

	Medtronic Lead Pacemaker RVDR01	Medtronic Leadless Pacemaker MC1VR01
Length	45 mm	25.9 mm
Volume	12.7 cm ³	1 cm ³
Weight	21.5 g	1.75 g
Pacing Mode	Varying	VVI
Battery	12 years*	12 years*
* This is the maximum battery duration. The battery duration depends on the pacing settings.		

Both lead or leadless pacemakers, however, suffer with the same problem: the battery life. Both pacemakers have a battery life of approximately 5-12 years, after which the pacemaker has to be replaced [2]. As stated in the introduction, vibration energy harvesting could be a solution. Vibration energy harvesting is the conversion of ambient vibrations to energy. These vibrations are the heart wall vibrations, which bounce at a certain acceleration and frequency. Via an energy harvesting mechanism designed to use these vibrations in order to generate electrical energy the battery is recharged. However, these mechanisms must meet many technical and safety requirements before it can be used in pacemakers. These requirements and the testing procedures are discussed in Appendix A.

3

Discussing the Current Development Status of Energy Harvesting for Powering a Pacemaker

This chapter contains the literature research paper, presenting the literature study investigating the state of the art. The heart signal measurement methods found in literature are analysed, followed by an overview of nonlinear techniques currently used in MEMS low frequency energy harvesters. The dynamical behaviour of energy harvesters is discussed. The testing signals used for testing in the lab are reviewed and the interaction between the signals and the dynamical behaviour of an energy harvester is analysed.

Discussing the Current Development Status of Energy Harvesting for Powering a Pacemaker

R. Bastiaanse, T.W.A. Blad and N. Tolou

This article discusses the current status of energy harvesters for powering a pacemaker. To test if an energy harvester is sufficient for powering a pacemaker, a representative human heartbeat signal is needed. The signal should contain information about the input frequency and the input acceleration. Methods performed to measure the human heart signal with the required information are ultrasonic measurements and measurements with an accelerometer. Energy harvesters operating in a pacemaker should operate at a broad range of low frequencies, and at MEMS scale. This research contains an overview of nonlinear techniques used in low frequency MEMS energy harvesters. For instance, a large displacement, stoppers and the material stiffness of piezoelectric material are used to obtain nonlinearities in energy harvesters. The majority of nonlinear MEMS low frequency energy harvesters are tested on harmonic signals. This is a good first step, but energy harvesters for a specific application will have to be tested on the signal intended for that application to obtain the dynamical performance of the energy harvester.

Keywords: Energy Harvesting, Pacemaker, Nonlinear, MEMS, Ambient Vibrations

3.1. Introduction

Energy harvesting refers to the method in which ambient vibrations are converted to electricity [4]. This electricity can be used as a power source for biomedical devices or wireless sensor nodes [35]. An example of a biomedical device that is suited for this method is a pacemaker. Now, a pacemaker runs on a conventional battery that must be replaced every 5-12 years [3]. This accounts for approximately 25% of all pacemaker implantation procedures [36]. As these procedures come with complications such as infections or bleeding [3], powering the pacemaker through an energy harvester has been considered a promising alternative. However, this also comes with its own challenges, since there are several requirements for an energy harvester to power a pacemaker [37]. Examples are size ($< 1 \text{ cm}^3$), a long lifetime (more than 20 years) and being capable of delivering 1-10 μW of power output [37, 38].

The human heartbeat normally has a heart rate that varies between the 60 and 100 beats per minute (bpm). This corresponds to a frequency range of 1-1.67 Hz. During an activity, like sports, this range can increase up to 3 Hz [39]. An energy harvester for a pacemaker should, besides the aforementioned requirements, thus also be able to operate on a broad frequency spectrum. Different techniques can be investigated to achieve a broad bandwidth in an energy harvester. Twiefel and Westermann [40] categorize and describe techniques for broadband energy harvesters. This categorization contains linear generators, nonlinear generators and advanced electronic networks. Toshiyoshi et al. [41] review and evaluate recent examples of MEMS velocity-damped resonant generators (VDRG) in terms of the power density, with the focus on size. Todaro et al. [42] discuss piezoelectric MEMS vibration energy harvesters and compare them using several figures of merit. Also, challenges in vibration energy harvesters are discussed, including widening the working bandwidth. Daqaq et al. [43] write about the role of nonlinearities in vibration energy harvesters and give a broad description of the nonlinear energy harvesters under different types of excitations. They specify three different excitation groups, namely harmonic excitations, random excitations and other common ambient vibrations. Comparing energy harvesters for different input excitations can give different outcomes [44].

However, the majority of the developed nonlinear energy harvesters are tested on a harmonic signal and research is focused on broadening the bandwidth of energy harvesters. The investigation of the ambient vibrations on which the harvester must operate on becomes second priority [45]. Hence, it

can be speculated whether conclusions found under a harmonic signal can be translated to an ambient vibration, such as the human heartbeat, that is periodic but non-harmonic [4]. The objective of this paper is to discuss the current status of energy harvesting for powering a pacemaker. In Section 3.2 energy harvesters that are tested on a human heartbeat signal are reviewed. In Section 3.3 signal measurements are discussed, used to obtain the human heartbeat signal for the testing of energy harvesters. In Section 3.4 an overview of current techniques used for nonlinear MEMS low frequency energy harvesters is given and the nonlinear characteristics are described. Furthermore, in Section 3.5 the testing conditions for energy harvesters are reviewed. Section 3.6 contains the discussion. Finally, Section 3.7, is the conclusion.

Literature Search Method

The literature for this research has been found via Google Scholar and Scopus. During the search for the overview some boundaries were specified. The first boundary is specified for the volume of the harvesters. As stated by Galayko D et al. [46] a volume of 1 cm^3 can be assumed as standard and should be the size for the power source for autonomous micro-scale systems. The second boundary specified is for the input frequency. Ansari and Karami [47] state that the energy harvester should be designed for a frequency below 50 Hz, to generate sufficient power for a pacemaker. This boundary of 50 Hz is maintained. Only the articles that performed an experiment with a prototype are taken into account.

3.2. Energy Harvesters for Pacemakers

Several researchers already developed energy harvesters intended for powering a pacemaker. Some of these energy harvesters are discussed below. The harvesters are sorted in different categories, these categories represent the methods used to obtain the heartbeat signal to test the harvester on. These methods will be elaborated in Section 3.3.

Ultrasonic Signal

For the first harvester discussed, the ultrasonic measurements performed by Kanai et al. [8] are used as heart signal input vibrations and the acceleration profile and frequency spectrum of the heartbeats is estimated in [4]. With this signal, linear, monostable and bistable harvesters are simulated. They state $1 \mu\text{W}$ as a boundary for providing sufficient power for pacemakers. A millimeter-scale zigzag linear structure could obtain enough power output to satisfy the boundary condition, but this depends on the frequency of heart signal. However, they found that a linear zigzag structure on microscale could not provide sufficient power. The nonlinear harvester consists of two external magnets, one magnet attached to the frame and one tip magnet, making the harvester monostable or bistable depending on the distance between the magnets [4], this is shown in Figure 3.1a. Both the nonlinear harvesters provide enough power output to satisfy the boundary condition. Moreover, they found that the bistable nonlinear energy harvester had the largest power output over an extra wide range of the heart rate. Although the type of vibrations and the power output change with the heart rate, the bistable energy harvester generates more than $3 \mu\text{W}$ over the heart rate range, which is 7-700 bpm [4, 48]. Furthermore, experiments on the Kanai waveform also showed that the nonlinear piezoelectric energy harvesters obtain a power output that meet the conditions if the human heart rate is between 20-700 bpm [4]. Ansari and Karami [47] simulated a fan-folded geometry with a tip mass of 21 grams on the Kanai waveform, which can be observed in Figure 3.1b. The device has a first natural frequency at 16.18 Hz and an average power output $10.24 \mu\text{W}$. The harvester is simulated for different heart rates and it is stated that the output power does not change significantly for different heart rates. This harvester is further developed and also experimentally tested on the Kanai waveform [49]. The theoretic and experimental results are compared and they found that the prototype is robust to a heart rate variation over a wide range.

Accelerometer Signal

The heart signal obtained with an accelerometer by Deterre et al. [39] is used to perform a preliminary design study. This study presents parameters specified via simulations on the obtained signal to get a $100 \mu\text{W}$ power output. The found parameters are a mass of 3.5 g of tungsten, a stiffness of 100 N/m

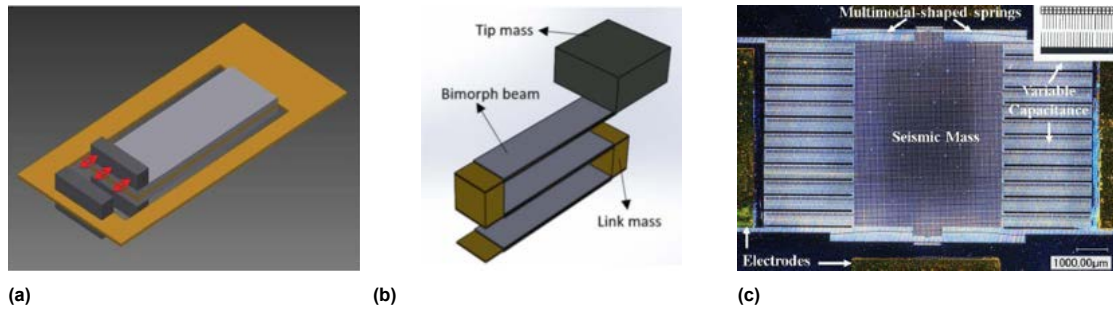


Figure 3.1: Energy harvesters discussed for powering a pacemaker. (a) Nonlinear energy harvester with magnets, from [4]. (b) The fan-folded design, from [47]. (c) The multimodal-shaped spring design, from [50].

and an electrical damping ζ of 0.1 at a frequency of 25 Hz. Obviously, further research is needed to use these parameters in an energy harvester design. The signal of Deterre et al. [39] is also used by Vysotskyi et al. [50], for testing a nonlinear energy harvester having multimodal-shaped springs, shown in Figure 3.1c. The device orientation influences the average output power. A maximum average power of $2.38 \mu\text{W}$ is measured, with a heart rate of 116 bpm and 10 m/s^2 acceleration amplitude. However, it is known that a heartbeat is time-varying, so this power output also changes with time.

Animal Tests

Zurbuchen et al. [36] tested an electromagnetic induction based energy harvester on measured heart motions from a pig and implanted the harvester in the right ventricle apex of a pig's heart. At a heart rate of 84 bpm, the harvesting device generated a total mean output power of $0.78 \mu\text{W}$. The output power per heartbeat increased with an increasing paced heart rate up to $1.7 \mu\text{W}$ at 160 bpm. The simulation on the three heart signals obtained from animals, as described in Section 3.3, predicted a mean output power of 14.5, 41.9, and $16.9 \mu\text{W}$. Li et al. [3] designed a piezoelectric energy harvester with an elastic skeleton and two piezoelectric composites. Placed into the apex of the heart of an adult Yorkshire swine, the maximal output of approximately 20 V is found. Furthermore, the measurements performed in [4] are experimentally tested on a shaker, the harvester can generate $25 \mu\text{W}$ if tested on the signal from the heart base, $5.5 \mu\text{W}$ at apex, $5.4 \mu\text{W}$ at the lung, and $1.4 \mu\text{W}$ below the diaphragm. Zurbuchen et al. [2] sew an energy harvester onto a sheep's heart resulted in a mean power of $16.7 \mu\text{W}$.

Subconclusion

The mentioned studies are a good step in the development of energy harvesters for powering a pacemaker. However, much remains to be done before energy harvesters can be implemented in pacemakers. There are three aspects which are important in the development process to deliver a sufficient energy harvester for powering a pacemaker. These three related aspects are the heartbeat signal, the energy harvester design and the testing process. Of course the energy harvester design itself is needed to power the battery. The heartbeat signal is needed to test the energy harvester and to align the dynamic behaviour of the energy harvester. The heartbeat signal should contain the required information to be used for the testing process. To investigate in which aspect the design process can be improved, this paper will elaborate on them separately.

3.3. Heart Signal Measurements

Several methods are known to measure the heart signal. The most basic method is listening to the sound of the heart with a stethoscope or a phonocardiograph, which use the heart sounds to measure the heart rate [51]. An electrocardiogram (ECG) provides information of the electrical activity of the heart muscle [52]. The heart rate can be estimated from the intervals of the ECG peaks, i.e. the beat-to-beat intervals [53]. Kim et al. [54] and Massagram et al. [53] designed a low-cost non-contact phase-detection radar, that continuously detects the real-time heartbeat, such that one can measure the heartbeat rate variability. This radar is developed to measure 40 cm from the chest, and uses a bandpass filter for separating the heartbeat and respiration signals [54]. Pandia et al. [51] measured

the heart sounds with a chest-worn MEMS accelerometer. This signal contains not only of heart information, but also of information of the motion artifacts [51], so signal filtering is needed. The heart rate gives information about the input frequency of the signal, but it does not give information about the heart motion. To perform experiments for energy harvesting on a human heartbeat signal, in addition to the heartbeat rate, information on the heart acceleration is also required. The methods mentioned above cannot provide this information. Methods that are able to provide this are discussed next.

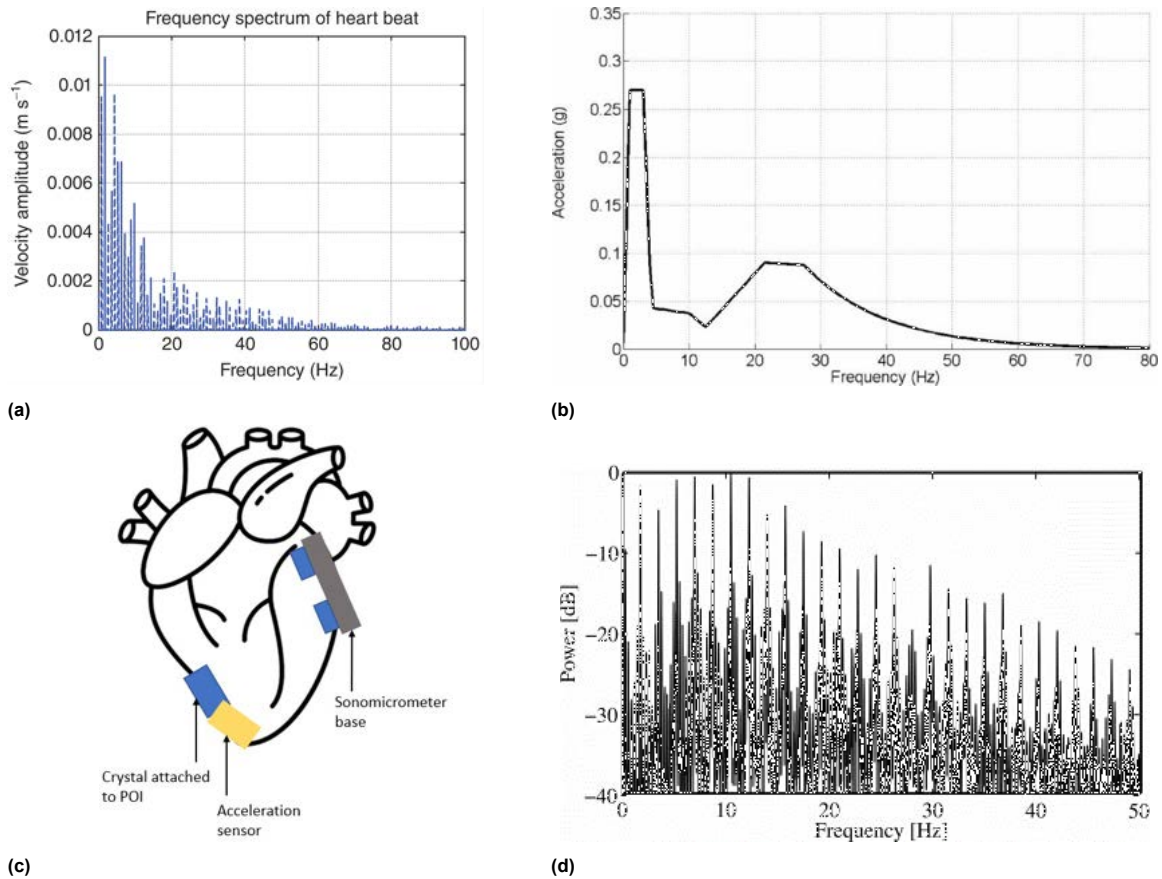


Figure 3.2: Heart Signal Measurements. **(a)** The heart wall motion from Kanai converted to an acceleration signal in the frequency spectrum, from [4]. **(b)** The acceleration spectrum of the heart measured with an accelerometer, from [39]. **(c)** The proposed scheme by Horiuchi et al. [55]. One crystal of the sonomicrometry system on the heart, four or more other crystals on a rigid base. A three-axis solid state microaccelerometer is placed on the target sonomicrometry crystal. **(d)** The power spectrum of the heart acceleration of a pig, from [56].

Ultrasonic Measurements

Kanai et al. [8] used ultrasonic diagnostic equipment to track the heart wall movement. An ultrasonic beam is passing through two points, one at the surface of the left ventricular side and one at the right ventricular side of the interventricular septum. Via this, the position of the heart wall is determined and a velocity signal is estimated, for six heartbeat periods. The obtained signal is used for experiments, where the acceleration signal is obtained by the derivative and it is converted to the frequency spectrum [4]. This signal can be seen in Figure 3.2a. However, it is questionable whether the velocity found in the measurements is the required velocity or a different velocity, since this is a 2D method. It cannot be assured that only one point is continuously followed.

MRI

McVeigh [57] analysed the heart wall motion with a cardiac MRI. With MRI images of the heart can be obtained, using a combination of breath-holding, tagging and velocity-encoding. However, quantitative analysis of the data takes a long time and lacks an appropriate interface for data acquisition, which is a problem for all cardiac MRI [57].

Accelerometers

Measurements are also performed with the use of accelerometers. Deterre et al. [39] implanted accelerometers into several heart cavities to measure the acceleration spectrum of the heart, transferred to the frequency domain. This signal has the main excitation component on a frequency between 1-1.5 Hz and a frequency plateau is found at the range of 10-30 Hz and shown in Figure 3.2b. However, the study does not elaborate on how the measurements are performed. Due to this it cannot be established for certain that the heart signal obtained is also the correct heart signal. Furthermore, Horiuchi et al. [55] presented a method to estimate the heart motion with a 3D point of interest position on the heart surface. They propose a sonomicrometer, that measures the moving soft tissue via ultrasound signals with crystals attached to the heart, in combination with an accelerometer that measures the target crystal, to increase the accuracy of the heart signal. This method is evaluated by simulations and is presented in Figure 3.2c. However, this is an open heart surgery of which it is not certain whether this may be performed on humans.

Animal Tests

Researchers have performed tests on animals to imitate the human heartbeat. Hoff et al. [56] used acceleration sensors to measure the heart motion during surgery on pigs. The first sensor was placed near the apex of the heart and the second acceleration sensor placed higher, on a region supplied by the circumflex coronary artery. The power spectrum of the heart acceleration can be observed in Figure 3.2d. The heart motion is reproduced in detail and by integrating the filtered acceleration data, the heart wall velocity and position are obtained. Furthermore, the heart vibrations of a pig are measured with a laser Doppler vibrometer, a non-contact method in [4], to measure the velocity of the moving surface. The vibrations were measured at the apex of the heart, the base of the heart, the lung, and at one point beneath the diaphragm on the liver. Also, Zurbuchen et al. [36] used a custom-made motion tracking unit to obtain acceleration data, the measurements are performed on three pigs. The methods discussed are open heart surgeries of which again is not certain whether this may be performed on humans.

Subconclusion

From the measurements that provide the acceleration and frequency data, the following signal characteristics can be concluded. The heartbeat signal consist of a broad low frequency spectrum. Furthermore, the acceleration amplitude of the heart signal is not constant for the entire frequency range. The highest acceleration amplitude can be seen at the lower frequencies, while for higher frequencies the amplitude decreases. This also means that the power is higher for low frequencies and decreases for higher frequencies [8]. It is good to mention that the expectation was to see a frequency response of the heart rate, which is around 1-1.67 Hz. However, a broader frequency response is seen. This can be explained due to the fact that each heartbeat acts as an impulse [49]. This signal characteristics could be used during the design process of an energy harvester intended for powering a pacemaker. The measured heartbeat signals discussed do not match. This could be due to the different measurement methods used. However, important to note is that the moment of measuring and the subject of whom the signal is measured can also influence the found signal. More heart measurements are needed to verify this difference.

3.4. Energy Harvester Overview

As seen in previous section, pacemakers require harvesters that can operate on a real, broad and low frequency signal. Furthermore, a harvester that is MEMS scale ($< 1 \text{ cm}^3$) and has a high power output (1-10 μW) is required. Although linear energy harvesters can generate a high power, this power is distributed over a narrow bandwidth [58], which could be solved by frequency tuning. In addition, the size of a linear energy harvester operating at a low frequency would be larger than a nonlinear energy harvester for the same range [59]. Ramlan et al. [60] indicate that for a linear harvester to operate on a low frequency, a large mass and a soft spring element are required. Adding extra weight to a small device is not preferred and a large mass supported on a soft spring may result in nonlinearity, due to geometric stiffness. Altogether, frequency tuning for linear energy harvesters is not always an option due to geometrical or dynamical constraints [61]. Nonlinear energy harvesting could be the solution for this small size, in combination with a required high power on a low frequency signal. As stated by Green et al. [62] a lot is still unknown about the use of dynamic nonlinearities to aid the harvesting of

energy from low-frequency vibrations. These nonlinear effects increase the operating bandwidth [40] and could positively influence the power output. The operating bandwidth is defined as the range between the half-power cut-off frequencies [63].

3.4.1. Overview of Nonlinear Techniques

Different techniques can be used to obtain nonlinear behaviour in energy harvesters. Figure 3.3 gives an overview of the currently used techniques in MEMS low frequency energy harvesters. Sources of nonlinearities in MEMS are forcing, damping, and stiffness [64]. According to Younis [64], forcing nonlinearities can be induced by actuation and detection mechanisms, such as electrostatic forces or with harvesters that are operated or in-use, like capillary forces and Van der Waals forces. Another example of forcing is with the use of external magnets. External magnets introduce a force that is dependent on the distance. This force opposes the elastic restoring force of the bent beam [61]. Varying this distance can result in a nonlinear monostable harvester or a nonlinear multi-stable harvester [7]. Finally, pre-buckling is categorized under forcing. Due to preloading a beam buckles, giving a bistability [50, 65]. The next category, stiffness nonlinearities, consists of stoppers, geometric stiffness and material stiffness. Nonlinearities can be inherently present in the dynamics of an energy harvester due to its geometric or material properties [43, 64]. Material stiffness is a stress-strain relation, while geometric stiffness is a displacement-strain relation in which a large displacement causes an increase in strain, giving a nonlinear spring behaviour [43]. This can be of the softening type, with a decreasing force with the tip deflection, or of the hardening type, with an increasing force with the tip deflection [43, 66]. Mahmoodi et al. [67] analyse a piezoelectric actuated microcantilever and relate the stress-strain relation for piezoelectric material. The equation of motion of the cantilever is obtained, where quadratic nonlinearities were found. They state that these quadratic nonlinearities are the result of material nonlinearities in the piezoelectric layer, so when deformed they add material nonlinearities to the structure [64]. Finally, the third form of stiffness nonlinearities are stoppers, which have a piecewise-linear equation of motion [43]. On impact, the resonant branch of solutions of the harvester is broadened [43]. This impact causes a sudden increase in the stiffness, a nonlinear hardening effect [43]. Stoppers covered by this category are objects that limit the diversion of the harvester and cantilever stoppers.

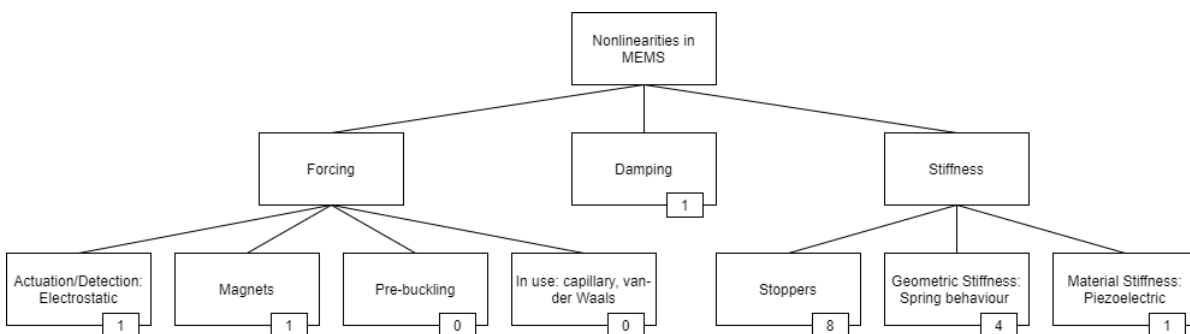


Figure 3.3: Overview of nonlinear techniques currently used in MEMS low frequency energy harvesters. The numbers represent the techniques used to design nonlinear energy harvesters, consisting of fifteen reports found in the literature.

In Figure 3.3 the numbers represent the techniques used by researchers to design a nonlinear energy harvester, found in the literature, that meet the boundary conditions of MEMS and low frequency energy harvesters specified in Section 3.1. Some articles use multiple techniques to obtain the broadband behaviour. Techniques used more often in literature are stoppers and the nonlinear spring behaviour due to large displacements.

3.4.2. Nonlinear Characteristics

Nonlinear energy harvesters have some dynamic behaviour characteristics. The characteristics discussed are found in the MEMS low frequency nonlinear energy harvesters articles, but also general characteristics found in other literature. The characteristics described are the non-uniqueness, need

for a specific input acceleration, the quality factor and robustness.

Non-uniqueness

Due to nonlinearity the harvester can show a hysteric behaviour, meaning that the harvester could have a different response depending on the direction of the frequency sweep and the initial conditions. In other words, it has a non-unique solution [43]. The frequency response curve of a frequency sweep is shown Figure 3.4. Here a large-amplitude branch of solutions, the upper branch, and a small-amplitude branch, the lower branch can be observed. Sets of initial conditions can be indicated to a basin of attraction for the equilibrium points. The basin of attraction determines for which initial conditions the harvester ends up on which branch [43, 68]. The nonlinearity determines the bending direction, the bending degree of the frequency-response curve and does not influence the peak height. The peak height can be influenced by the input acceleration and the damping [43].

Input acceleration

For some nonlinear energy harvesters, the performance depends on the input acceleration. Meaning that to enter the nonlinear regime, to enlarge the bandwidth, sometimes a large input acceleration is required [69]. For a small input acceleration, a monostable harvester behaves similar to a linear harvester and a bistable harvester behaves the same as a monostable harvester. A bistable energy harvester needs a certain input acceleration to activate the interwell oscillations [43]. Furthermore, for stoppers the broadening effect is influenced by the distance of the stopper and the amplitude of the input acceleration by which the harvester is excited. A higher acceleration and a smaller stopper distance broadens the bandwidth. However, there is a trade-off between the bandwidth and output power. A smaller stopper distance decreases the maximum output power and the average power, due to impact losses [70].

Quality factor

For a nonlinear harvester it is given that a higher quality factor enlarges the bandwidth [71]. This is in contrast to a linear energy harvester, where a higher quality factor reduces the bandwidth. The bandwidth of the harvester depends on the damping ratio, the nonlinearity and the input acceleration [60].

Robustness

When a nonlinear energy harvester operates on the upper branch of solution it is more tolerant to variations in the excitation frequency, because of this enhanced bandwidth [43]. When a nonlinear energy harvester is designed in a way that the dominant excitation frequency occurs in the middle of the bandwidth, the harvester will have a good margin of error for when the dominant frequency shifts [72].

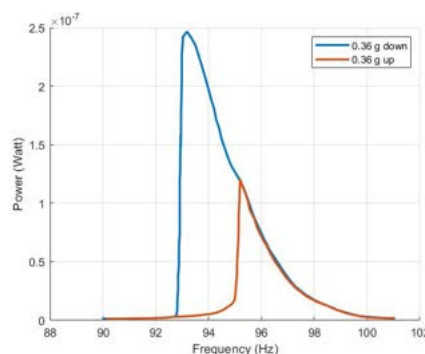


Figure 3.4: An example of a frequency-up and -down sweep at input acceleration of 0.36 g for an out-of-plane MEMS electret energy harvester, from [73].

Subconclusion

The mentioned nonlinear characteristics should be taken into account when designing a nonlinear energy harvester. Further research is needed to address these characteristics for a nonlinear energy

harvester that is MEMS scale and operating at a low frequency. Under certain conditions, nonlinear energy harvesters have a wider steady-state frequency bandwidth than linear energy harvesters, leading to a common belief that they can be used to enhance the performance in ambient environments [43]. However, the dynamic behaviour of harvesters can be different for varying testing signals, because of non-uniqueness, the need for a specific input acceleration and the quality factor characteristics of a nonlinear harvester. Altogether, the performance of a harvester should be verified on multiple testing signals.

3.5. Testing Signals

Of the fifteen studies analysed for the nonlinear techniques overview, thirteen energy harvester designs are tested on a harmonic frequency sweep. The output response and the bandwidth increases with an increase in the acceleration of the input signal. Lu et al. [74] have, besides testing the electrostatic energy harvester on a frequency sweep, also shaken the energy harvester by hand with a frequency of 7 Hz and an acceleration of 2.0 g. At this low frequency an output power of $0.06 \mu\text{W}$ is found. However, during the frequency sweep between 10-180 Hz at an acceleration of 2.0 g, a power output from 0.1-0.9 μW is found. Furthermore, Vysotskyi et al. [38] and Vysotskyi et al. [50] tested the same nonlinear energy harvester on a harmonic frequency sweep and a human heart signal, respectively. However, during the frequency sweep from 5-100 Hz at an acceleration of 10 m/s^2 , the harvester starts with a power output of $0.5 \mu\text{W}$ at 5 Hz and increases to a maximum of $10 \mu\text{W}$ at 55 Hz. For the same harvester tested on the heart signal an output power of $1.26 \mu\text{W}$ is found at 130 bpm and an acceleration of 10 m/s^2 . These two examples show a different response of the harvesters on different testing signals. In other words, testing signals have an influence on the performance of the energy harvester. This makes analysing the testing conditions interesting.

There are multiple conditions to test an energy harvester on. A first testing signal is a harmonic frequency sweep, consisting of a certain fixed amplitude and frequency. However, it is thought that Gaussian white noise is a more representative signal for ambient vibrations. A characteristic of Gaussian white noise is that the power is equal in each frequency [62]. To further improve the testing conditions for ambient vibrations energy harvesters, coloured Gaussian noise is used. Some ambient vibrations could have a Gaussian white noise distribution, but according to Daqaq [75], the energy of most ambient vibrations is present in a frequency bandwidth. They give an example of a sensor on a bridge, where the frequency and intensity vary due to environmental conditions. The ambient signal can be approximated with a coloured Gaussian noise, since the bridge acts like a filter and only frequencies of a certain bandwidth are allowed to pass. In research coloured Gaussian noise is obtained by low pass filtering Gaussian white noise [75–77].

A comparison of the discussed testing conditions with characteristics of the human heartbeat signal found in Section 3.3, can be observed in Figure 3.5. The human heart signal is a broad signal, consisting of a varying acceleration amplitude at low frequencies. The power of the signal decreases for higher frequencies. Differences between the testing signals and the heartbeat signal can be seen. The influence of testing signals on the behaviour of energy harvesters is discussed.

3.5.1. Harmonic Signals

In most cases, testing is performed by a frequency up or down sweep [78]. This applies also for the MEMS low frequency nonlinear energy harvesters as discussed in Section 3.4. Some researchers indicate that when a harvester is tested under a harmonic frequency sweep and the nonlinear energy harvester shows a broader bandwidth, it is more suitable for ambient vibrations [58, 79–81]. However, according to Tran et al. [44], many nonlinear harvesters have an enhanced performance when excited by a harmonic input, but this response is diminished for other types of excitations. Daqaq et al. [43] addresses that when a bistable harvester performs well under harmonic excitations, the harvester might not perform as well under random or nonstationary input. In a real environment, vibrations such as a frequency sweep of constant magnitude cannot be expected, this means that a response found under a frequency sweep, is not the response found under a noise excitation [78].

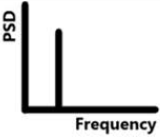
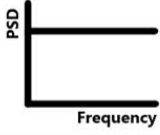
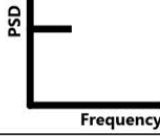
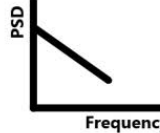
	PSD	Broadband	Low Frequencies	Varying Power
Harmonic Signal		✗	✗	✗
Gaussian White Noise		✓	✗	✗
Gaussian Colored Noise		✓	✓	✗
Human Heart Signal		✓	✓	✓

Figure 3.5: Overview of the comparison of testing signals with the human heartbeat signal.

3.5.2. Random Signals - Gaussian White Noise

Several researchers performed experiments with Gaussian white noise. For instance, Cottone et al. [61] found that a bistable energy harvester can outperform a linear harvester under Gaussian white noise, where the distance from external magnets determines the linear or bistable behaviour. Jiang and Chen [82] produced nonlinearity by a snap-through mechanism. Comparing this to a linear harvester of the same size shows that the nonlinear energy harvester outperforms the linear harvester under Gaussian white noise excitations. Green et al. [83] found that under Gaussian white noise, the nonlinear spring term is used to reduce the moving space of the device. However, the same energy harvester has been tested on ambient vibrations, where this reduced displacement space also influences the power output negatively [62, 83]. According to Daqaq et al. [43], to design a bistable energy harvester that can outperform a linear harvester under Gaussian white noise, knowledge about the excitation intensity is needed. They also state that, for Gaussian white noise excitations, nonlinear hardening cannot improve the harvesters performance. This in contrast to nonlinear softening, which may improve the performance.

3.5.3. Random Signals - Coloured Gaussian Noise

Testing under Gaussian coloured noise gave diverse results when comparing linear, monostable and bistable energy harvesters. For instance, Daqaq et al. [43] indicate that under coloured Gaussian noise a bistable energy harvester, in comparison to a monostable energy harvester, has a wider bandwidth response. It is also less sensitive to variations in the center frequency of the excitation. Furthermore, Daqaq [75] indicates that, with an excitation frequency close to the natural frequency of a linear harvester, a bistable harvester produces less power under coloured Gaussian noise. However, this does not mean that a linear harvester is better under coloured Gaussian noise, since the performance could differ for an other excitation frequency. Daqaq [84] found an enhanced bandwidth response under harmonic excitations. Under coloured excitations with small bandwidths, however, a deterioration of the mean power was observed, due to the nonlinearity. This different response under different input signals is also found by Blystad and Halvorsen [76]. They use stoppers to obtain the nonlinear behaviour and a different harvesting response is observed for a sinusoidal excitation compared to a coloured Gaussian noise. With a sinusoidal excitation the output power reaches a plateau. For coloured Gaussian noise the output power continues to increase when the stopper is hit, but at a slower rate than without a stopper. This comparison has also been made by Lee et al. [72], where for a harmonic excitation

the harvester was able to oscillate at the large-amplitude branch. In the coloured Gaussian noise the response drops back to the small-amplitude branch after a certain time. Also Lu et al. [85] simulated their MEMS electret-biased energy harvester on a harmonic frequency sweep and a coloured Gaussian noise signal. An interesting difference in the response of the harvester is that under the Gaussian noise two frequency components, the main resonance and the asymmetric vibration, can be observed in the output that are not seen during the frequency sweep.

3.5.4. Ambient Signals

Beeby et al. [86] have tested energy harvesters on ambient vibrations. Piezoelectric and electromagnetic harvesters were simulated on real vibration data from a diesel ferry engine, a combined heat and power pump, a petrol car engine, a helicopter and Gaussian white noise. The results show that for the four real vibrations data, in the piezoelectric case the linear energy harvester with a high Q-factor outperforms the other harvesters. Only under Gaussian white noise a bistable energy harvester has the highest power output. For the electromagnetic harvesters, the linear high Q-factor has the highest power output for all the vibrations [86]. However, Neri et al. [7] experimented with an energy harvester where the nonlinearity depends on the distance from external magnets. These experiments were performed on a car, a train and microwave oven signal. They found that the distance between the magnets to obtain the maximum output depends on the shape and intensity of the used signal. Finally, Boisseau et al. [87] used nonlinear springs to improve the output power simulated on a car engine signal at 3000 rpm and a human walking down of a staircase. On a drill signal or the car engine at 2000 rpm, however, nonlinear energy harvesters have a lower power output.

3.5.5. Testing according FDA

The Food and Drug Administration set the requirements which a medical implantable device should meet. They also specify the testing requirements. According to the Food and Drug Administration, for the implementation of new implantable pacemakers in vitro (bench) test are needed to verify the mechanical and electrical working principle. This shall be tested under the conditions of the operational environment [10]. During the clinical trial of a new device, the pilot phase, consisting of 10-30 subjects, the preliminary safety and performance information is investigated [11]. Since the mechanical and electrical working principle depends on the energy harvester's performance, which dynamical behaviour depends on the input signal, it is likely that the in vitro (bench) tests should also be validated on 10-30 different input signals.

Subconclusion

During the discussion of the testing signals it was observed that harvesters tested on various input signals gave a different output response. The behaviour of nonlinear energy harvesters depends on the driving force [7, 78]. For nonlinear energy harvesters, understanding the characteristics of the excitation signal is important to match the dynamic behaviour of the harvester to the source, since the type and strength of ambient excitations influence the performance [7, 44, 62]. Inconsistent input accelerations are a challenge for nonlinear energy harvesters [45]. Due to the different characteristics in ambient vibrations, it is difficult to find a general solution for the energy harvesting problem [88]. Testing a harvester with signals that reproduce the main characteristics of the operational environment gives an optimal working setup [7]. As stated before, for powering a pacemaker with an energy harvester, detailed knowledge is needed of the heartbeat signal of a human. There can be a difference in the response of a nonlinear harvester when comparing the response from a heartbeat waveform to a harmonic oscillation [4]. This means that testing an energy harvester on a harmonic signal is a good first step, however, further testing on a heart signal is needed to obtain the actual power output.

3.6. Discussion

The current status of energy harvesters for powering a pacemaker is discussed in this article. However, only three subjects are highlighted: the heartbeat signal, the designed energy harvesters and the testing conditions. More components are required to integrate an energy harvester in a pacemaker. Take for instance the transition from the obtained electrical energy to the battery. It is questionable whether

the quality of the battery is good enough to keep up with the developments or that it will eventually end up depleting faster, as with a smartphone for instance. In addition to the technical aspects, one may wonder if, for pharmacists, it is economically feasible to produce pacemakers based on energy harvesters. Instead of selling a pacemaker every 5-12 years, they will sell one for a whole lifetime. Despite the importance of the other factors, this discussion focuses on the nonlinear energy harvesters and the testing conditions on the heart signal.

3.6.1. Nonlinear MEMS Low Frequency Energy Harvesters

The volume boundary condition, in this paper specified as 1 cm^3 , can be questioned. In some of the found articles it is not clearly specified what is defined as the volume given. It is debatable whether the volume only includes the harvester mechanism or that the volume also contains the motion range of the harvester. For a pacemaker the best maximum volume specified, is the volume including the harvester's motion range. Furthermore, the volume of a leadless pacemaker is smaller than the specified boundary condition, since volumes of 0.5 cm^3 and 0.8 cm^3 are found [36]. The volume of 1 cm^3 is chosen for a broader scope during the research, but it should be considered that the design of energy harvesters with the purpose of powering a pacemaker should be smaller.

Not all the nonlinear techniques found are suitable for a pacemaker, as for instance harvesters using magnets. A pacemaker without magnets is preferred for reasons of compatibility with MRI [38]. Multiple of the discussed harvesters that are tested on heartbeat signals consist either of magnets or of mass of approximately 20 grams to lower the resonance frequency. Current pacemakers are approximately 20 grams in total, making the increase in weight when a harvester is added significant. Furthermore, it must be ensured that the harvester does not impede the heart rhythm.

3.6.2. Testing Heart Signals

Energy harvesters designed for a certain application should be tested on the ambient input signal from that specific application. To obtain the heartbeat signal, measurements with accelerometers and ultrasonic measurements have been performed. Ultrasonic measurement performed by Kanai et al. [8] gave information about heart wall vibrations. However, only the vibration signals of the period of the second heart sound, which is the closure of the aortic valve, are analysed in the frequency spectrum and a correlation analysis of other periods in this spectrum is needed [8]. The measurement with ultrasound of the full cardiac cycle has been performed by Takahashi et al. [89]. This method is feasible for the longitudinal axis view. Further research is needed to use this method in various cardiac views, such as the short axis and apical views of the heart. Furthermore, this method shows a serrated heart wall region, caused by lumen misclassified as heart wall [89]. Further research is needed to overcome this difficulty in tracking points in the lumen and to recover the shape of the heart wall [89]. The measurements by Kanai et al. [8] show a heartbeat waveform containing a wide range of frequencies [49]. Ansari and Karami [49] state that this is because each beat acts similar to an impulse. This is different from the frequency of the heart rate, which for a normal heart rate is around 1-1.5 Hz [49]. The acceleration profile and frequency spectrum of the different researchers that use the Kanai waveform show small differences that could be explained by the way the data has been fitted or edited. This could also influence the dynamics of the nonlinear energy harvester during testing.

Furthermore, it is not specified how the results from the acceleration measurements performed by Deterre et al. [39] are obtained and therefore the results from this measurement cannot be adopted. Some other measurements with accelerometers require an open heart surgery, which was performed on animal experiments. The interpretation of these signals obtained with the accelerometer are complicated, because of movement due to respiration and movements of the pig as a whole [56]. Pacemakers with an energy harvester have been placed in animals. Despite the positive results from this test, the conclusions can not be translated to a human heart, due to the differences between humans and animals.

The major challenge of gaining the heart signal are the different measurement conditions. First, the location where the pacemaker is implanted has an influence on the received heartbeat signal. Commercial cardiac pacemakers are implanted under the skin near the clavicle [90], but a new leadless pacemaker is placed in the heart wall [91]. The location of measurement influences the acceleration and

frequency of the obtained signal. Second, the heartbeat signal depends on the moment of measuring. Zurbuchen et al. [36] obtained the heart signal from one animal twice, which showed a different peak accelerations along the device's axis and heart rates, namely 7.7 m/s^2 at 94 bpm and 15.3 m/s^2 at 165 bpm. This implies that there is a relation between acceleration and bpm. Third, the obtained heart signal also depends on the subject of whom the signal is measured, for instance, a subjects age or health condition [8, 9].

3.6.3. Future Research

The outcome of this research results in two recommendations for future research. The first recommendation is the development of nonlinear MEMS low frequency energy harvesters, working without a magnet and without a large mass to achieve the low resonance frequency. Instead, it is suggested to use piezoelectric material. The broadening of the bandwidth could be achieved with stoppers, however, it should be taken into account that the harvester does not impede the heart rhythm. The broadening effect could also be achieved by an energy harvester consisting of a buckled beam, with an additional advantage that this could be designed as a compliant mechanism. The mentioned nonlinear characteristics should be taken into account and further research is needed to address these characteristics for the designed energy harvesters. The second recommendation is to perform more heart measurements to obtain a signal that can be used to test whether an energy harvester is sufficient to power a pacemaker. This signal should contain the heartbeat frequencies and the input accelerations of the heart. To obtain more signals, more testing subjects are needed. A measurement method that is medically allowed and could be carried out easily is needed. An example is the detection of the heart wall movements using ultrasonic measurements. The location of measuring and different conditions should be taken into account, in order to obtain a representative test signal. With more signals available it could be verified if the harvester could be used widely.

3.7. Conclusion

In this article the current status of energy harvesters for powering a pacemaker has been discussed. Researchers have performed various measurements to obtain the input signal of the human heart. The input signal for testing energy harvesters should contain the heartbeat frequency and input acceleration information. Two methods to measure the heartbeat signal are described: ultrasonic measurements and measurements with accelerometers. The human heart signal is a broadband signal, consisting of a varying acceleration amplitude at low frequencies. The signal has a high power at low frequencies, which decreases for higher frequencies. Thereafter, an overview of the nonlinearities of low frequency MEMS energy harvesters is given. Popular techniques used are nonlinearity due to a large displacement and stoppers. Nonlinear energy harvesters have characteristics which could influence the performance namely, the need for a high input acceleration, the quality factor, the non-uniqueness and the robustness of the harvester. For pacemakers, energy harvesters without magnets and large masses are required. Furthermore, different testing conditions for an energy harvesting are discussed. It can be concluded that when an energy harvester is designed for a certain application, the harvester should be tested on the input signal of that specific application. The dynamical behaviour of the harvester could be different for different input signals, which could influence the performance of the harvester. The majority of the found nonlinear MEMS low frequency energy harvesters are tested on a harmonic signal. This is a good first step, but further research is necessary. Several researchers tested energy harvesters on a human heartbeat signal, which gives information about the behaviour of the energy harvester on the heart signal. The heart signal will show a different response for different people. More heartbeat signals are needed to verify the energy harvesters performance under different input conditions, since the different input characteristics of testing signals in combination with the harvesters own characteristics can influence the dynamic behaviour of energy harvesters.

Contributions

- Overview of nonlinear techniques currently used in MEMS low frequency energy harvesters.
- Addressing that experiments with energy harvesters should be specifically on the signal of the environment where it will operate, to obtain a realistic performance of the harvester.
- Overview of heart signal vibration capturing results.

- Overview and comparison of results in nonlinear energy harvesting.

4

Combining Cardiac Measurement Techniques to Improve Testing for Energy Harvesting Pacemakers

This chapter presents the experimental research paper. Three different heart sources are analysed, namely: open-chest pig heart acceleration signals, human heart ultrasound measurements and human chest motion signals. The found heart signal characteristics are processed in a human heart signal generator. With this generator various heart signals are generated and used for testing in the lab. An energy harvester with moving magnets is used and the power output on the different signals are compared.

Combining Cardiac Measurement Techniques to Improve Testing for Energy Harvesting Pacemakers

R. Bastiaanse, J. Roos, T.W.A. Blad, N. Tolou and J.W. Spronck

In this research, a first step towards the testing of energy harvesters on human heart signals is made. A heart signal generator has been developed in order to improve the test facilities for the testing of energy harvesting pacemakers. Three different sources of heart signals are combined in order to obtain a new source of heart signals, an approximation of reality, which can be used for testing. The first source are open-chest acceleration measurements of pig hearts, used as the building block of the generator. Second, ultrasound heart measurements of human hearts are used for the scaling of the pig heart accelerations. Finally, human chest motions are measured, in order to investigate the human heart's acceleration trajectory and to determine whether an increasing amplitude results from an increasing heart rate. The output of the generator are various acceleration heart signals. An energy harvester with moving magnets and static coil is tested on signals generated by the heart signal generator. The mean power output on the various heart signals is compared. For ten heart signals generated by the heart signal generator for a heart rate of 160 bpm, an average power output between $0.15 \mu W$ and $4.81 \mu W$ is generated by the energy harvester. This shows that the dynamic behaviour of an energy harvester is different for various heart signals, so broad testing is needed.

Keywords: Energy Harvesting, Pacemaker, Heart Wall Motion, Human Heart Acceleration Signals

4.1. Introduction

Each year 600.000 new pacemakers are implemented [1]. The activity of the pacemaker necessary to combat the arrhythmia determines the battery life. Nowadays, a pacemaker runs on a conventional battery, that lasts for approximately 6-12 years, after which the pacemaker must be replaced [2]. This means a new pacemaker implantation is needed, accounting for approximately 25% of all pacemaker implantation procedures. These procedures come with complications, such as infections or bleeding [3], a new leadless pacemaker has also high costs, approximately \$10.000 [92]. A potential alternative to limit this, is the use of energy harvesting. Energy can be harvested by heat, wind or vibration, for example. Vibration energy harvesting refers to the method in which ambient vibrations are converted into electricity [4]. These vibrations can be anything in the environment, from machines that vibrate, the oscillations of a bridge and, in this case, the pulsation of the human heart wall. Due to these vibrations electricity is generated, to recharge the battery.

An energy harvester designed for a certain application, should be tested on the input signal of that application to accurately estimate the performance [6]. For instance, Neri et al. [7] experimented with a nonlinear energy harvester. It is found that the design for a maximum power output depends on the shape and intensity of the used input signal. The dynamical behaviour of the harvester differs per input signal. This means that an energy harvester intended for powering a pacemaker should be tested on a heart signal in order to obtain the matching dynamic behaviour.

However, the majority of the energy harvesters are tested on a harmonic signal. This is a good first step, but further research is needed, since the characteristics of a harmonic signal do not match the characteristics of the human heart signal. The human heart acceleration signal is a broadband signal, consisting of a varying amplitude at low frequencies. Briand et al. [4], Ansari and Karami [93] and Karami and Inman [48] used the heart velocity signal, obtained with an ultrasonic measurement by Kanai et al. [8], for the testing of their designed energy harvesters. It is questionable, however, whether the velocity found in the ultrasonic measurement is the velocity of one point that is continuously followed, since this is a 2D method. By Zurbuchen et al. [2] a heart signal measured with MRI

is used for testing. The temporal resolution of the MRI measurement was 40 fps, which is too low for obtaining a detailed heart signal. In addition, the ultrasonic signal and MRI signal were obtained from a single human. However, the heart signal can differ per person, since it also depends on, for instance, a subject's heart rate, age or health, the time of measuring and measurement location [8, 9]. Deterre [94] analysed that the magnitude of these variations can go up to 50%, this means that more input signals are needed. Then, Zurbuchen et al. [36] and Li et al. [3] performed tests on heart signals obtained from pig heart measurements and implanted the harvester in the right ventricle apex of a pig's heart. The tests performed with pig heart signals and on the pig hearts, are open-chest tests of which the signals could contain an overestimation. Furthermore, Deterre [94] used 3D measurements performed on pig hearts and 1D acceleration data of the right atrium of humans, to obtain the heart acceleration signals. Deterre et al. [39] and Vysotskyi et al. [50] used these obtained signals for the testing of energy harvesters. The signals found are a combination of pig heart measurements with human signals. These signals used, however, are obtained from the atrium. A leadless pacemaker is fixated in the apical septal region, which is close the apex. This can give a wrong signal amplitude, since the heart moves from the base to the apex. This means that there is little movement at the bottom of the heart, relative to the top. The tests performed on the heart signals give information of the behaviour of the energy harvester on the needed operation signal, but the signals used have their drawbacks. More heartbeat signal are needed to verify the energy harvesters performance for different input conditions, such that it could be widely used in pacemakers.

The aim of this research is to develop a human heart signal generator, where the signals contain the required information that is needed for the testing of energy harvesters. With this generator multiple heart signals can be generated that approximate a human heart wall acceleration signal. The database of heartbeat signals is expanded, helping the researchers with the verification of the performance of the energy harvester in a realistic manner. The generated heart signals are demonstrated with the use of an electrodynamic shaker to analyse the power output of an energy harvester on different input heart signals.

First, in *background*, the technical requirements of an energy harvester intended for powering a pacemaker are discussed, followed by an overview of current human heart measurement options. In *methods* the measurement methods of the heart motion sources used for the generator are discussed. Furthermore, the heart signal characteristics are analysed from the heart motion sources. These characteristics are processed in the heart signal generator, of which the working principle is explained. This followed by a short description of the energy harvester used for the demonstration and the experimental test setup used. Then, in *results*, the results of the heart signal generator and the experiment are shown. The final sections are the *discussion*, discussing the results, followed by a *conclusion* on the research.

4.2. Background

First, the *Technical Requirements of an Energy Harvester* intended for powering a pacemaker are discussed, followed by an overview of current *Human Heart Measurement Methods* used in the hospital.

4.2.1. Technical Requirements of an Energy Harvester

An energy harvester for a pacemaker should meet several technical requirements. First of all, when analysing the power usage of a Micra leadless pacemaker, a pacemaker directly placed in the right ventricle, the power usage for 100% inhibition is $1.2 \mu W$ and $1.95 \mu W$ for 100% stimulation per heart cycle [34]. This is an average power output that the energy harvester should meet every heart cycle. Second, the total volume of the Micra leadless pacemaker is 1 cm^3 , where the battery is approximately 60% of the volume. Taking into account that a spare battery is needed, the maximum volume of the harvester is determined at 0.3 cm^3 [95, 96]. Third, a Micra leadless pacemaker weigh 1.75 g . For not impeding with the heart rhythm, the energy harvester should not weight more than 1-2% of the heart mass, which is approximately 3-6 g [97]. Resulting in that the energy harvester should have a weight of 1 g at max. Zurbuchen et al. [98] concluded that when a heavier weight is attached on the heart wall, the heart needs more force to move and thus the acceleration amplitude increases. In the hospital a resistance of the heart motion is also seen due to a pacemaker. However, when visually analysing

the heart motion obtained with ultrasound measurements, no difference can be observed between the motion of the heart wall with a lead attached from a lead pacemaker or the Micra leadless pacemaker fixated in the heart wall (E.R. Holman, personal communication, December 21, 2020). Finally, another important requirement is that the harvester should operate on a heart signal, with a varying frequency and amplitude. The contribution of this paper is to facilitate the signals for the validation of this last requirement.

4.2.2. Human Heart Measurement Methods

The human heart wall motion can be measured via a CT-scan, MRI, Tissue Doppler Imaging (TDI) and Speckle Tracking Echocardiography (STE). In Table B.1 a comparison of the four measurements methods is made for five important specifications: the source of measuring, the temporal resolution, the spatial resolution, the dimensions and the usability. In this table it can be seen that the preference for measurement method lies with STE and TDI. The usability and availability of the measurement methods in the hospital are important to take into account for the method decision. The CT-scan and MRI are less available and more difficult to perform than STE and TDI. Furthermore, the temporal resolution of a CT-scan and MRI is low. The temporal resolution and spatial resolution are important to obtain a representative and accurate motion signal of the heart wall without aliasing, resulting in a preference for STE and TDI. When comparing STE and TDI, STE measurements can obtain a signal consisting of multiple consecutive heart cycles, instead of 1-2 heart cycles with TDI. Furthermore, TDI measurement have an angle-dependency and measurements are only possible in one direction [99]. More comparison details can be found in Appendix B. The STE measurements are one of the three heart signal sources used for the analysis in this research.

Table 4.1: Comparison of the different human heart measurement methods for five specifications [100–102].

	CT-Scan	MRI	TDI	STE
Source	X-Ray	Magnetic Field	Echo	Echo
Temporal Resolution	14 fps	50 fps	100 fps	70 fps
Spatial Resolution	0.5-0.625 mm	1-2 mm	0.5-2 mm	0.5-2 mm
Dimensions	Three	Three	One	Three*
Usability	In Machine	In Machine	Bedside	Bedside

* At an approximation of the same location

4.3. Methods

The three *Measurement* methods, that measure the heart signals sources used in this research, are discussed. The signals are analysed, resulting in *Heart Signals Characteristics*. These heart signal characteristics are processed in the *Heart Signal Generator*, of which the generated signals are used in an *Experiment* with the use of an electrodynamic shaker.

4.3.1. Measurements

Besides human ultrasound measurements obtained via *Speckle Tracking Echocardiography*, are also *Pig Heart Wall Motion* measurements obtained with an accelerometer used. Furthermore, *Human Chest Motion* measurements with an accelerometer attached on the chest located near the apex are analysed.

Speckle Tracking Echocardiography

Speckle Tracking Echocardiography (STE) measurements are performed at the Leiden University Medical Center (LUMC), the Netherlands, on nine patients (4 woman/5 man, age 20-79) with normal hearts. A VIVID E95 (GE Healthcare) with a 2.5 MHz transducer is used and the data is analysed offline in EchoPAC. The patients held their breath in order to prevent influence from respiratory motion and the drift compensation mode was turned on. The mean spatial resolution is 0.25 mm per pixel and the mean temporal resolution is 62 fps. The longitudinal direction is measured in the four chamber view

and the circumferential and radial directions are measured in the apical short axis view, giving an approximation of the same apical septal location analysed in the four chamber view, Figure 4.1a. For the longitudinal and radial direction the displacement (mm) is obtained and for the circumferential direction the motion is obtained in the rotation angle (degrees). In order to process the rotation angle, the radius of the heart in the apical view is determined in EchoPAC, to calculate the tangential velocity. In EchoPAC each heartbeat had to be analysed separately and was pasted one after the other for further analysis. The derivative of the displacement signals is taken to obtain a velocity signal, Figure 4.1b. Here an average velocity signal can be seen with the IVV-peak and s-wave, the contraction of the heart, and the e-wave and a-wave, the relaxation of the heart.

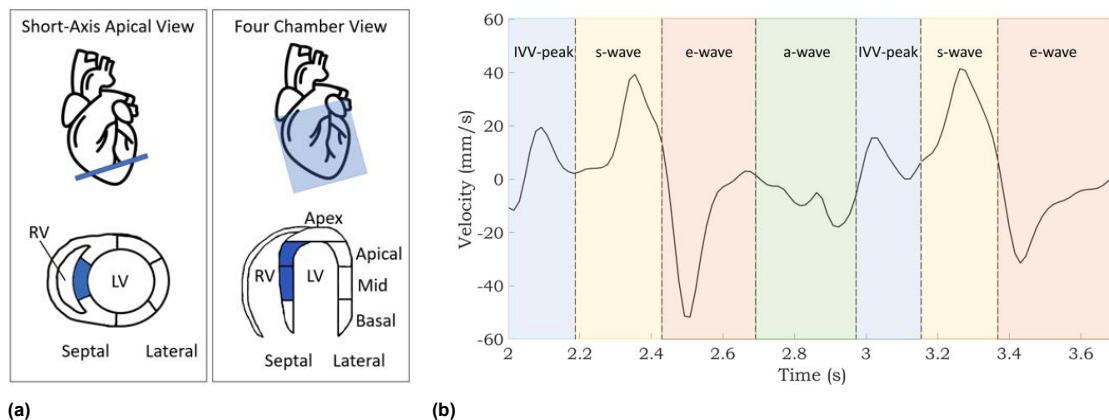


Figure 4.1: Human ultrasound measurements. **(a)** The short-axis apical view and four chamber view, used for the STE measurement in order to obtain the radial, circumferential and longitudinal axis, respectively. The blue part are the placement location of a leadless pacemaker. LV is the left ventricle and RV is the right ventricle. Also the heart regions, Apex, Apical, Mid, Basal, Septal and Lateral are labeled in the figure. **(b)** An example of a longitudinal velocity signal from a patient. The IVV-peak, s-wave, e-wave and a-wave are shown, the parts that make up a heart cycle.

Pig Heart Wall Motion

A second source are heart acceleration signals measured with an accelerometer attached on five pig hearts, performed in [103]. The accelerometer used is a 3D accelerometer (KXM52-1040, Kionix, Inc., NY, USA) with a dimension of $5 \times 5 \times 2$ mm and a sampling frequency of 500 Hz. One accelerometer is placed in the left ventricle apical region and the second one is placed in a basal lateral region. During the measurements the chest was left open and the pigs were placed in dorsal supine position (lying on their back).

Human Chest Motion

A third source used are measurements performed with an accelerometer attached on the human chest. The accelerometer used for this experiment is also a 3D accelerometer (356A32, PCB, NY, USA) with a dimension of $11.4 \times 11.4 \times 11.4$ mm and a sampling frequency of 2048 Hz. Measurements are performed on three men (age 23-28) with normal hearts during rest and exercise. The accelerometer is attached on the chest at the location of the apex of the heart. During the measurements the test persons were also lying in the dorsal supine position and the breath was held.

4.3.2. Heart Signal Characteristics

The heart signal sources are analysed and the found heart characteristics are discussed. These characteristics are categorized in *Trajectory*, discussing the course of the heart signal, followed by *Scaling*, where it is explained how the pig heart signals are scaled to a human heart amplitude. Finally, the *Influence of Heart Rate* on the amplitude is discussed.

Trajectory

The open-chest pig heart acceleration signals contain the longitudinal, radial and circumferential direction, measured in five pig hearts. Figure 4.2a shows an example of the longitudinal direction of one of the five acceleration signals. Every heart cycle consist of first a contraction peak, followed by a relaxation peak. When analysing the five different acceleration heart signals, there are differences in the details of these peaks. They differ, for instance, in duration, amplitude and number of oscillations per peak. The contraction and relaxation peaks will be used as the building block for the heart signal generator, since the signals are obtained with a high sampling frequency and the accelerometer was attached directly on the heart wall. Because of this high sampling frequency the shape of the signal represents the acceleration accurately. Analysing acceleration signals found in literature, the same shape can be observed for dogs, sheep, pigs and humans [104–107]. Furthermore, in the signals obtained from the measurement with the accelerometer attached on the human chest, the same trajectories are observed. A detailed analysis can be found in Appendix D. It should be kept in mind, however, that these signals are measured epicardial instead of endocardial. The placement location of a leadless pacemaker is endocardial. It is known that the heart wall motion is different when comparing epicardial and endocardial [24]. When analysing the acceleration signals from Eggen et al. [108], where the accelerations are obtained with an accelerometer placed in a leadless pacemaker, fixated in the heart of a sheep. It is observed that the same shape is seen in the contraction and relaxation. Because of this observation, it is stated that the pig signals can be used as a first step to obtain an approximation of human heart acceleration signals. However, more details are needed.

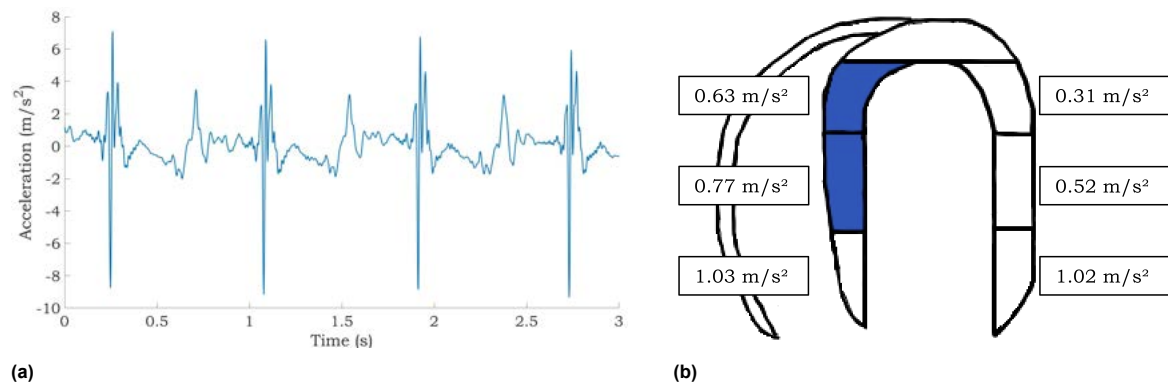


Figure 4.2: Two heart signals. **(a)** An example of an acceleration signal measured at the heart wall of the pig with an accelerometer in the longitudinal direction. **(b)** The left heart ventricle with the mean acceleration values measured with ultrasound from nine patients at the different regions.

Scaling

Comparing open and closed heart measurements, an overestimation of 100% is observed in open-chest measurements [109]. Furthermore, the gravity component gives also an overestimation in the acceleration signals [110]. This can not be compensated, since the rotation angles of the accelerometer are unknown. To compensate for the overestimation the STE measurements are used to determine the scaling factor. The temporal resolution and spatial resolution of the STE measurements are too low to obtain a detailed acceleration signal. The STE data must be differentiated twice and due low resolution, these details are not visible in the differentiated signals and the signal-to-noise ratio is rather low. However, a scaling factor to scale the pig acceleration signals in order to mimic a more realistic human heart acceleration signal can be obtained from the data. The mean accelerations for the different heart regions in the left ventricle are shown in Figure 4.2b. A higher acceleration is seen for the basal regions and the acceleration decreases when analysing the mid and apical region. The peak acceleration for the heart signal generator is randomly chosen out of a range of accelerations determined from the STE measurements. It is chosen to vary the acceleration with a range between 0.26 – $1.82 m/s^2$. This because of several reasons. First of all, the heartbeat signals differ per person, including the amplitude of the acceleration and velocity. In order to include this human factor a range is used. Second, the placement location of a leadless pacemaker differs per surgery. The fixation location depends on the patient

and circumstances during surgery. Finally, the range is applied because of the ambiguous acceleration and velocity values found in literature [111–117] and in this research when comparing STE and Tissue Doppler measurements. Due to the range, any inaccuracies of the measurement method used in this study are covered when scaling the heart signal generator signals. The details of this analysis can be found in Appendix C.

Influence of Heart Rate

For an increasing heart rate, the heart has a positively increasing acceleration amplitude. This was also observed in the chest motion lab measurements, where the acceleration amplitude was greater during exercise than in rest. To process this in the heart signal generator, the research of Roche et al. [118], Cifra et al. [119] and Nguyen et al. [120] are used. Here a linear increase for the contraction and relaxation velocity and an exponential increase for the contraction acceleration is observed. It is assumed that the relaxation acceleration has also an exponential increase. For the determination of the slope, two tangents are used, one between 70-100 bpm and one between 100-180 bpm, shown in Table 4.2. Since the relaxation velocity has a steeper increase, the tangents of the relaxation are estimated larger. Pauliks et al. [121] showed that for a lower heart region the difference between the acceleration values for a heart rate in rest and a heart rate in exercise are smaller than for a higher heart region. So, the tangents found have been reduced in order to avoid an overestimation, since a leadless pacemaker is placed in a low region. Besides the amplitude, the duration of a heart cycle is also influenced by the heart rate. In percentage, the duration of the relaxation decreases for an increasing heart rate, while the percentage of the contraction increases for an increasing heart rate. This means, that for a heart in rest, the duration of the relaxation is larger than the duration of the contraction. For an increasing heart rate, however, the relaxation time decreases more than the contraction time of the total heart cycle [122, 123]. This influence is incorporated in the heart signal generator.

Table 4.2: The slope numbers of the tangents to the graphs of the exponential growth of the heart acceleration due to the rise of the heart rate. The slope numbers are shown for the contraction and relaxation.

	HR <70 bpm	70 bpm <HR <100 bpm	HR >100 bpm
Contraction	0	0.014	0.054
Relaxation	0	0.017	0.060

4.3.3. Heart Signal Generator

The input for the heart signal generator is a chosen heart rate and the number of desired heart cycles. The output of the generator is a one-dimensional acceleration signal, approximating the human heart acceleration signal in the longitudinal direction. The energy harvester can harvest energy in one direction and in the apical domain the longitudinal direction has the highest velocity and acceleration. The heart signal generator uses the pig signals as building blocks, where a simulated time response of the dynamic model of the contraction and relaxation peaks is obtained. The dynamic systems are obtained from a transfer function estimation. This estimation is found from an input vector and the original measurement data using a nonlinear least-squares search method. The dynamic systems are loaded into the generator. Every run a new input vector is generated for both the contraction and relaxation, varying in impulse locations and peak heights, causing a different simulated time response. The fact that every person has a different heartbeat is imitated. More details are explained in Appendix F. The obtained simulated time response of the contraction and relaxation parts are scaled according to the acceleration values determined from the STE measurements. Every run a random value is selected from the range with a little variation for each heart cycle. This is added to mimic the human factor in the signal, and the influence of the heart rate is applied. The parts between the contraction and relaxation are a sum of cosine and sine with varying amplitudes and frequencies. When analysing the pig heart acceleration signals these parts have a low acceleration around zero that will not affect the movement of the energy harvester and therefore the amount of power generated.

4.3.4. Experiment

The signals generated with the heart signal generator are used in an experiment in the lab. The *Energy Harvester Device* and the *Measurement Setup* used are discussed.

Energy Harvesting Device

The energy harvester used during the experiments is an electromagnetic energy harvester consisting of a stack of eight moving magnets and a static coil, Figure 4.3b. On both ends of the moving magnets, repulsive magnets are placed in 3D printed end caps, resulting in a nonlinear spring. The tube is made of transparent PVC and ferrofluid is added around the magnets. The energy harvester has a total length of 70 mm and a diameter of 16 mm. The moving magnets have a total mass of 12.47 g. Further details of this energy harvester can be found in Appendix G.1.

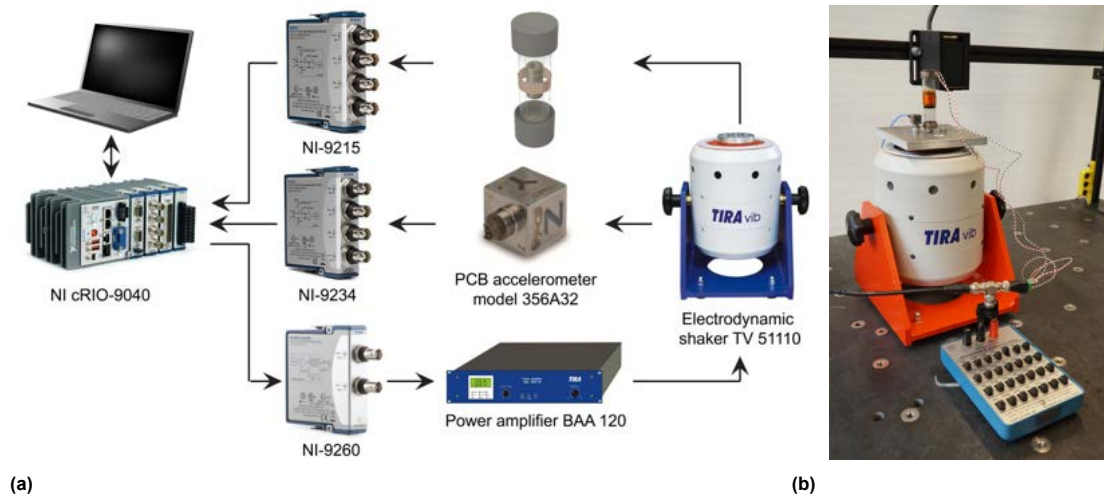


Figure 4.3: The experimental setup. (a) A schematic overview of the measurement setup used during the experiments. (b) The energy harvester attached on the shaker.

Measurement Setup

The performance of the vibration energy harvester on the human heart signal is experimentally validated on an electrodynamic vibration exciter. Figure 4.3a schematically depicts the various components in the setup, where the NI cRIO-9040 with the depicted modules act as an actuator, data sampler and controller. The actuation signal is sent to the amplifier and successively to the shaker. On top of the shaker, a PCB accelerometer is attached next to the energy harvester. During the experiments the acceleration signal was measured simultaneously with the harvester's output voltage over a 100 Ω resistance.

In order to excite the desired human heartbeat on the shaker, a feedforward controller was used. A system identification as described by Martini [124] was performed in order to determine the shaker's transfer function. Based on the shaker's transfer function, a feedforward controller was designed as described by Della Flora and Gründling [125]. Successively, the controller was implemented on the cRIO, where the desired heartbeat signal from the heart signal generator is adjusted before being sent to the shaker.

Heart signals generated with the heart signal generator are used as input signal for experiments to analyse the power output and efficiency of the energy harvester on different heart signals. The heart signals are generated for a heart rate of 120-200 bpm in steps of 20 bpm. High heart rates are chosen, otherwise no magnet motion was obtained, this results in no power generation to compare. The efficiency is calculated by dividing the measured power output of the energy harvester by the power present in the input signal, which is obtained in Equation 4.1. Where a is the acceleration, m is the mass of the moving mid magnet and T is the measurement period of the signal.

$$P_{in} = \frac{\int a^2 dx}{T} \cdot m \quad (4.1)$$

4.4. Results

4.4.1. Heart Signal Generator

In Figure 4.4, three examples of acceleration signals obtained with the heart signal generator can be observed, with the corresponding velocity signals. The first two signals are both generated for a heart rate of 70 bpm, the third signal is generated for a heart rate of 130 bpm.

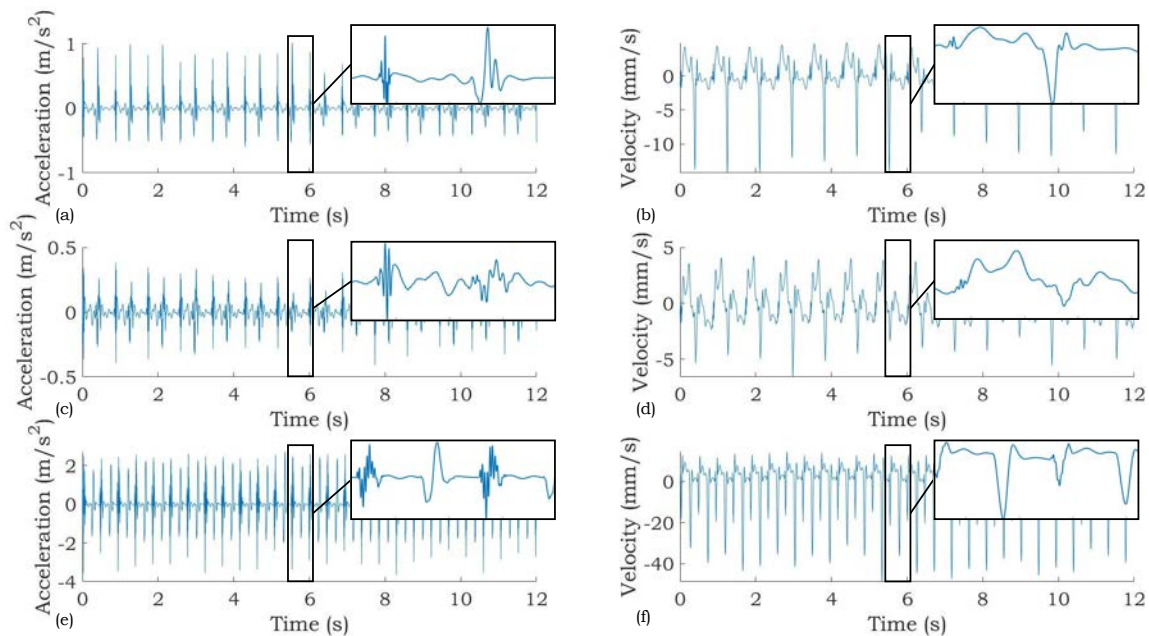


Figure 4.4: Three examples of signals generated by the heart signal generator for a heart rate of 70 bpm and 130 bpm. **(a,b)** The acceleration and velocity profile of a heart signal of 70 bpm. **(c,d)** The second acceleration and velocity profile of a heart signal of 70 bpm. **(e,f)** The acceleration and velocity profile of a heart signal of 130 bpm.

4.4.2. Experiment

The acceleration signal, velocity signal and the corresponding power output of 160 bpm and 200 bpm can be observed in Figure 4.5. The average power output and the corresponding efficiency of the signals with a heart rate of 120-200 bpm, in steps of 20 bpm, are shown in Figure 4.6a and Figure 4.6b.

4.5. Discussion

4.5.1. Heart Signal Generator

Comparing the two 70 bpm signals, it can be seen that details in the peaks are different and the velocity signals have differences, but in both velocity signals the IVV-peak, s-wave, e-wave and a-wave can be detected. When comparing the 70 bpm signals to the 130 bpm signal, differences can be seen in the peak height and duration of the heart cycles. It is validated that the heart rate indeed has a linear influence on the velocities and an exponential influence on the acceleration. The heart signal generator generates different heart signals, in order to mimic the fact that everyone has a different heartbeat. The information provided by the measurements is brought together in the generator, in order to mimic a human heart acceleration signal within the possibilities. The results of the three heart sources are combined in order to obtain an accurate and detailed heart signal, in which the disadvantages of one method are compensated by the advantages of another method.

Heart signals that have been used for testing so far, are a heart signal obtained by an ultrasonic

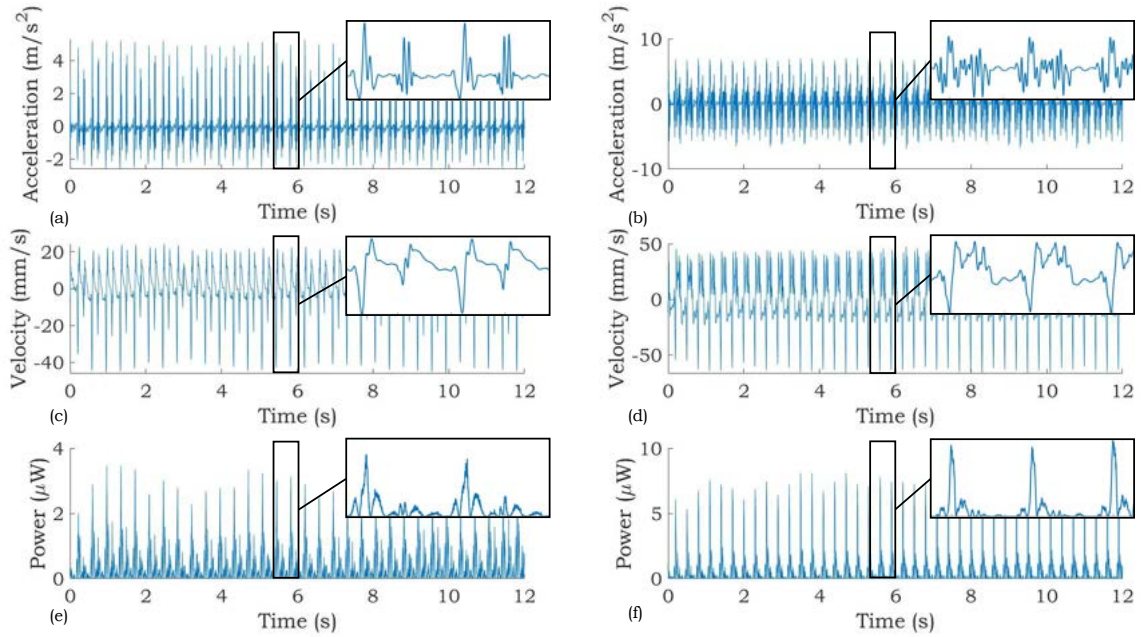


Figure 4.5: Two examples of signals generated by the heart signal generator for a heart rate of 160 bpm and 200 bpm and used for the experiment. (a,c,e) 160 bpm heart rate acceleration and velocity profile with the power generated by the energy harvester. (b,d,f) 200 bpm heart rate acceleration and velocity profile with the power generated by the energy harvester.

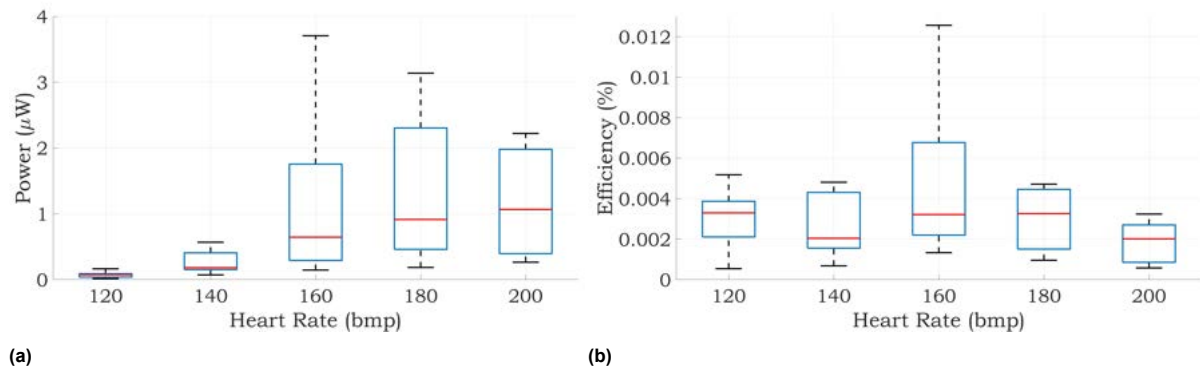


Figure 4.6: The experiment results. (a) The boxplot for the mean power measured for the ten heart signals generated per heart rate. (b) The boxplot for the efficiency calculated for the for ten heart signals generated per heart rate.

measurement and a MRI measurement [2, 8] or acceleration signals obtained from pig measurements [3, 36]. It is questionable whether the measurement methods used gave a correct signal of the heart wall accelerations. The ultrasonic measurement is 2D and MRI has a low temporal resolution. A measurement of a single person is not representative for the population and it is known that pig heart acceleration signals contain an overestimation. This heart signal generator takes these drawbacks into account by means of combining detailed pig heart signals with human ultrasound measurements. The pig heart accelerometer measurements ensure that one point is continuously followed with a good resolution, but the ultrasound measurements add the human factor in the generator signal. Another contribution of this generator is that multiple, varying heart signals can be generated, without the need of difficult and against ethical requirements, heart measurements. Varying heart signals, for different heart rates can be generated quickly, which makes it easier to validate whether an energy harvester can generate sufficient power in order to power pacemakers. In this generator human heart signals measured in the apical septal and mid septal region, are used to scale the pig heart signals in order to prevent an overestimation in the testing signals. Due to this scaling with amplitudes measured in the apical septal region, the fixation location of a leadless pacemaker is taken into account.

4.5.2. Experiment

Analysing the power output in Figure 4.5, a higher power output is generated for the relaxation part of the heart signal. This can be explained by the fact that the surface underneath the acceleration signal, and thus the velocity, of the relaxation part is larger than the contraction part, giving a larger motion to the energy harvester. This is not always true, as everyone has a different heartbeat. As shown in Figure 4.6a and Figure 4.6b for different acceleration signals, generated for the same heart rate, the energy harvester has a varying power output and efficiency. For example, when analysing the measurements performed for signals generated at a heart rate of 160 bpm, a mean power output between $0.15 \mu W$ and $4.81 \mu W$ is measured and an efficiency between 0.0013-0.013% is calculated. Analysing the mean power output and efficiency for the measurements performed at other heart rates, spread power and efficiency values are also observed. When analysing the mean power for 120 bpm, the variance is lower. This can be explained by the fact that this energy harvester has little motion for the low acceleration in the 120 bpm signals, this means that little power is generated. The efficiency calculated with Equation 4.1 can be compared with the efficiencies of other harvesters, as it is dependent on the mass. Figures of merit designed to compare various energy harvester designs, as for example from Blad and Tolou [126], can not be used, because this requires a harmonic input signal, which a heart signal is not. In addition to the varying power output and efficiency, it was expected that for a higher heart rate the power output would increase due to more power in the input signal. In Figure 4.6b it can be observed that this is true when analysing the median of the mean power for the ten signals generated for an increasing heart rate. For different heart signals generated by the heart signal generator this energy harvester has varying power outputs and efficiencies, showing that the dynamic behaviour of the energy harvester changes for different signals. This observation shows the importance of the testing of energy harvesters on multiple heart input signals.

The average power output of this energy harvester is too low in order to charge the battery of a leadless pacemaker since, for 100% inhibition a leadless pacemaker uses $1.2 \mu W$ and $1.95 \mu W$ for 100% stimulation per heart cycle [34]. This energy harvester is not specially designed for this input signal. When performing a frequency-sweep with an acceleration of 1 g, at 12.5 Hz an average peak power output of $13.44 mW$ is measured, with a calculated efficiency of 2.16%. When optimizing the design of an energy harvester for the intended input signal, the efficiency can be increased, increasing the power output. Blad and Tolou [126] analysed different types of energy harvesters and their efficiencies are calculated. It is observed that for the same types of energy harvesters diverse efficiencies are found and that large profits can be made by optimizing the design. Further advice for energy harvester designs intended for pacemakers are harvesters that can generate power at a heart rate in rest and without moving magnets, since this is not desired inside a human body for safety and potential medical investigations. The final orientation of the energy harvester design depends on the positioning of the leadless pacemaker, which is different for each person during surgery. In a non-optimal position the energy harvester should generate still enough power in order to recharge the battery of the pacemaker.

4.5.3. Recommendations

When comparing the velocity signals generated with the heart signal generator the s-wave amplitude is relatively low to what is seen in both literature and the STE measurements from the LUMC of the mid septal and apical septal regions. The heart has different motions for different heart locations. When analysing the location of the accelerometer placed during the pig heart measurements, the location of this sensor is between the apical septal region and the apex. This could explain the fact that the generated velocity signals have more similarities with this location than with the motion at the mid septal segment. Scaling the signals with the peak amplitudes from the apical septal and mid septal segments does not change the shape of the velocity signal. It is advised to measure the pig heart wall motion at different locations from the apex to the mid apical heart wall location, in order to further improve the heart signal generator.

Another challenge is to test the energy harvester under real life circumstances that can influence the reliability of the energy harvester and the amount of energy harvested. Examples of circumstances to take into account are the heart wall rotation, and the fact that the leadless pacemaker is fixated in soft tissue, making the leadless pacemaker move in a wobbly motion. The next step, after testing the

energy harvester on a shaker, is to test the energy harvester with the heart wall environment imitated. The energy harvester should be fixated in a material just as soft as the heart wall and after that be tested on the three dimensional motion.

4.6. Conclusion

In this work a heart signal generator has been developed in order to improve the test facilities for the testing of energy harvesters intended for powering pacemakers. Three different sources of heart signals are combined in order to obtain a new source of heart signals, an approximation of reality, which can be used for the testing of energy harvesters. The detailed contraction and relaxation parts of pig heart wall acceleration signals are used as building blocks. The pig acceleration signals are scaled according to the acceleration values found in the human STE measurements performed at the LUMC. The influence of the heart rate is added in the generator. Humans have a positive force-frequency relation between the heart rate and the signal amplitude for the contraction and relaxation, observed in the human chest motion measurements. The heart signal generator can be seen as a first step towards the testing of energy harvesters on human acceleration signals on a broad range of human heart wall acceleration signals, where the dynamic behaviour on the different signals can be investigated. Heart signals generated by the heart signal generator at a heart rate of 120-200 bpm, with steps of 20 bpm, are used for experiments in the lab on an energy harvester. Analysing the measurements performed for signals generated at a heart rate of 160 bpm, the average power output measured for the different signals is varying between $0.15 \mu W$ and $4.81 \mu W$, with an efficiency varying between 0.0013-0.013%. The varying power output and efficiency show that the energy harvester has a different dynamic behaviour on the different heart signals. Testing energy harvesters intended for powering pacemakers on various heart signals is needed, since it is important that the energy harvester generates sufficient power to charge the battery on all human heart signals. This heart signal generator is a first step to validate if energy harvesters have a sufficient performance on different heart signals.

4.7. Acknowledgments

We would like to thank R.W.C. Scherptong (Interventional Cardiologist) and E.R. Holman (Imaging Department) of the Heart Lung Center Leiden, Leiden University Medical Center for for sharing their medical knowledge and support with the Speckle Tracking Echocardiography measurements. Furthermore, we would like to thank E. W. Remme and A. Wajdan from the Oslo University Hospital for sharing the five pig heart acceleration signals and the discussions about the signals.

5

Discussion, Conclusion and Recommendations

This chapter contains a reflection on the project progress. The successes, learning points and unsuccessful attempts are described, followed by the project conclusions and recommendations for further research.

5.1. Project Reflection Discussion

The project reflection is divided in successes and unsuccessful attempts, where the successes are divided in project successes and personal successes.

One of the major project successes is the collaboration with the cardiologist from the LUMC. It is known that doctors are busy and have little spare time. Despite this, fortunately, the doctors were able to free up enough time to assist me during this project. This has taken the project to the next level, because the aim of this project is to improve the testing facilities, requiring human heart signals. The cardiologists have the medical knowledge. The fact that this thesis combines the knowledge from the cardiologist with the technical knowledge is a success. Eventually, the goal of powering a pacemaker with an energy harvester is that this technical devices will be used in hospitals. Therefore it is important that during the research process, those who eventually use the device are involved in the design process. This project is a small step in the long way to implementation. Via this thesis a first attempt is made by testing the energy harvesters on the signal sources for which they are intended. To bring the project of powering a pacemaker by an energy harvester to a successful end, an interaction of several specialisms is required.

The personal successes gained during this project, besides going through a project from start to finish and being your own project manager, can be described as three life lessons. Three lessons that I have learned and I will take with me in my further career. The first lesson is that you have to do what you like, stay true to yourself and what makes you unique. That may sound like a hackneyed life lesson, but during this project I started with a different project direction. In this first project the skills that make me unique were not used. On the contrary, I thought they would not be useful. But nothing could be further from the truth. After the project switch the progress went more smoothly and pleasure was taken from the research. A second life lesson is: 'focus'. While working on a project, the actual goal of the project can sometimes be forgotten and is it easy to drift away. During the process is it important to sometimes take a step back and analyse the whole project. What am I working on? Does this help achieving my goal? What are the steps needed to achieve the goal? It is important that these questions are asked from time to time. The third life lesson is there is a solution for everything. During the project there were challenges. Ultimately, by making certain choices, asking for advice or getting a good night's sleep something that seemed impossible at first, turned out to be possible. The work could be continued and this has led to a beautiful end result.

Besides the successes, there were also unsuccessful attempts in the project that were not used for the end result. The first unsuccessful attempt is the electromagnetic energy harvester design, which not used during the experiments (Appendix G). Designing an energy harvester with the lowest possible stiffness has taken some time. The focus of this thesis was obtaining the heart signals in order to improve the testing facilities and not designing an energy harvester that can operate on these heart signals, which is a research by itself. It would have been better to take a step back and see what was available in the lab, than start with designing immediately. However, it was educational to go through the design process and to simulate the dynamic behaviour of the energy harvester.

A second unsuccessful attempt is the investigation of how to imitate the heart wall material. It was thought that in order to improve the testing facilities the heart environment could be better imitated when the energy harvester was pinned in a soft tissue. It turned out that the investigation of how to imitate the soft tissue of the heart wall is more difficult than expected (Appendix H). The silicone tests were a good first approach, however, more detailed research is needed to obtain the finer details of the heart wall tissue. Furthermore, despite the fact that the aim of this thesis is to improve the testing facilities the mimicking of soft heart wall tissue with silicone was out of the scope of this research.

5.2. Conclusion

In this work, first, the current status of energy harvesters for powering a pacemaker has been discussed. Different heart measurement techniques are discussed, varying from ultrasound measurements to measurements with an accelerometer. All the methods have their advantages and disadvantages. Obtaining detailed heart signals from humans is a challenge, because of the measurement

methods available in the hospital and the ethical rules. In the literature research, it is concluded that when an energy harvester is designed for a certain application, the harvester should be tested on the input signal of that certain application. The dynamical behaviour of the harvester could be different for different input signals, which could influence the performance of the harvester. The majority of the found nonlinear MEMS low frequency energy harvesters are tested on a harmonic signal. This is a good first step, but further research is needed. Several researchers tested energy harvesters on a heartbeat signal of a single human, which gives information of the behaviour of the energy harvester on the operation signal. However, the heart signal differs per person. Different signals have varying characteristics, that can influence the dynamic behaviour of the harvester. To verify the performance of energy harvesters under multiple heart conditions, more diverse heartbeat signals are needed. In order to fulfill this demand, a heart signal generator has been designed in order to improve the test facilities for the testing of energy harvesters intended for powering pacemakers. Three different sources of heart signals are combined in order to obtain a new source of heart signals, an approximation of reality, which can be used for testing. The detailed contraction and relaxation parts of pig heart wall acceleration signals are used as building blocks. The pig acceleration signals are scaled according to the acceleration values found in the human STE measurements performed at the LUMC. The influence of the heart rate is added in the generator. Humans have a positive force-frequency relation between the heart rate and signal amplitude, which was observed in human chest motion measurements. The results of the three heart sources are combined in order to obtain an accurate and detailed heart signal, in which the disadvantages of one method are compensated by the advantages of another method. The heart signal generator is a first step towards the testing of energy harvesters on human acceleration signals on a broad range of human heart wall acceleration signals, where the dynamic behaviour on the different signals can be investigated. Heart signals generated by the heart signal generator at a heart rate of 120-200 bpm, with steps of 20 bpm, are used for experiments in the lab on an energy harvester. Analysing the measurements performed for signals generated at a heart rate of 160 bpm, the average power output measured for the different signals is varying between $0.15 \mu W$ and $4.81 \mu W$, with an efficiency varying between 0.0013-0.013%. The varying power output and efficiency show that the energy harvester has a different dynamic behaviour on the different heart signals. Testing energy harvesters intended for powering pacemakers on various heart signals is needed, since it is important that the energy harvester generates sufficient power to charge the battery on all human heart signals. This heart signal generator is a first step to validate if energy harvesters have a sufficient performance on different heart signals.

5.3. Recommendations

Although this thesis is a first step towards the testing of energy harvesters intended for powering pacemakers, further research is needed in order to further improve the facilities.

First, the heart has different motions for different heart locations. When analysing the location of the accelerometer placed during the pig heart measurements, the location of this sensor is between apical septal region and the apex. This could explain the fact that the generated velocity signals have more similarities with this location than with the motion at the mid septal segment. Scaling the signals with the peak amplitudes from the apical septal and mid septal segments does not change the shape of the velocity signal. It is advised to measure the pig heart wall motion at different locations from the apex to the mid apical heart wall location, in order to further improve the heart signal generator.

Second, in the heart signal generator only the heart rate has an influence on the heart signal. However, it is known that the a heartbeat is influenced by multiple factors, as for instance someone's age or health. Further research is needed in order to process these differences in the heart signal generator.

Third, testing an energy harvester on a human heart wall signal is a first step of imitating the heart environment. However, it is known that the heart motion is not one-dimensional, but has translations and rotations in three dimensions. In addition, it is known that the heart wall is a soft tissue, influenced by connective tissue formation, scar tissue and the blood flow in the heart ventricle. The influence of this phenomena on the leadless pacemaker motion and thus the energy harvester motion or reliability is unknown. It should be investigated if these phenomena should be included in the testing of an energy

harvester intended for powering pacemaker or not.

Finally, the energy harvester design must be further improved. Besides the fact that the harvester must generate enough power, at least $1.95 \mu W$, it must be small, approximately 0.3 cm^3 , light weighted, must not contain toxic material, and be made of a material that lasts for a lifetime. The energy harvester should also operate on different heart signals with varying heart rates. It must be investigated if one general energy harvester can be designed for the entire population. A few energy harvesters, where the right energy harvester is allocated on the base of signal characteristics. Or that a personal energy harvester should be designed. A person's heart rate also differs with time. It is different when someone is asleep, in rest, or during exercise. The energy harvester should generate sufficient power on all the different moments.

Acknowledgement

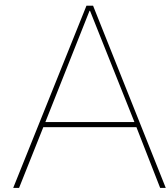
I would like to thank a lot of people, not only for the support during my thesis, but for the long way I have had to come during my entire studies.

First of all, I would like to thank my friends. With whom I studied together, worked together on various projects and with whom I did completely the opposite: forgetting about studying and just focusing on having fun. Thank you Flip, 8op8, TB friends, WB friends, Hudito friends, and Bennebroek friends.

Second, I would like to thank my supervisors Nima and Thijs. Who understood very well what I am about. I would like to thank Nima for alerting me every time I strayed from the main topic and steer me in the right direction. I would like to thank Thijs for all the sparring and the amount of time you put into my project. I never felt like I could not come to you with a question. Here I also thank the Stroomgraiers, for all the discussions on Mondays and the help in the lab.

Then, I would like to thank my family. For immediately jumping in the line of fire when needed. For the always warm and loyal support. All the times that I could catch up on sleep in Bennebroek and enjoy a freshly squeezed orange juice. Here I specially want to name my mother and my cousins Mar and Anne.

Last, but certainly not least, I would like to thank my boyfriend Paul, for all the mental support and help. For always cheering me up and having my back. Thank you for always being there for me.



Leadless Pacemaker Requirements

In medicine there are different classes for medicines and medical devices, specifying the test procedure. A class III device is a device that supports or sustains human life [127]. A leadless pacemaker is a class III device, meaning that Premarket Approval Application (PMA) is required, consisting of assurance of safety and effectiveness, bench-animal-human tests and clinical studies [128]. This appendix discusses the technical requirements and questions that arise using energy harvesting for a leadless pacemaker. The testing conditions required in order to meet the PMA specifications are also discussed.

A.1. Technical Requirements

The use of energy harvesting for powering a pacemaker raises several technical questions and should meet challenging requirements, such as mass, volume and power requirements. These requirements and more are discussed.

- **Mass** A leadless pacemaker is attached in the heart wall of the right ventricle, making that the leadless pacemaker and the heart interact. This interaction should not impede the heart rhythm, in other words the pacemaker should not be too heavy. For not impeding the heart rhythm, the energy harvester should not weigh more than 1-2% of the heart mass, which is approximately 3-6 g [97]. A leadless pacemaker weigh 1.75 g (Micra MC1VR01, Medtronic) [34], meaning that the energy harvester ideally, in order not to disturb the heart rhythm, should have a weight of 1 g at max.
- **Volume** The total volume of the Micra leadless pacemaker is 1 cm³ [34]. In Figure A.1 a cross section of the Micra leadless pacemaker is shown. In this figure, the battery of the pacemaker is also visible. This takes approximately 60% of the total volume. With an energy harvester in the mechanism, a battery is still needed in order to store any extra generated power by the harvester. This means that in order to fit the originally needed electronics, a battery and the energy harvester in the leadless pacemaker, the energy harvester should have a volume of 0.3 cm³ [95, 96]. The leadless pacemaker has an outer diameter of 6.7 mm, so the area in which the energy harvester should operate is not flat but cylindrical. In order to match this form, the energy harvester should also be three-dimensional [93].
- **Power** The third requirement discussed is the power. For this, the Micra leadless pacemaker is taken into account again. For the Micra leadless pacemaker the power consumption during 100% inhibition is approximately 0.8 μA, giving, with 1.5 V, a power usage of approximately 1.2 μW. The power consumption of the pacemaker during 100% stimulation is 1.3 μA, giving, with 1.5 V, a power usage of 1.95 μW [34]. This is the power usage with a full battery at VVIR-mode at 60 bpm and a pulse width of 0.24 ms. So the power generated by an energy harvester should be 1.95 μW at minimum. When the pacemaker is not in stimulation mode, the remaining energy can be stored in the existing battery as a buffer. A calculation of the average power usage can be seen in Equation A.1, A.2, A.3. Where the average power usage is calculated for a leadless pacemaker pacing at 60 bpm, a pulse width of 0.24 ms, 1.5 V, 120 mAh and a resistance of 500 Ω. Leading to a battery life of 11.7 years (102492 hours) [34]. The average power usage is 1.7 μW.

$$hours = \frac{mAh}{Amps \cdot 1000} \quad (A.1)$$

$$Current = \frac{120mAh}{102492hours \cdot 1000} = 1.17 \cdot 10^{-6}A \quad (A.2)$$

$$Power = Voltage \cdot Current = 1.5V \cdot 1.17 \cdot 10^{-6}A = 1.7 \cdot 10^{-6}W = 1.7\mu W \quad (A.3)$$

- **Material** A leadless pacemaker is in contact with human tissue for a long time. The piezoelectric material, consisting of lead, used in most energy harvesters is toxic [4]. However, the energy harvester is located inside the leadless pacemaker. For the Micra leadless pacemaker that is a case made of titanium, a bio-compatible material [34]. So the toxic material does not make contact with the human tissue.
- **Material Failure** An important question to ask is if the material of which the energy harvester exist lasts long enough. Fatigue failure can occur in materials when the same motion is often repeated, which is the case for energy harvesting. For energy harvesting for powering a pacemaker the material experiences the same motion between 60-100 bpm, meaning 86.400-144.000 cycles per day. The material also undergoes high heart accelerations, of which no plasticity may arise [36]. In literature, piezoelectric energy harvesters are found that can experience one million cycles before deformation occurs. This leads to a decrease in the power output due to a change in

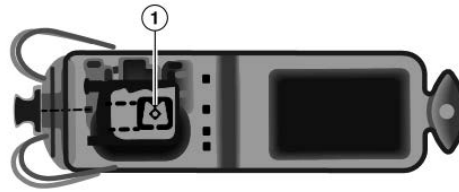


Figure A.1: X-ray image of the Micra leadless pacemaker showing the battery size. (1) is the x-ray identification. Figure obtained from [34].

the eigen frequency [129–131]. An energy harvester that can last for one million cycles, last for approximately 2-3 years on a heartbeat vibration. However, this depends on the bpm, the acceleration and on the energy harvesting design. In order to be able to draw conclusions, testing on the human heartbeat signal is needed. However, it can be said that further development of the piezoelectric material is needed in order to operate for a lifetime.

- **Heartbeat** Another important question is if the energy harvester can operate on a heartbeat. Does the heartbeat make the energy harvesting mechanism move, in other words is the acceleration of the contraction and relaxation sufficient to make the harvester vibrate? It is also important to investigate whether the other motions present in the heart contraction, for example the twisting of the heart, influences the harvester. Do gravity and the respiratory motion have an influence? For this the heartbeat signal should be used to test the energy harvester.

Besides the main requirements and questions mentioned above, there are a few side questions that should be taken into account. For instance: does the motion of the energy harvester in the pacemaker influence the force acting on the heart wall? A leadless pacemaker is attached to the heart wall with the usage of tines. Does the motion of the energy harvester influences how the tines are attached in the heart wall? Connective tissue grows around a leadless pacemaker. Does this influence the motion of the pacemaker, and thus the motion of the energy harvester inside the leadless pacemaker? Furthermore, is the quality of the battery good enough to keep up with the developments or will the battery eventually end up depleting faster (as with a smartphone for instance)? Should an extra sensing system be added to measure the battery fatigue?

A.2. Testing Requirements

Besides technical requirements, have medical devices also testing requirements in which, among other things, the technical requirements are tested. These testing requirements are specified by for instance the American Food and Drug Administration (FDA). As stated, a leadless pacemaker is a class III device so the testing is strict. The timeline for the testing can be seen in Figure A.2.

In Figure A.2, the first phase consist of invention and prototype building. This phase interacts with the second phase, which is the preclinical studies. The prototype is tested in the preclinical phase, redesigned if needed and is preclinically tested again. This preclinical phase includes bench testing, technical testing, computer simulations and animal studies. With computer simulations it can be modeled how the device should operate in the human body. During the bench testing and technical testing the performance and safety is measured. The accuracy and reliability of the elements used in the prototype are also tested. In these tests it is established that the designed device operates as it should. Finally, in the animal studies the efficacy is tested, whether the bio-compatibility and toxicology [132, 133]. Animal studies are performed to mimic the device operating in humans.

After the preclinical testing the next tests are in the clinical trials. First, the testing plan has to be approved during the regulatory and ethics review. There are four phases in the clinical trials, the first-in-human phase consists of 10-30 subjects, the traditional feasibility phase consists of 20-30 subjects, the pivotal phase consists of 100 subjects and the post market phase consists of 1000 subjects. In these phases again the efficacy, safety, effectiveness, device performance are tested, but now in humans.

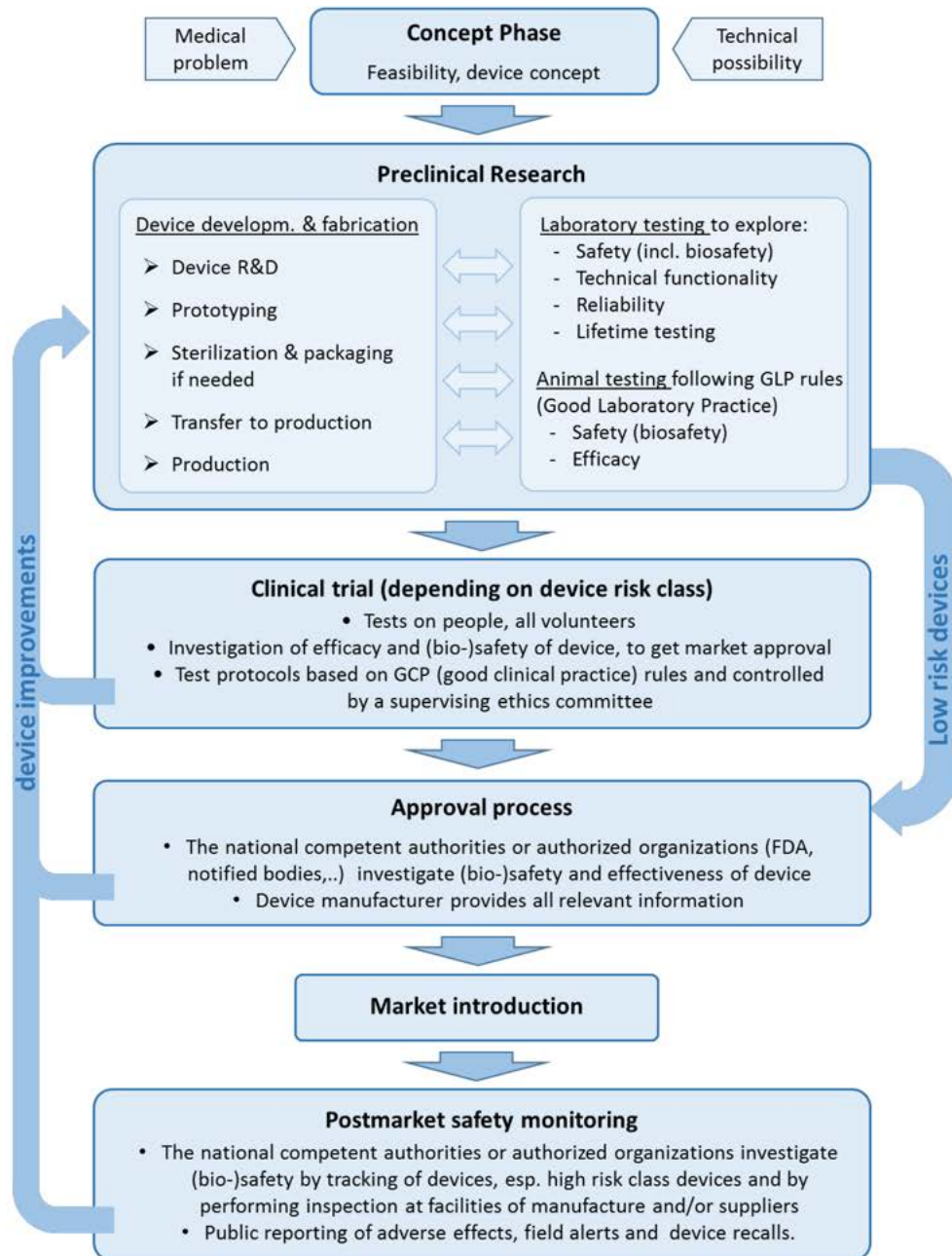
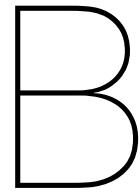


Figure A.2: An overview of the phases that a medical device should go through in order to be accepted at the market. Figure obtained from [133].

These testing requirements are specified for a pacemaker without an energy harvester. A pacemaker generating power with an energy harvester to recharge the battery requires more testing. Since, in such a pacemaker, it must sense the heart signal in order to obtain information if it should stimulate the heart and it should also operate on the heart signal in order to generate power. Tests must be performed to assess whether energy harvesters produce enough power to recharge the battery. The developments of energy harvesting for powering pacemakers are in the invention and prototyping phase. The challenge is to design an energy harvester that is small enough to fit into the leadless pacemaker, operate on a low frequency and to generate sufficient power. For an energy harvester, the power output depends on the signal where it operates on. The dynamic behaviour can vary per input signal. To validate if an energy harvester generates enough power, tests are needed on a human heart signal consisting of the acceleration and the frequency information of the signal. In literature, tests are performed on measured heartbeat signals (Chapter 3). Further bench testing is needed to validate the mechanical and electrical working principle of energy harvesters in pacemakers. For the validation, multiple human heart signals are needed as input, in order to guarantee a sufficient performance of an energy harvester on a broad scale. As can be read in Chapter 3, heart measurements are performed in order to obtain a signal with the needed input. However, in order to investigate if the dynamical behaviour of energy harvesters differs also per different heart signal more input signals are needed, particularly human heart signals (Chapter 3).



Heart Signal Measurement Method

This appendix elaborates on the decision for the heart signal measurement method. Four methods are highlighted, namely: Computer Tomography-Scan, Magnetic Resonance Imaging, Tissue Doppler Imaging and Speckle Tracking Echocardiography. The pros and cons of the methods are discussed, leading to a chosen method used in this research.

B.1. Heart Signal Requirements

A signal intended to test the performance of energy harvesters in the lab should contain the frequency and acceleration information of the specific ambient vibration. This means that for energy harvesters intended for powering pacemakers, the frequency and acceleration information of the heart wall vibration is also required. The heartbeat signal is a low frequency signal consisting of a varying acceleration and the heart rate in rest is between 60-100 bpm. In order to obtain an accurate signal of the heart wall acceleration, a temporal resolution of 100 frames per second (fps) is needed [134]. This is needed to prevent aliasing and to resolve all relevant events in the time-dependent parameters. To determine the spatial resolution required for the measurements Equation B.1 is used. Here the displacement of a sine wave is calculated for a specific acceleration a and frequency f . For instance, with an acceleration of 5 m/s^2 and a frequency of 22 Hz, the estimated displacement is 0.52 mm. This results in a spatial resolution with a pixel size of 0.50 mm as sufficient for capturing the displacement. The minimal needed pixel size during the measurements is specified at 0.50 mm. In the calculations it is shown that for an acceleration of 1 m/s^2 and a pixel size of 0.50 mm, the displacements can be captured until 10 Hz and for an acceleration of 10 m/s^2 a displacement can be seen until 30 Hz.

$$d = \frac{a}{(2\pi f)^2} \cdot 2 \quad (\text{B.1})$$

In previous research it is seen that the highest power in the signal is at the heart rate frequency, varying between 1-2 Hz for humans [39]. The power in the signal decreases for an increasing frequency. At a frequency of 20 Hz, the power in the signal is significantly lower than at the heart rate frequency. However, higher frequencies present in the signal are needed in order to obtain a representative signal to mimic the heart signal during the testing of energy harvesters. The displacement was calculated for accelerations varying from 1 m/s^2 to 10 m/s^2 . During this research, it must be critically examined whether this is indeed sufficient and if the signal contains enough frequency information in order to be representative. The apical region of the heart has a displacement of around 1-5 mm during the cardiac cycle [135]. This means that the estimated pixel size should be sufficient in order to capture the heart wall motion. According to the Nyquist theorem the pixel size should be at least the halve of the spatial resolution. In order to reduce noise, the pixel size should be smaller: the spatial resolution divided by three [136, 137]. This results also in a pixel size of approximately 0.50 mm.

The spatial resolution and temporal resolution depend on each other. Increasing the temporal resolution usually worsens the spatial resolution or vice versa [134]. The measured signal must be at least ten seconds long in order to analyse the frequency content in the signal. When the duration of the same signal is longer, the lower frequencies in the signal can be analysed.

B.2. Measurement Method

The functioning of the heart can be analysed in different ways. For instance, a first simple and fast analysis of the heart is via the heart sounds, this is done via a stethoscope [51]. Another method is an electrocardiography (ECG), showing the electrical activity of the heart. With these measurements heart arrhythmia can be seen. However, these methods do not provide the required heart information, the motion. Methods that can obtain heart images are discussed.

B.2.1. Computer Tomography-Scan

The first measurement method discussed to obtain heart images is the Computer Tomography-Scan (CT-scan). This method uses X-rays to produce images. X-ray beams are pointed at a patient and rotating around the body, the signals obtained are processed and computed in images, so called slices of a thickness of 1 to 10 mm [138]. Recently, new developments around CT-scans are made. They developed a CT system containing two tubes in a 90 degree geometry, this new development improve the temporal resolution of the CT-scan [139]. An example of a CT-Scan is shown in Figure B.1.

The CT-scan has a high spatial resolution, since the pixel size is between 0.5-0.625 mm, giving that a lot of detail can be seen in the images [100]. The reproducibility is also high and it has a fast acquisition. However, the temporal resolution is relatively low, since it has a frame rate of 14 fps

[101]. This low temporal resolution makes that the functional imaging of the heart can not be captured accurately. During a CT-scan, breath-holding is needed in order to compensate for the respiratory movement. Besides, it cannot be used bed sided and the ionizing radiation can cause harmful effects in living tissue. For the measurement decision the availability of the method in the hospital should also be taken into account, which of a CT-scan is low (E.R. Holman, personal communication, May 15, 2020). A comparable, but less risky method without the radiation is MRI. This method is discussed next.

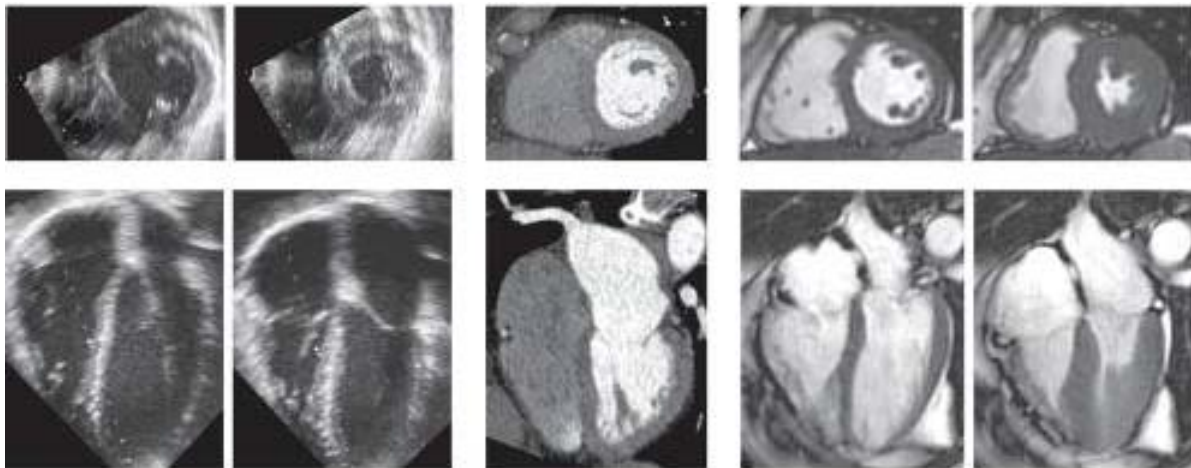


Figure B.1: Heart images obtained with three different measurement methods in the short-axis and long-axis views of the heart. At the left, ultrasound images are shown at two different moments in the heart cycle. In the middle, images obtained with a CT-scan are shown. At the right, heart images obtained by MRI are shown, during two moments in the heart cycle. The images are obtained from [101].

B.2.2. Magnetic Resonance Imaging

The second method for imaging is Magnetic Resonance Imaging (MRI). For measurements of the RV functions, MRI is referred to as the gold standard [2]. MRI uses the magnetic field naturally present in the body. This magnetic field is changed by electric coils, when switching of this radio frequency source a signal is emitted. With this signal the images are obtained [140]. With MRI 2-, 3- and 4-chamber views, so both the left and right side of the heart, can be obtained. An example of a CT-Scan is shown in Figure B.1.

The temporal resolution of MRI is higher than the CT-scan, it is 50 fps. However, the set temporal resolution depends on the heart rate [102]. In literature varying temporal resolution settings have been seen, varying between 20 fps and 50 fps. The spatial resolution associated with a temporal resolution of 50 fps, found in literature, is a pixel size of 2x2x8 mm [101]. According to other literature, however, MRI can have a spatial resolution of 1-2 mm [100]. As stated, the temporal and spatial resolution depend on each other. Lowering the spatial resolution, negatively influences the temporal resolution. The acquisition of MRI images depends on whether patients hold their breath or not. With breath-holding the acquisition time varies between the 5-8 s/slice, without breath-holding this increases up to 60 s/slice. For the measurement of the heart wall movements, in order to recharge the pacemaker's battery, it is interesting to measure the heart wall movement including a leadless pacemaker. However, on an image obtained with MRI distortion close to the metal can be seen [140]. Due to this the movement of the region of interest can not be specified. Furthermore, just as the CT-scan, the availability of the MRI-scan is poor and it has high costs. This should be taken into account for the measurement method decision [141].

B.2.3. Tissue Doppler Imaging

The third measurement method is Tissue Doppler Imaging (TDI). With TDI an echo is made using ultrasound, following a point of interest. An example of an image obtained via echo is shown in Figure B.1. It indicates the rate at which a specific point, the chosen point of interest, moves towards or away

from the transducer used for the measurements, see Figure B.2a [114]. The frequency shift between received ultrasound waves, reflected from the tissue to the transducer, indicate if the tissue moves towards the transducer or away. The resulting Doppler frequency, calculated with the phase change of the received waves, is used to obtain the tissue velocity [142]. TDI velocity can be obtained by pulsed Doppler, M-mode Doppler or two-dimensional colour Doppler. The difference between pulsed Doppler and colour Doppler is that in colour Doppler the mean velocity is measured, in contrast to the peak velocity measurements in pulsed Doppler [142]. In M-mode Doppler a chosen ultrasound line is followed and the velocities are analysed as a function of time [143, 144]. In order to obtain the heart wall movement in the colour Doppler mode, the echo is analysed by an algorithm that gives the displacement and the velocity signal of the heart wall [145].

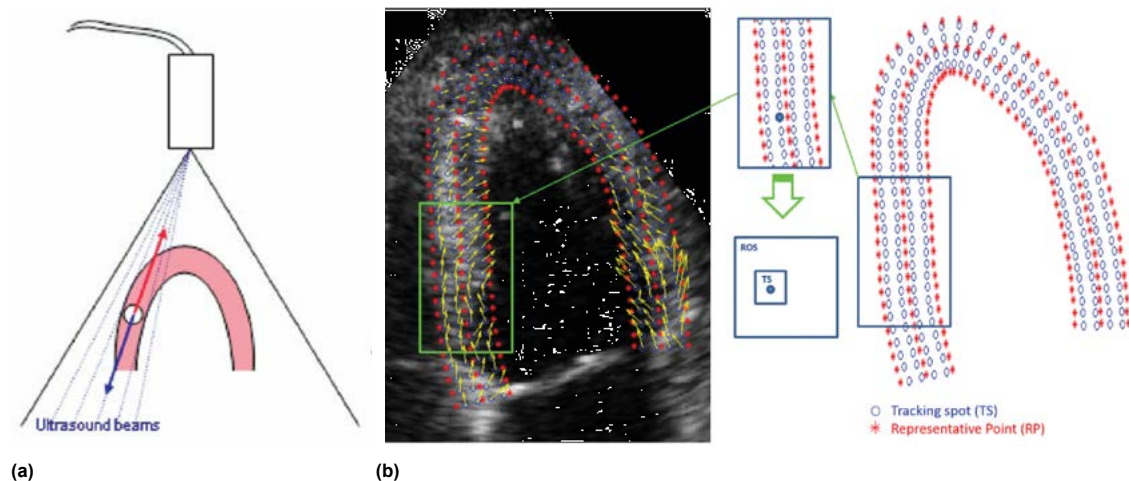


Figure B.2: The two ultrasound measurement methods. **(a)** The working principle of TDI obtained from [146]. Where the heart wall moves towards and away from the probe. **(b)** The working principle of STE. Where bright dots are obtained with two ultrasound waves and followed. The tracking of the displacement of the markers is also shown. The figure is obtained from [147].

In literature it is stated that TDI is a robust method for measurement of the myocardial contractile function and the relaxation [148]. An advantage is that with TDI global myocardial areas can be analysed, just as a detailed analysis of areas [145] and that it can be used bed sided. TDI has a high temporal resolution of 100 fps (E.R. Holman, personal communication, May 13, 2020) and the spatial resolution of TDI discussed in literature has a pixel size of 3x3 mm [149]. However, in other literature a spatial resolution of 0.5-2 mm is specified for echocardiography [100]. The frame rate for M-mode is the highest, it is lower for pulsed Doppler and the lowest for colour Doppler TDI [114]. A disadvantage of this method is that it is a 2D method, so the movement of the heart wall can only be analysed in plane and not out of plane. Furthermore, this method is angle dependent. This means that the ultrasonic beam must be perpendicular on the movement direction of the heart wall. When this angle exceeds 20 degrees, the calculation of the velocity may be underestimated by 6%. For an angle of 30 degrees this is an underestimation of 13% and for 45 degrees 29% [150]. The reproducibility differs per view, for the long axis it is better than for the short axis, however, it is also dependent on the observer experience [151]. Then, TDI is sensitive for cardiac translational motion and tethering, since it measures heart wall motion at a single point with a transducer outside the chest [114].

B.2.4. Speckle Tracking Echocardiography

The fourth and last method discussed is Speckle Tracking Echocardiography (STE). In this method echo's are also obtained using ultrasound. However, this method analyses the wall movement in a different manner than TDI. In STE, B-mode images are used. In B-mode images bright dots are generated by the reflecting of ultrasound beams, resulting in a speckle pattern. The speckles are generated randomly due to reflections, refraction and scattering of echo beams [152, 153]. These speckles are markers on a specific point on the heart wall. These speckles or a cluster of speckles are followed during the cardiac cycle, frame by frame by the software, Figure B.2b. Via this, the cardiac motion

is followed and the tissue velocity is estimated from the shift of the speckle between two successive frames. With STE, besides the longitudinal deformation, the radial and circumferential deformations can also be obtained [154].

STE is usually performed with a temporal resolution of approximately 70 fps. Furthermore, the spatial resolution lies between 1-2 mm for echocardiography [100, 102]. However, there is a trade-off between the temporal and spatial resolution. An increase in the temporal resolution increases the pixel size [134]. With STE, just as TDI, a global and detailed area of the heart wall can be analysed. In STE, however, this is without the angle dependency and the dependence on cardiac translational motion [141]. Additionally, STE is more robust and reproducible [154]. However, STE is also a 2D method, this means that only the in plane heart wall motion can be analysed and not the out of plane motion. Furthermore, STE requires a high image quality in order to follow the speckles [154]. Other limitations of STE are the detection of borders and the fact that the used software is a black box. This results in that it is not known what for influence the used filters have on the found data [154].

B.3. Method Decision

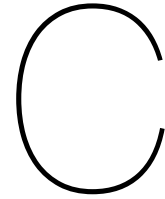
In Table B.1 a comparison of the four measurements methods for the most important requirements: the source of measuring, the temporal resolution, the spatial resolution and the usability is tabulated. In this table it can be observed that the preference for measurement method lies with STE and TDI, since these methods have more green marked requirements when compare this with the CT-scan and MRI. The usability and availability of the measurement methods in the hospital are important to take into account for the method decision. The CT-scan and MRI are less available and more difficult to perform than STE and TDI. Furthermore, the temporal resolution of the CT-scan and MRI is low. The temporal resolution and spatial resolution are important to measure a representative and accurate acceleration signal of the heart wall, without aliasing. This results in a preference for STE and TDI. These are the two methods that will be used for the heart wall measurements in this thesis.

Table B.1: Comparison of the different human heart measurement methods for five specifications.

	CT-Scan	MRI	TDI	STE
Source	X-Ray	Magnetic Field	Echo	Echo
Temporal Resolution	14 fps	50 fps	100 fps	70 fps
Spatial Resolution	0.5-0.625 mm	1-2 mm	0.5-2 mm	0.5-2 mm
Dimensions	Three	Three	One	Three*
Usability	In Machine	In Machine	Bedside	Bedside

* At an approximation of the same location

It must be kept in mind that all the discussed measurement methods have their drawbacks, including TDI and STE. TDI has an angle dependency, which can influence the found heart wall velocity. On the other hand, the temporal resolution of STE is lower than the needed resolution, which can result in that high-pitched velocity signals could be missed by this method. However, by van Dalen et al. [99] this dependence of the height of the temporal resolution was not found. They state that this could be explained by the algorithm used by STE, that uses temporal and spatial smoothing. The fact that both methods use an algorithm in order to obtain the velocity is another drawback, since these algorithms are a black box. Furthermore, both methods are 2D methods, so the out of plane velocity can not be measured. These drawbacks should be taken into account during the analysis of the found data. In order to verify the found data, the measurements are compared to those performed with an accelerometer on pigs heart. This will be elaborated in Appendix D. However, since both methods are based on echocardiography, both methods are used and are compared with each other. This comparison can be found in Appendix C.



STE and TDI Measurements

In this appendix the STE and TDI measurements are discussed. First, the measurement methods are explained in more detail, followed by how the data is processed. Both methods are compared to each other. Finally, it is discussed how the signals from the STE and TDI measurements are used later in this research for the characteristics analysis.

C.1. Measurement Method

Both the STE and TDI measurements are performed at the LUMC, the Netherlands. For these measurements a VIVID E95 from GE Healthcare with a 2.5 MHz transducer is used and the data is analysed offline in EchoPAC. The measurements are performed on nine patients for STE and on eight patients for TDI with normal hearts (4 woman/5 man, age 20-79). During the measurements the patients held their breath in order to prevent influence from respiratory motion. The drift compensation mode was turned on during the measurements. The TDI measurements are performed in the four chamber view. The STE measurements are performed in the four chamber view and in the short-axis apical view, Figure C.1. In this manner the motion of the heart can be analysed in the apical septal and mid apical regions.

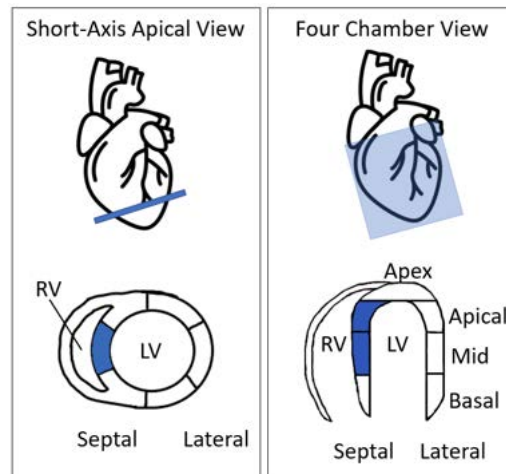
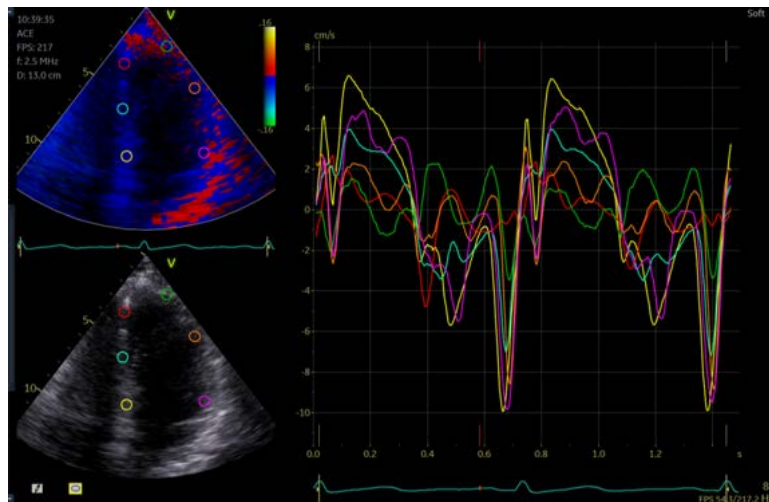


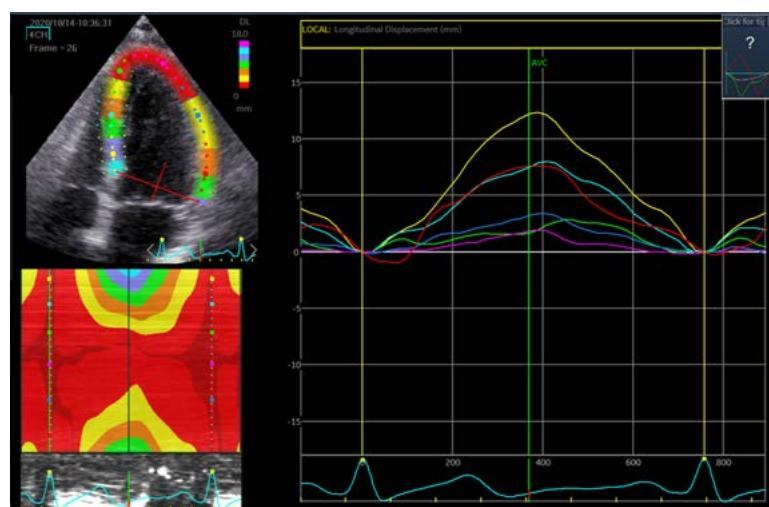
Figure C.1: The apical short-axis view and four chamber view used during the TDI and STE measurements. The blue segments represent the placement locations of a leadless pacemaker.

During the TDI measurements a signal of 1-2 heartbeats is obtained with colour Tissue Doppler in the longitudinal direction. The mean spatial resolution for the eight measurements was 0.24 mm per pixel and the mean temporal resolution 180 fps. The analysis of the velocity signal (cm/s) in EchoPAC is shown in Figure C.2a. Here blue and red heart images are seen, this is because the probe emits two ultrasound beams during TDI measurements. For the eight patients the left chamber is divided into six segments. From these six segments the heart wall velocity is obtained, see figure C.2a.

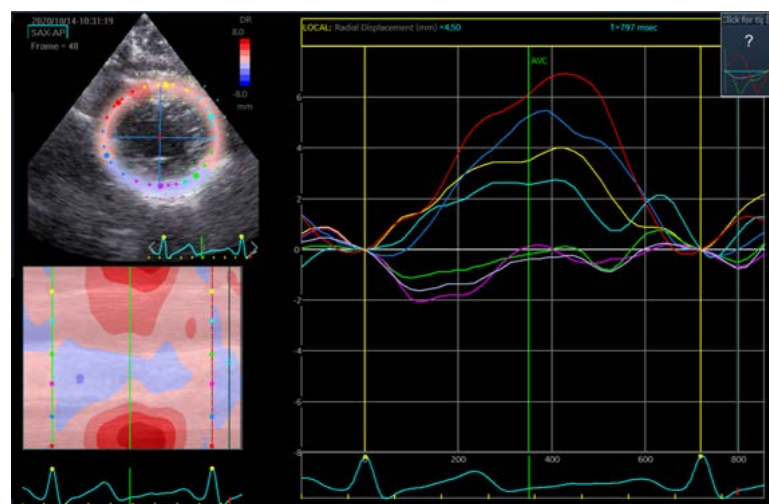
The signals obtained with STE contain several heart cycles in a row (varying from 8-12). The mean spatial resolution is 0.25 mm per pixel and the mean temporal resolution is 62 fps. With STE an approximation of the motion in all three directions can be measured. This means that the longitudinal direction is measured in the four chamber view. The STE analysis in EchoPAC can be seen in Figure C.2b. Here the displacement (mm) is analysed in the same six segments as analysed for TDI. In order to obtain the motion in the circumferential and radial direction, the heart motion is also measured in the short-axis view on apical height, giving an approximation of the same apical septal location analysed in the four chamber view. In Figure C.2c the analysis in EchoPAC is shown. For the radial direction the displacement (mm) is also obtained. However, for the circumferential direction the rotation angle (degrees) is obtained. In order to process the rotation angle, the radius of the heart in the apical view is also determined in EchoPAC. With this the tangential velocity can be calculated. For the analysis in EchoPAC the short-axis images are also divided into six segments. Two of these segments are located at the apical septal and apical lateral regions. Two locations that were also measured in the four chamber view, Figure C.1. In other words, the location of the pacemaker placement and the location of the sensor during measurements in pig hearts, which will be further elaborated in Appendix D. It should be kept in mind that these are an approximation of the same location as measured in the four chamber view. More will be explained about this later. For both STE analysis in EchoPAC, each heartbeat had to be analysed separately. The data extracted from EchoPAC was pasted one after the other before analysis in Matlab.



(a)



(b)



(c)

Figure C.2: TDI and STE analysis in EchoPAC. **(a)** Velocity signals obtained with TDI measurements during one heart cycle measured in the six segments. The signal colour corresponds to the measurement location marked in left ventricle in the four chamber view in the top left. **(b)** STE measurements performed in the four chamber view. The displacement signals are shown, where the colour corresponds to the segment location in the left ventricle in the top left. **(c)** STE measurements performed in the short-axis apical view. The rotation angles are shown, where the colour corresponds to the segment location in the short-axis in the top left.

C.2. Signal Processing

In this section, it is discussed how the human ultrasound data is processed in order to be usable. First, the filtering is discussed, followed by the discussion of obtaining the velocity from the STE measurements.

C.2.1. Filtering Pre-processing Stage

For both STE and TDI the heart wall velocity is obtained via an algorithm. This algorithm is a black box and it is hardly known what filters are used. In literature, some filters are mentioned and are discussed below. Because of the filtering in the pre-processing stage the signals are already smooth and no further filtering is needed. Furthermore, the ultrasound measurements are not influenced by gravity and in order to avoid signal disturbances due to respiratory motion the patients hold their breath during the measurements (E.R. Holman, personal communication, October 14, 2020)[17].

Tissue Doppler Imaging

TDI uses the Doppler technique to obtain the tissue velocity. Another known application using this technique is flow Doppler imaging. The difference between Tissue Doppler Imaging and Flow Doppler Imaging is shown in Figure C.3. Here, in the left figure the flow velocity is obtained. In order to obtain this velocity a high pass filter is used to filter out the high amplitude, the wall motion. In the right figure, to obtain the wall motion the high frequency blood flow is eliminated by gain adjustment [151]. The gain is decreased, resulting in that only the high amplitude of the wall motion is collected. Furthermore, mentioned in [155], filter settings are used to remove noise from the velocity signal and smooth the signal. They state that in this filtering function a low pass filter can be varied between 16 and 100 Hz.

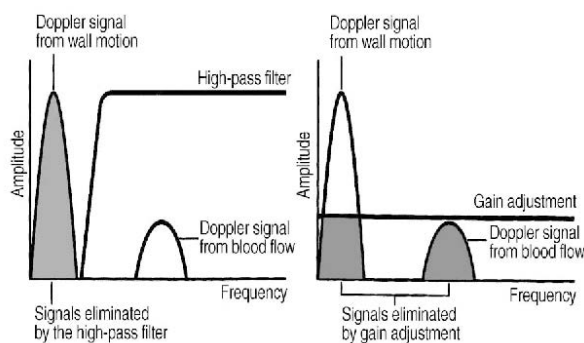


Figure C.3: Difference between Flow Doppler imaging and Tissue Doppler imaging. Figure obtained from [151].

In a study from Gunnes et al. [156] the influence of the temporal filter settings on the Doppler velocity is analysed. They found that the temporal filter behaves as a low pass filter and when the filtering is overdone it counteracts the effect of a high frame rate. This is also analysed by Manouras et al. [157] where they, besides the influence of the temporal filtering, also analysed the influence of the gain setting. Here it is found that the settings of both can alter the velocity measurements and an interaction between the temporal filtering and the frame rate is seen. For temporal filtering, decreasing velocity values are found for an increasing filter width. For an increase in gain saturation level the found velocities are also altered, in this case higher velocity values are found. These two studies show that it is important to keep in mind that the filter settings during the measurements can influence the found velocities, giving a distorted meaning of the reality.

Speckle Tracking Echocardiography

The STE signals found in this research are displacement signals and further processing to velocity is performed without the algorithm used in the software. However, in literature what is found about pre-processing filtering is for velocity signals obtained by the software. The information found of filters used in STE is scarce and different per research. It is stated that a Savitzky-Golay filter is used by Negoita et al. [158]. This filter smooths the velocity signal in order to remove noise. Here it is explained that for obtaining the s-wave (peak systolic wave) a third polynomial degree and eleven points are used, in

contrast to the e-wave and a-wave (the peak early and late diastolic waves) where a fifth polynomial degree and seven points are used. This is because the e-wave and a-wave are faster time-occurring [158]. In this research the influence of the high frame rate is also shown. At a lower frame rate, the velocities of the faster waves, and thus shorter waves (e-wave and a-wave), are inadequately tracked and underestimated. At a very low frame rate, this is the case for all the three waves. On the other hand, in [159] it is stated that the software uses a three-point median filter and a three-point Gaussian filter (of weight 0.25, 0.5, and 0.25). These filters are used to ensure a sufficient pixel resolution, spatial coherence, in order to follow the speckles during the cardiac cycle. Then, it is explained by Reant et al. [160] that the software tracks a large number of small regions and averages the motions with spline interpolation before obtaining the regional motion. STE and TDI signals are analysed by Jasaityte and D'Hooge [17]. Here it is concluded that the signals found with STE looks less noisy than the TDI signals, but that this is because of differences in smoothing. The fact that there is less noise in STE measurements is an illusion. The filtering in the algorithms should be kept in mind during this research, since this could influence the values found. However, it is unknown how much this influences the found velocity signals.

C.2.2. Velocity

With the TDI analysis in EchoPAC the velocity signals are already calculated within the algorithm. However, from the STE measurements a displacement signal is obtained of which the velocity signals must be calculated. For the velocity calculation the derivative is taken by dividing the displacement signal by the time signal. However, the temporal resolution of STE measurements is low, meaning that it can affect the shape of the signals when they are differentiated or integrated. Because of the low temporal resolution it can occur that specific moments in time are not captured, resulting in that they are not visible in the velocity graph. An example of a velocity graph obtained from the derivative of the STE displacement is shown in Figure C.4. First, the isovolumic contraction velocity (IVV) peak can be observed. The IVV-peak represents the early systole or contraction, resulting in pressure build-up in the ventricles. The second peak seen in the signal is the s-wave. The s-wave represents the blood ejection into the body. The s-wave is followed by the e-wave, the early diastole or relaxation. The last phase of the heart cycle is the a-wave, or the late diastole. This is represented by the fifth peak in the signal. After the a-wave, the cycles starts over with the early systole and the IVV-peak can be observed in the signal.

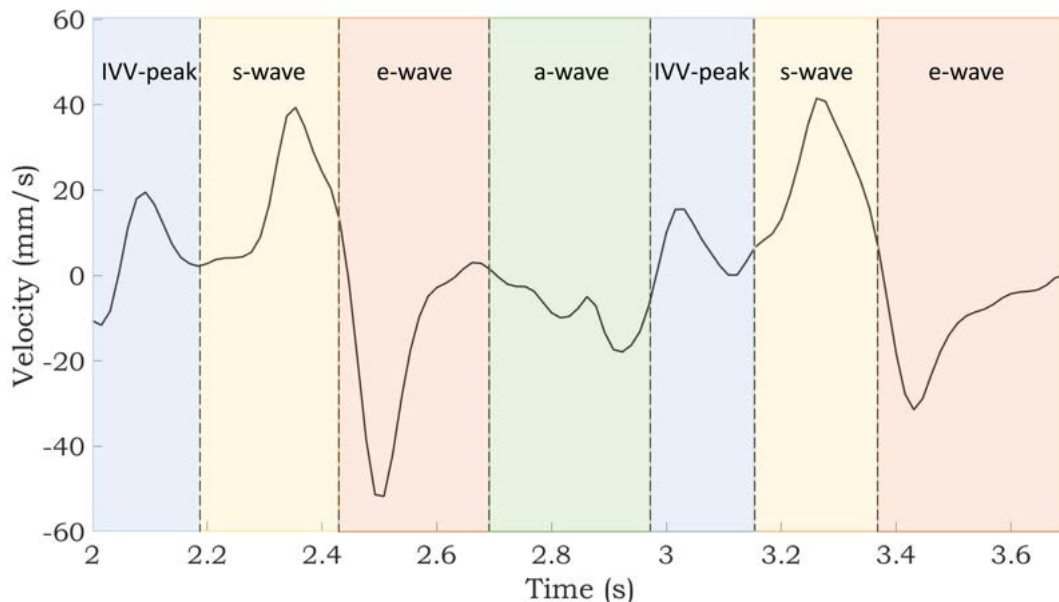


Figure C.4: Example of a velocity graph obtained with the derivation of the displacement signal found with STE.

For the circumferential direction, STE gives the rotation angle in degrees. The tangential velocity is calculated using Equation C.1. Where ω is the angular velocity in radian/s and r is the radius of the heart. The radius is obtained from the heart images in EchoPAC.

$$V_t = r \cdot \omega \quad (\text{C.1})$$

C.3. Comparison STE and TDI Measurements

This section compares the velocity signals obtained with STE and TDI measurements in order to validate if velocity signals found with STE could be used for further analysis in this research. It was thought to compare the two measurement methods statistically. Despite that the measurements with both methods are performed on the same patients, are there differences in the signals. For instance the signal length, the STE measurements are signals of 10 seconds, while the signals of the TDI are only 1-2 seconds, existing of one heart cycle. For statistical comparison it is desired to obtain the mean of the peak values, but for the TDI measurements no average can be calculated, since there are only 1-2 heart cycles. This does not result into representative velocity values and therefore not a representative comparison. Furthermore, the two methods are not measured at the same moment. With the TDI measurement only representing one heart cycle, this can also be misleading. Therefore, it is chosen to compare the signals visually and with information found in literature.

C.3.1. Visual

First, the two obtained velocity signals are visually compared. An example of the velocity signals obtained with TDI and STE can be observed in Figure C.5, from one patient measured at approximately the same location of the heart wall. In both signals the same heart cycle characteristics can be seen, the IVV-peak, s-wave, e-wave and a-wave. However, small differences can be seen in the amplitude height. In this particular example, the two measured velocities are almost similar. However, when analysing the velocity signals obtained with STE and TDI measured from other patients, the signals do not match as well as this example in Figure C.5. The same trajectory is seen, the IVV-peak, s-wave, e-wave and a-wave, but the amplitude and timing is different. This could be explained by the fact that the two velocity signals are not measured simultaneously. This results in differences because of natural differences, in the heart rate or a slightly different measurement position. The differences in the peak height are analysed and compared with other research found in literature in the next section.

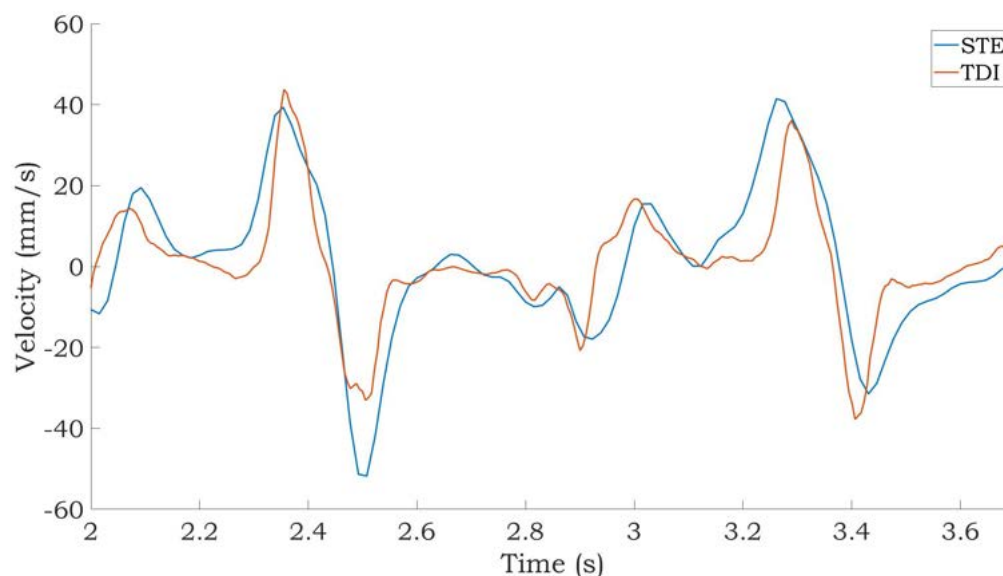


Figure C.5: The velocity signals measured with STE and TDI of the same patient at the same location.

In Figure C.6 the STE measurements of the six segments in the longitudinal direction are shown from one patient. Here it can be observed that the velocity is higher for the basal segments and is decreasing for the mid and apical segments. This is in line with the fact that the heart moves from base to the apex. In the figure differences in the six velocity trajectories are also seen, what can be

explained by the fact that the heart has a different motion for the different regions of the heart.

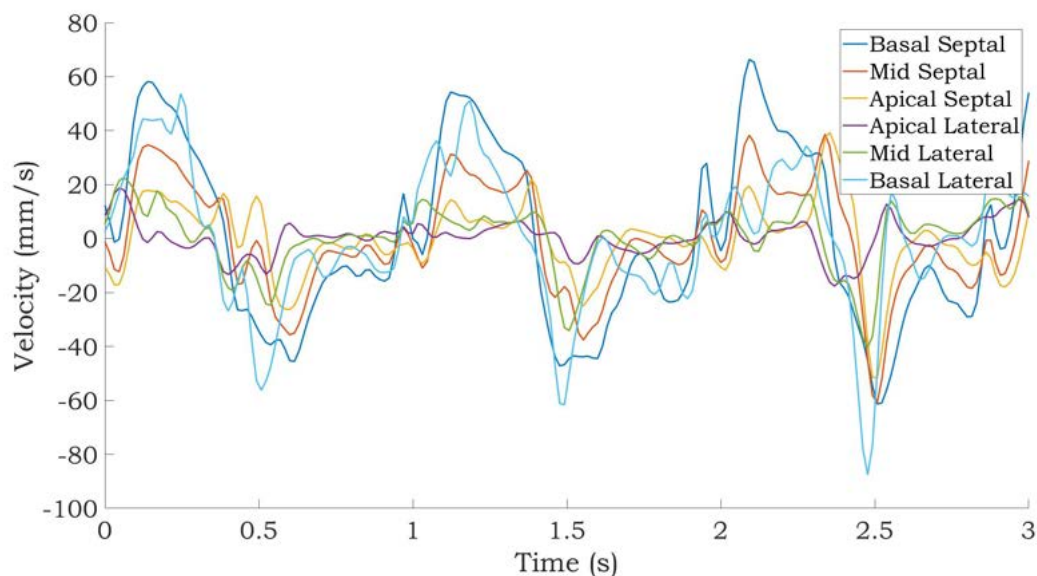


Figure C.6: The velocity signals of the six segments from one patient. Differences in amplitude and trajectories can be observed.

C.3.2. Literature

In literature several studies are found that compare STE and TDI measurements. For example, Wess et al. [161] analysed the heart wall velocity from 100 healthy dogs. They found that STE and TDI have small differences for velocities measured at the interventricular septal wall. In [99] no significant differences were found and there were good correlations between the velocities. However, they also changed the angle of insonation of the probe and observed that the velocities measured with TDI are lower than STE. They state that TDI is angle-dependent and that an increase of the angle of the position of the probe, underestimates the velocity values of the heart wall. With the motion parallel to the ultrasound beam, both STE and TDI measure accurately the velocities. The angle-dependency and the underestimation of the velocity was also observed in [99], here they state that in the clinical setting the velocity signals measured by STE had higher values when comparing these values to TDI, probably due to the angle dependency.

The mean velocity values measured with STE and TDI in this research are visualized in Table C.1. Here it can be observed that for most locations the STE velocities are higher than the TDI velocities. It should be kept in mind that the TDI velocities are only measured for 1-2 heart cycles, so the mean velocity is not entirely representative and can give a wrong impression, since for a person the heartbeat differs per heart cycle. However, for some velocities the difference is from such a proportion, that it is thought that the angle-dependency has its influence in these measurements. Only the lab technician was present during the measurements, so this cannot be validated. Furthermore, all the ultrasound measurements are performed by a different lab technician, which can also influence the observations.

In literature it is stated that in order to capture the heart motion, a temporal resolution of 100 fps or higher is needed [134]. The average temporal resolution used for TDI in this research is 180 fps. In [99] the influence of the frame rate of the STE measurements on the velocity values found is investigated. The hypothesis is that because of the low temporal resolution of STE, high-pitched velocity signals are missed. They found that increasing the frames per second did not influence the result of the velocity values measured. It is stated that this could be due to the speckle tracking algorithm, where some temporal or spatial smoothing and a larger sample size is used, compared to TDI [99]. In [158] the underestimation of the velocity is also investigated by increasing the frames per second. Here they found that the s-wave can be accurately measured with a frame rate of 20 fps. The e-wave and a-wave need at least a frame rate of 40 fps, but a higher frame rate is desired [158]. They measure also for

Table C.1: Comparison of TDI and STE velocity measurements from the IVV-peak, s-wave, e-wave and a-wave.

	TDI				STE			
	IVV-peak (mm/s)	s-wave (mm/s)	e-wave (mm/s)	a-wave (mm/s)	IVV-peak (mm/s)	s-wave (mm/s)	e-wave (mm/s)	a-wave (mm/s)
Basal Septal	23.77	57.52	-71.46	-59.88	21.23	86.87	-81.69	-60.68
Mid Septal	16.80	40.64	-56.59	-37.55	19.13	59.84	-65.16	-38.38
Apical Septal	13.84	23.54	-27.48	-11.92	18.87	38.74	-43.02	-25.12
Apical Lateral	14.62	17.39	-16.05	-14.24	9.79	15.03	-22.06	-7.91
Mid Lateral	27.31	23.13	-28.64	-25.30	17.92	22.87	-33.47	-12.73
Basal Lateral	33.12	44.19	-69.62	-39.99	38.12	58.86	-77.30	-31.06

different heart rates and conclude that no higher frame rate is needed for higher heart rates.

When comparing the STE values measured in this study with STE values found in other research is it seen that different velocity values are found, but of the same order of magnitude. The measured velocity values show that from basal to apical measurements the velocity values decrease, what is also observed in this research [113–117]. However, the values found in literature can not be compared one-on-one with the values found in this research, since details of the measurement methods are unknown. The measurements can differ in the location of the segment selection, the STE analysis algorithm and the location of the ultrasound probe.

For the further research in this report the STE velocity signals are used. The ultrasound measurements are not influenced by gravity or other overestimation components. When comparing TDI and STE measurements the values found with STE are higher than with TDI, which could be because of the angle-dependence of TDI. Furthermore, the STE signals are ten seconds and thus contain more information than the TDI measurement, which are 1-2 seconds. The STE measurements obtain an approximation of a three dimensional signal, where the circumferential and radial axes are measured in the apical short-axis view. This is an approximation, since the height of the cross section, the apical region, is determined by the lab technician. However, it should be kept in mind that the STE measurements are not very accurate, because a different unit is measured than used for the energy harvesting testing. The STE measurement provide a displacement signal, while velocity and acceleration signals are desired. Furthermore, the algorithm to obtain the displacement signal is a black box. It is not precisely known how the signals are processed. The velocity signals are used to obtain the acceleration amplitude for a human heart. Because of the known drawbacks, the found acceleration values are only used in order to scale the obtained acceleration signals from the heart signal generator, Appendix F.

C.4. Acceleration Amplitude

For the testing of energy harvesters an acceleration signal is needed as input for the experimental setup. The ultrasound measurements discussed are used to obtain the height of the peak amplitude for the acceleration signals for humans. This amplitude is used to scale the acceleration signals, which are discussed in Appendix D. The isovolumic myocardial acceleration (IVA) is a parameter used in literature to assess the systolic function of both ventricles. The IVA is calculated by dividing the peak myocardial velocity (IVV) by the acceleration time (AT) [162]. Besides the IVA, the relaxation acceleration is also determined, in order to obtain the complete heart cycle overview. Despite the fact that the frame rate is high enough to measure the velocity amplitude, is it too low to obtain a detailed and precise acceleration signal. The trajectory as analysed in Appendix D is not observed. As a result, the acceleration trajectory can not be used for the testing of an energy harvester and only the amplitude is used for scaling.

In Figure C.7 the mean IVA for the ten heart cycles of the nine patients can be observed. A higher acceleration is seen for the basal regions and the acceleration decreases when analysing the mid and apical region. When comparing the found acceleration values with the acceleration measurements

thoroughly analysed in [111], it can be concluded that the acceleration values are within the same order of magnitude. Just as the velocity values, the acceleration values in literature and measured in this research are decreasing for the basal region to the apical region. In [112] the same order of magnitude for the acceleration values are also found. However, here it is also seen that the found values are different, when analysed by different observers.

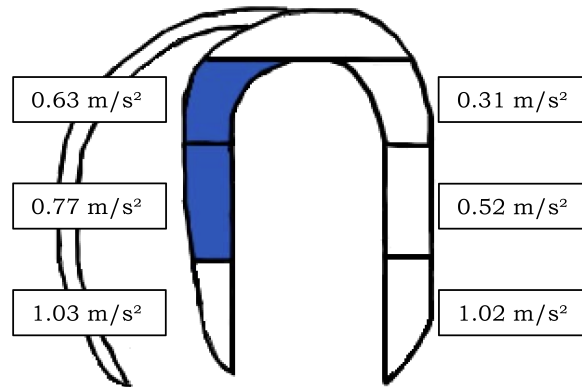
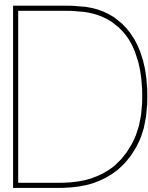


Figure C.7: The six segments of the left ventricle presented in the four chamber view. The blue segments represent the placement location of a leadless pacemaker. The mean contraction acceleration of the nine patients measured with STE per segments is shown.

The input acceleration for the heart signal generator, used for the scaling of the obtained acceleration signals, is randomly chosen out of a range of accelerations determined from the STE measurements of the nine patients. It is decided to vary the acceleration within a range of $0.26-1.82 m/s^2$, for several reasons. First of all, as stated multiple times, the heartbeat signals are different per person, including the height of the acceleration and velocity. In order to obtain this human factor a range is used. Second, the placement location of a leadless pacemaker is different for every surgery. The best location to fixate the leadless pacemaker in the heart wall depends per person and what seems to be the best location during the operation. Finally, the range is chosen because of the ambiguous values found in literature and in this research between the STE and TDI measurements. Due to the range, any inaccuracies of the measurement method used in this study are covered when scaling the heart signal generator signals.



Accelerometer Measurements

This appendix elaborates on the acceleration signals of the open-chest pig heart measurements and the human chest motion measurements. First, both measurement methods are described. Second, the human and the pig hearts are compared. Then, this chapter describes how the acceleration data is processed in order to prepare the signals for the analysis, followed by a comparison of the STE and acceleration data. After this comparison, this chapter analyses the trajectory observed in the acceleration signals, and how this is used for further research. Finally, the influence of the heart rate on the acceleration signal is described.

D.1. Measurement Method

Besides human ultrasound measurements, the signal analysis in this report is based on accelerometer measurements. Accelerometer measurements are performed on the heart wall of pig hearts and on the chest of humans. This section further elaborates on these two accelerometer measurements.

D.1.1. Heart Wall Motion Pig Signals

One of the sources of heart signals used in this report are heart acceleration signals measured with an accelerometer attached on five pig hearts. These measurements are performed by Grymyr et al. [103]. The accelerometer used is a 3D accelerometer (KXM52-1040, Kionix, Inc., NY, USA) with a dimension of $5 \times 5 \times 2$ mm and a sampling frequency of 500 Hz. In Figure D.1a the location of two accelerometers are shown: one is placed in the left ventricle apical region and the second sensor is placed in the basal lateral region. In the figure the X-, Y- and Z-axis directions are indicated, or the longitudinal, circumferential and radial directions, respectively. The heart wall acceleration signals of five pig hearts were made available in order to make comparisons. The signal length is ten seconds each and during the measurements the chest was left open and the pigs were placed in dorsal supine position (lying on their back) [103].

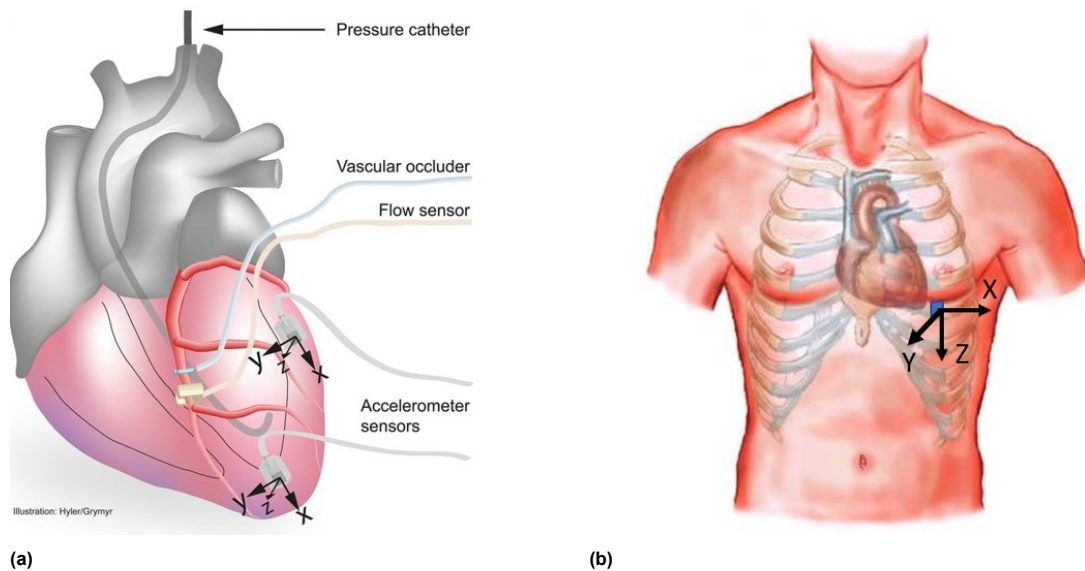


Figure D.1: The locations of the accelerometer sensors. **(a)** The two locations of the pig heart measurements: one sensor in the apical region and one in the basal region. For this analysis the apical region is used. Figure obtained from [103]. **(b)** The location of the accelerometer attached on the human chest, near the apex. The figure used is obtained from [163].

D.1.2. Chest Motion Human Signals

A third source of measurements are the measurements performed with an accelerometer attached to the human chest. The accelerometer used for this experiment is also a 3D accelerometer (356A32, PCB, NY, USA) with a dimension of $11.4 \times 11.4 \times 11.4$ mm and a sampling frequency of 2048 Hz. For the measurements a portable measurement setup was used, by using a laptop in combination with a NI-cDAQ 9171, where the accelerometer was connected to the first three terminals of the NI-9234. Measurements are performed on three men (age 23-28) with no known heart condition. The accelerometer is attached to the chest, near the apex of the heart, see Figure D.1b. The figure indicates the direction of the axes, with the Z-axis pointing downwards, the Y-axis pointing out of plane and the X-axis pointing to the left (test person's perspective). During the measurements the test persons were lying in the dorsal supine position, the signal length was fifteen seconds each and the breath was held during the measurements.

D.2. Heart Comparison

During this research pig heart measurements are used as an approximation of human heart acceleration signals in order to test energy harvesters for pacemakers. Before the pig heart measurements can be used, however, it is important to analyse in what ways human hearts and pig hearts are similar or different. Table D.1 provides an anatomical comparison of the characteristics of the two hearts. The hearts of a human and a pig are comparable in mass and size, and both have four chambers. For pigs, the heart rate (in rest) is slightly higher than for humans [164, 165].

Table D.1: Comparison of a pig and human heart for various properties, obtained from [165].

	Pig	Human
Mass	302.8 g	266.5 g
Broadest Transverse Diameter	8.9 cm	8.6 cm
Broadest Anteroposterior Diameter	6.6 cm	7.1 cm
Height	10.2 cm	9.8 cm
Chambers	4	4
Heart Rate	50-116 bpm	60-100 bpm

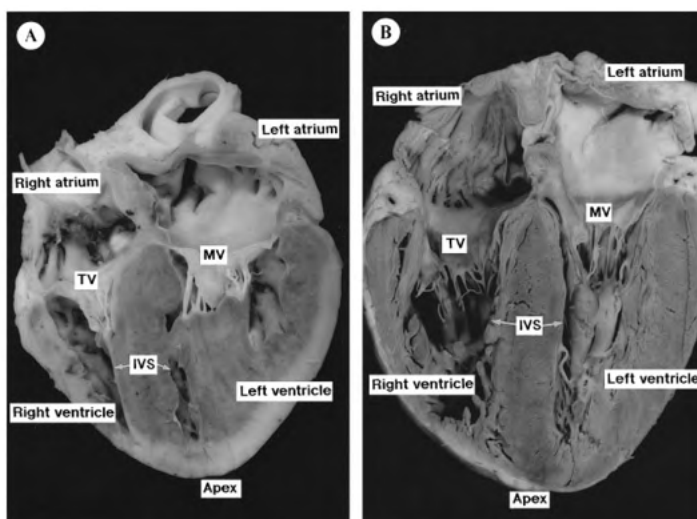


Figure D.2: The four chamber sections of a pig heart (left) and human heart (right) showing the similarities and differences. TV, leaflets of tricuspid valve; MV, leaflets of mitral valve; IVS, interventricular septum. The largest difference is the size of the left ventricle, and thus the differences of the location of the IVS. This influences also the location of the apex. Figure obtained from [166].

In Figure D.2 a pig heart and a human heart are shown, respectively. Here the four chambers in both hearts can be seen. The human heart and the pig heart share some important characteristics. Besides the fact that both hearts have four chambers, both hearts have also similarities when it comes to heart valves, major blood vessels, coronary arteries, the cardiac conduction system and cardiac motion [23, 167]. In both cases the left ventricles are the major pump, pumping the blood into the body, resulting in more muscular walls than the atrium- or the right ventricle walls. Both the human heart and the pig heart have three papillary muscles in the right ventricle and two in the left ventricle [166]. However, there are also differences when comparing the two hearts. A first difference is the orientation of the artery of the right ventricle of the heart. In a pig heart this component is directly aligned with the vein, but in a human heart this component is oriented at a slight angle to the vein. This difference can be explained by the stance of a pig and a human: an unguigrade stance versus an upright stance, respectively [166]. Furthermore, hearts have a cross-chamber muscle band, containing Purkinje fibers. The location of this band is higher in the pigs heart (on the septal wall), when compared to the human heart [168]. This difference in the position of this band explains the fact that the PR-interval in the

ECG of a pig is shorter than for humans. For a human this is 120-200 ms, versus 70-113 ms for a pig [166]. The shape and duration of the T-wave in the ECG, however, is the same for both humans and pigs, as is the activation sequence in the ventricles [169, 170]. A third difference is the thickness of the trabeculations, which are thicker in pig hearts and finer in human hearts. This difference could explain the higher efficiency of the ventricle activation and it is speculated that it could influence the ventricle contraction [171].

Human hearts and pig hearts are also similar when it comes to contraction and relaxation kinetics. The advantages and disadvantages of different animal hearts in cardiac contraction research are investigated by Milani-Nejad and Janssen [172]. Contraction and relaxation kinematics scale with body weight, and animal kinetics approaches human kinetics as the animal size increases. Milani-Nejad and Janssen [172] argue that "the closer the heart or body weight of the animal model to human; the more similar are the hearts" [172]. This research also includes swine hearts. The contraction and relaxation kinetics of swine hearts are slightly faster than human heart contraction and relaxation. Nonetheless, they are much more similar to human hearts than for instance rabbit hearts. Swine have, just as humans, a positive force-frequency relationship. Increasing the heart rate increases different indications of contractility, such as the maximal rate of pressure rise and the myocardial acceleration during during isovolumic contraction (IVA) [172]. For studies investigating changes in the contraction and relaxation kinetics in heart failure, it is thus appropriate to use large animal models to approximate human heart measurements. However, it should be kept in mind that the swine and human hearts are inherently different.

In Figure D.3 a TDI measurement at the basal region of a pig heart is shown. When visually comparing the signal with the human velocity signals from Appendix C, Figure C.2a, the described heart cycle moments can be seen. The peak amplitudes have the same order of size, where the s-wave, followed by the e-wave and a-wave are observed. In the next heart cycle, starting from the white vertical line, the IVV-peak, s-wave, e-wave and a-wave are seen. The velocity progress differs from person to person and from pig to pig, but the velocity signals at the heart base of both humans and pigs have generally the same structure.

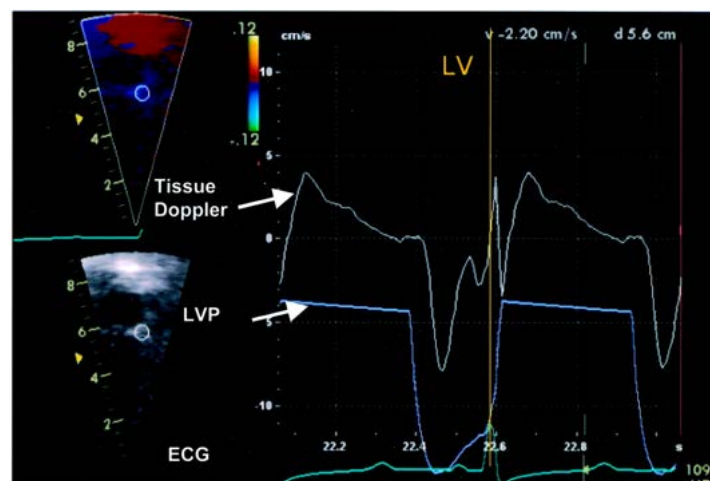


Figure D.3: The heart wall velocity of a pig heart measured with TDI. Figure obtained from [173].

All these analyses show that pig hearts are comparable to human hearts. Both hearts have matching properties, they have the same size and anatomy, the heart rate is slightly different and the velocity signals generally match. As stated earlier contraction and relaxation kinematics scale with body weight, and animal kinetics approaches human kinetics as the animal size increases making pig hearts comparable to human hearts in this area as well. However, there are also differences. Despite the fact that the acceleration pig signals are a good first approach to approximate human acceleration signals, it should be kept in mind that a pig and a human cannot be compared one-to-one (although it should be noted that humans cannot be compared one-to-one to other humans, either). In this research pig acceleration

signals are used to approach human acceleration signals for the testing of energy harvesting, further research is needed to validate this approximation or to obtain human acceleration signals.

D.3. Signal Processing

Before the data of the pig hearts can be used for analysis it should first be processed. This means that the data needs to be filtered in order to obtain a smooth acceleration signal without any noise or other movements besides the movement of the heart wall. Besides this, the human acceleration data must also be rotated, in order to align the human and pig data in the same coordinate system. This section provides a detailed explanation of both the filtering process and the data rotation.

D.3.1. Filtering

A high pass filter and a low pass filter are used to obtain a smooth acceleration signal. First, the pig heart signals are discussed, followed by the human chest motion signals.

Pig Measurements

The first step in the data processing of the pig hearts acceleration signals is the filtering of the data. Figure D.4 is a plot of the raw signals of one of the five pig heart measurements. In this figure the X-, Y- and Z-acceleration, or the longitudinal, circumferential and radial acceleration respectively, can be seen. The acceleration in the Z-direction is on average 9.8 m/s^2 higher than the other axes. Figure D.1a shows that the Z-axis is pointing downwards, in the direction of the gravity. The offset of the measurements in the Z-direction can therefore be explained by the pull of gravity.

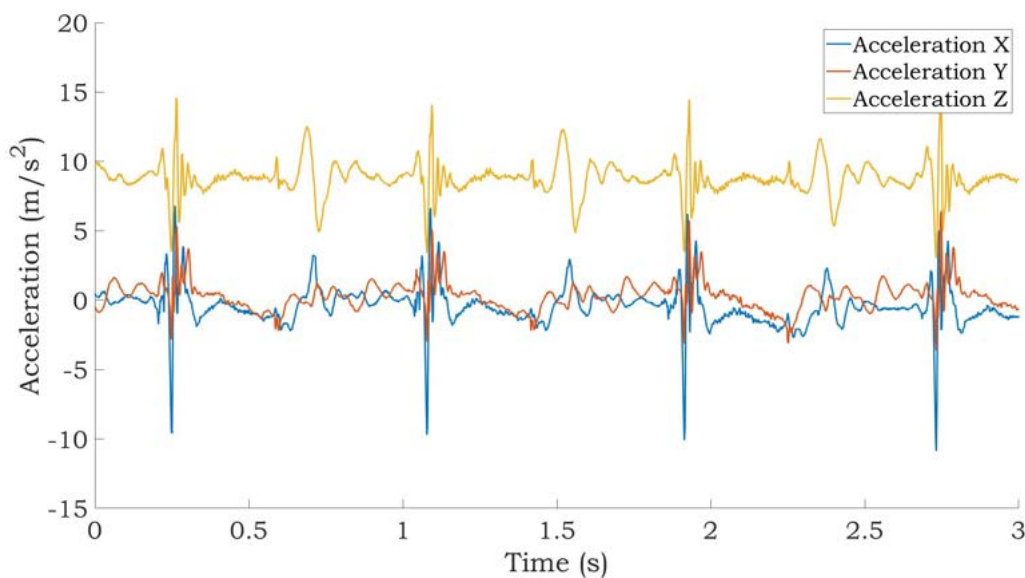


Figure D.4: Raw signal from one of the five measurements of the pig hearts in X-, Y- and Z-direction.

From the three axes the Fast-Fourier Transform (FFT) is calculated and the power is plotted against the frequency. This transformation is shown for the X- Y- and Z-axis in Figure D.5a, Figure D.5b and Figure D.5c, respectively. Looking closely at the power plot of the Z-axis, a high power can be seen at the very low frequencies. This high power is not seen in the other axes, meaning that this high power can be explained by the gravity present in the Z-axis. Looking at the power present in the X-axis and having a closer look at the low frequencies, shown in Figure D.5a, various peaks can be analysed. The figure shows the first peak at a very low frequency. This first peak is the offset from the accelerometer. Then a second peak at approximately 0.5 Hz can be seen, which can be attributed to the respiratory motion from the pig during the measurements [56]. These two peaks are followed by the highest peak of the power plot, which is the heart rate of the pig. This peak is at a frequency of 1.2 Hz, or 72 bpm. The power plot displays multiple following peaks, probably representing the higher harmonics of the

highest peak due to the heart rate. Analysing the power plot, the power indicated in the Y-axis is the highest. However, when analysing the raw acceleration data the amplitude of the X-axis seems larger than the other axes.

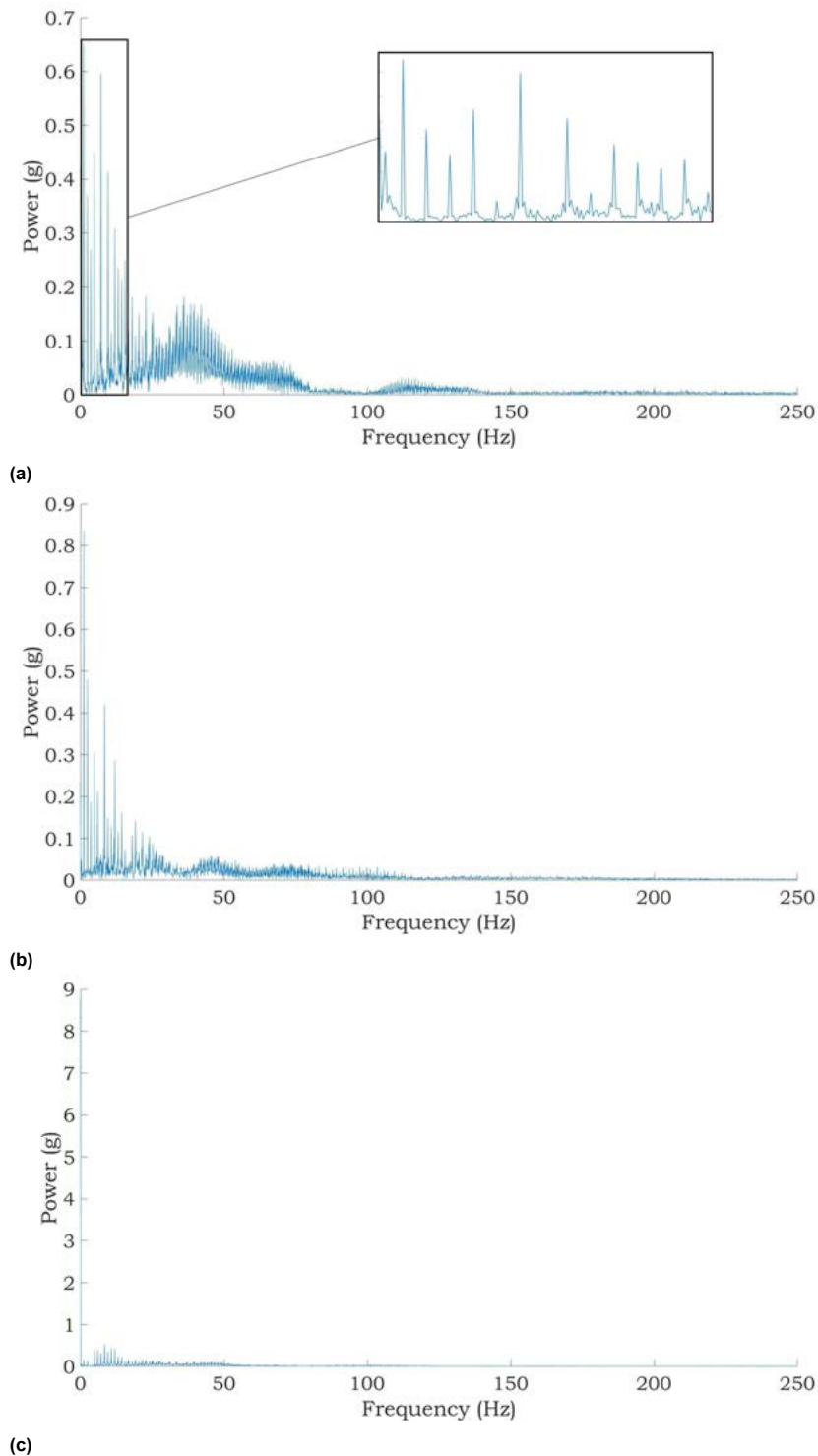


Figure D.5: The power plot of the FFT signals from the raw acceleration measurements with (a) The X-axis and a zoom of the FFT plot, (b) the Y-axis and (c) the Z-axis.

From the analysis of the raw acceleration signals and the corresponding power plots the following can be concluded: the acceleration signals consist of heart wall movement, gravity, respiratory motion,

DC offset and noise. Since only the heart wall movement is of interest in this research, the signal is processed in order to remove the other components. First, a high pass filter is used in order to remove the DC offset, gravity component and the respiratory motion. The high pass filter is set at a frequency of 0.5 Hz, since the respiratory motion has a frequency of approximately 0.5 Hz [23, 174]. The power of the frequencies below 0.5 Hz are removed from the signal, as is shown in Figure D.6a.

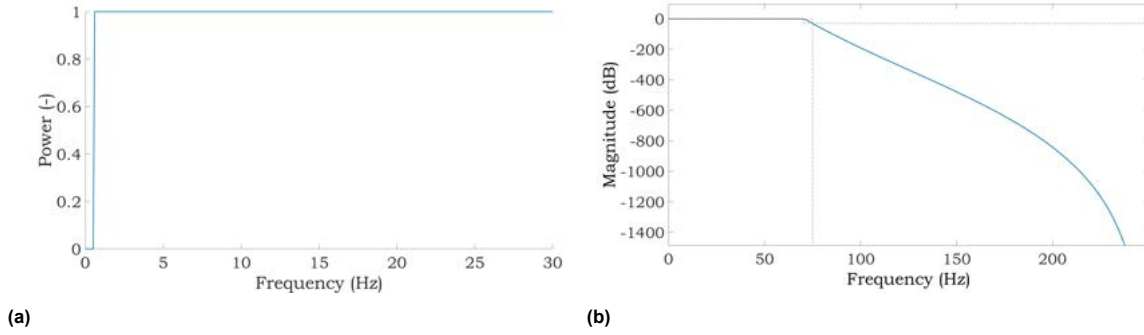


Figure D.6: The filters used for the processing of the acceleration signals (a) The high pass filter at 0.5 Hz and (b) The low pass filter at 75 Hz.

After the high pass filtering, a low pass filter is used in order to remove the measurement noise from the signal. For this filter the transfer function needs to be specified. Equation F.1 is a transfer function, where $Y(z)$ is the output and $X(z)$ is the input.

$$H(z) = \frac{Y(z)}{X(z)} = \frac{b_0 + b_1z^{-1} + b_2z^{-2} + \dots + b_Nz^{-N}}{1 + a_1z^{-1} + a_2z^{-2} + \dots + a_Dz^{-D}} \quad (D.1)$$

The gain of the filter is the ratio between the output and input. The design of a filter determines the a and b coefficients in such a way that the undesired frequencies are filtered out and the desired frequencies remain in the signal. For this signal processing it is important that the gain is 1, because the filter should not influence the other power peaks present in the signal at the frequencies of interest, as this would result in information loss. For filtering a finite impulse response (FIR) or infinite impulse response (IIR) can be chosen. The difference is that a FIR filter only operates using the input values and an IIR filter uses both the input and output values. A benefit from IIR is that the filter usually requires a lower filter order for meeting specifications [175].

A Butterworth filter is used as a low pass filter, the Fourier transform of the transfer function of this filter is Equation D.2.

$$H(jw) = \frac{1}{(1 + (\frac{jw}{jw_c})^2)^n} \quad (D.2)$$

Here w_c is the cut-off frequency and n is the filter order, the number of poles in the transfer function. Increasing the order increases the slope of the filter [175]. The cut off frequency for this filter was set at 75 Hz [174]. The order of the filter is 26 and the filter is stable. The magnitude response of the low pass filter can be seen in Figure D.6b. The stop band attenuation is set to 30 dB and the pass band attenuation to 1 dB. In Figure D.7 the filtered X-, Y- and Z-acceleration signals can be seen.

Human Measurements

For the human acceleration measurements filters have also been used in order to remove signal noise. The Fast-Fourier Transform (FFT) of the human signals does not show the correct frequencies, since the accelerometer is attached on the chest and the signal consist of damping because of the skin. Moreover, it is known that the accelerometer from PCB removes the static gravitation component. Despite this, it is chosen to still use the high pass filter at 0.5 Hz in order to remove the DC offset of the sensor. On top of that, the same low pass filter is used as for the pig acceleration signals, Figure D.6b.

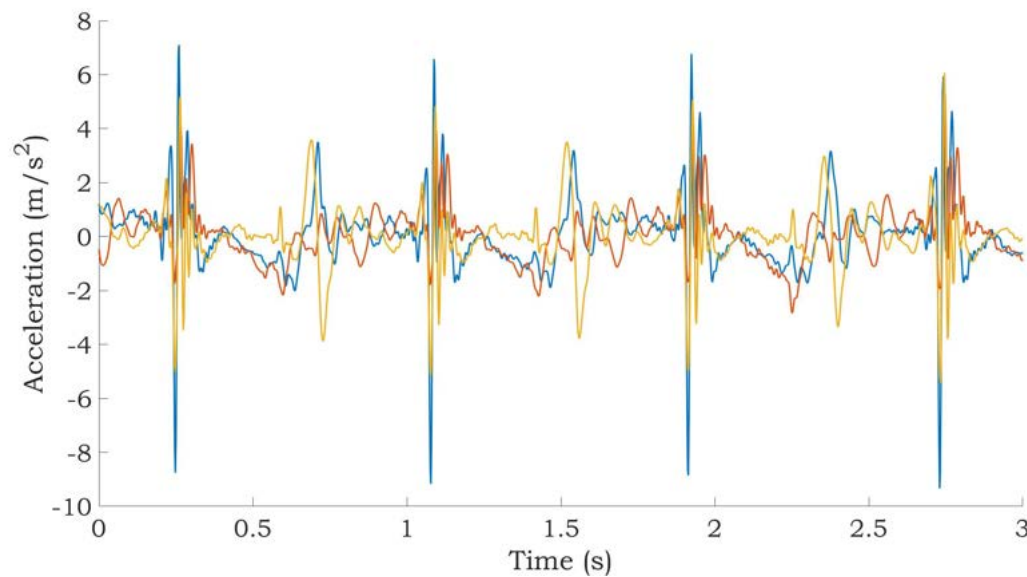


Figure D.7: The filtered acceleration signal from the acceleration signal shown in Figure D.4.

D.3.2. Rotating

In order to compare the axes of the acceleration signal from the pigs with the axes of the acceleration signals from the human, the signals should be aligned in the same coordinate system. The coordinate system from the accelerometer used on the pig's heart can be seen in Figure D.1a. Here the X-axis, or longitudinal axis, points from the base to the apex. The Y-axis, or the circumferential axis, follows the outer heart wall and the Z-axis, or the radial axis, points into the heart. The coordinate system of the human acceleration measurements can be seen in Figure D.1b. Here the longitudinal axis is the Z-axis and pointing downwards, the circumferential axis the X-axis pointing to the left and the radial axis the Y-axis pointing out of the heart, resulting in a different coordinate system. In order to align the signals in the same coordinate system a rotation matrix is used to rotate the human signals. For this rotation matrix two rotations are used, first a rotation of 90 degrees of the X-axis, followed by a rotation of 45 degrees of the Y-axis.

It should be taken into account that the rotations do not result in a Gimbal Lock. A Gimbal Lock occurs when two axes are locked together due to a rotation [176]. This means that one axis of movement is lost and a rotation of this axis has the same results as a rotation of the axis to which it is locked. A Gimbal Lock occurs when rotations are performed in a specific order with a rotation of 90 degrees around the Y-axis [177]. The Gimbal Lock can be bypassed by changing the rotation order. Here, however, the rotation around the Y-axis does not come near the 90 degrees, so the Gimbal Lock does not occur. It should also be taken into account that if the sensors are not placed in line with the cardiac coordinates, the acceleration values found can become inaccurate [103]. How the accelerometers were placed, however, during the operation is not precisely known and depends on the doctor performing the operation. It is assumed that the coordinate system in Figure D.1a is leading and it should be kept in mind that the location of the sensor could be different and influence the signals measured.

D.4. Comparison STE and Accelerometer Measurements

In this section the STE measurements from Appendix C and the accelerometer measurements are compared. They are compared in terms of resolution and in terms of overestimation because of external influences. This section then discusses differences, as well as pros and cons.

D.4.1. Resolution

The first component of comparison is resolution. A distinction is made between spatial resolution and temporal resolution.

Spatial Resolution

As discussed in Appendix C, the pixel size in the ultrasound measurements is 0.24 mm, which is the spatial resolution for displacement measurements. In order to compare the two spatial resolutions in the same units Equation B.1 is re-used, but now the acceleration is calculated in Equation D.3 instead of the displacement. The formula for spatial resolution for an accelerometer is shown in Equation D.4 [178]. Here N stands for the noise density. As shown in Table D.2, the noise density, or spatial resolution value, of the 3D accelerometer sensor is $35 \mu\text{g}/\sqrt{\text{Hz}}$ (x and y) and $65 \mu\text{g}/\sqrt{\text{Hz}}$ (z) [179].

$$a = \frac{d \cdot (2\pi f)^2}{9.81} \tag{D.3}$$

$$R = N \cdot \sqrt{1.6f} \tag{D.4}$$

With these two equations the two measurement methods can be compared when it comes to the spatial resolution. In Figure D.8 the smallest increment of acceleration detection for the two methods per frequency is shown. For all frequencies, the detection of the accelerometer is more accurate than the ultrasound measurements. This figure shows that when a signal contains a frequency of 12 Hz the detectable acceleration is 0.15 g for ultrasound. It is known that the acceleration of the heart signal contains frequencies higher than 12 Hz. These are acceleration values that occur in the human heart wall. When it comes to ultrasound, however, it can be seen that the detection acceleration increases exponentially in contrast to the accelerometer measurements which almost stabilizes. This means that for higher frequencies, only a higher acceleration can be detected. For the apical region it is known that these high accelerations rarely occur. This means that important characteristics of the acceleration signal of the heart can be visualized more accurately with an accelerometer than with ultrasound when it comes to spatial resolution.

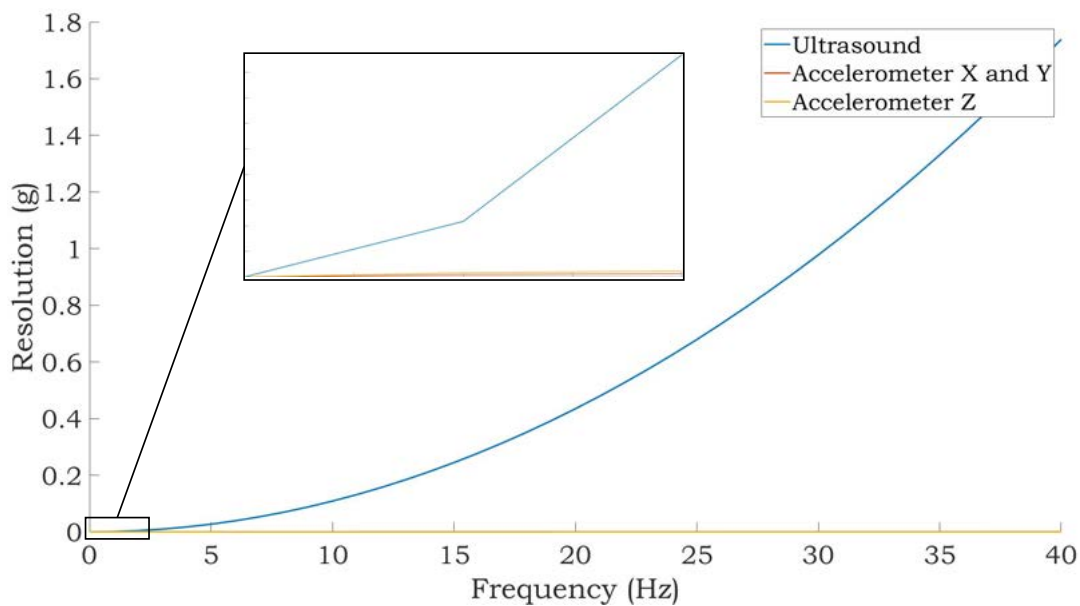


Figure D.8: Spatial resolution comparison of measurements with ultrasound and measurements with accelerometers.

Temporal Resolution

The temporal resolution values for ultrasound measurements are discussed earlier in Appendix C. The temporal resolution values are shown in Table D.2. For ultrasound measurement with TDI this is 180 fps, for ultrasound measurements with STE this is 62 fps and for accelerometer measurements this is 500 Hz. Taking the Nyquist theorem into account (meaning that the frequency present in the measured signals is half of the sampling frequency) the highest frequencies measured are 90 Hz, 31 Hz and 250 Hz, respectively. The influence of a lower sampling rate is shown in Figure D.9. Here it can be seen that due to this lower sampling rate peak values can be underestimated. In addition, it could occur

that the course of the signal is not displayed properly. In fact, the frequency represented by the contraction peak in different acceleration signals can vary between 20-60 Hz. With the contraction peak in the acceleration signal estimated with an existing frequency of 25 Hz, this should be visible in the ultrasound measurements. However, this is approaching the limit of the resolution of ultrasound. On top of that, this frequency present in this part of the signal is varying and depends on the heart rate. This means that it may be possible that these peaks can not be seen in the signals measured with ultrasound, because a lack of the sampling frequency. The acceleration signal contains information up to 50 Hz, which is shown in Figure D.5a. This information up to 50 Hz are probably the higher harmonics of the heart rate (approximately 30 higher harmonics). As stated by Hoff et al. [56] should all these harmonics be included in the signal to see the finer details of the heart motion. Furthermore, a low temporal resolution has also an influence for the integration or differentiation of the signal, since information is missing. This results in that tangents are underestimated. This influences the steepness and amplitude of the obtained signals. In order to analyse the shape of the acceleration signals, higher sampling rates are needed for ultrasound measurements.

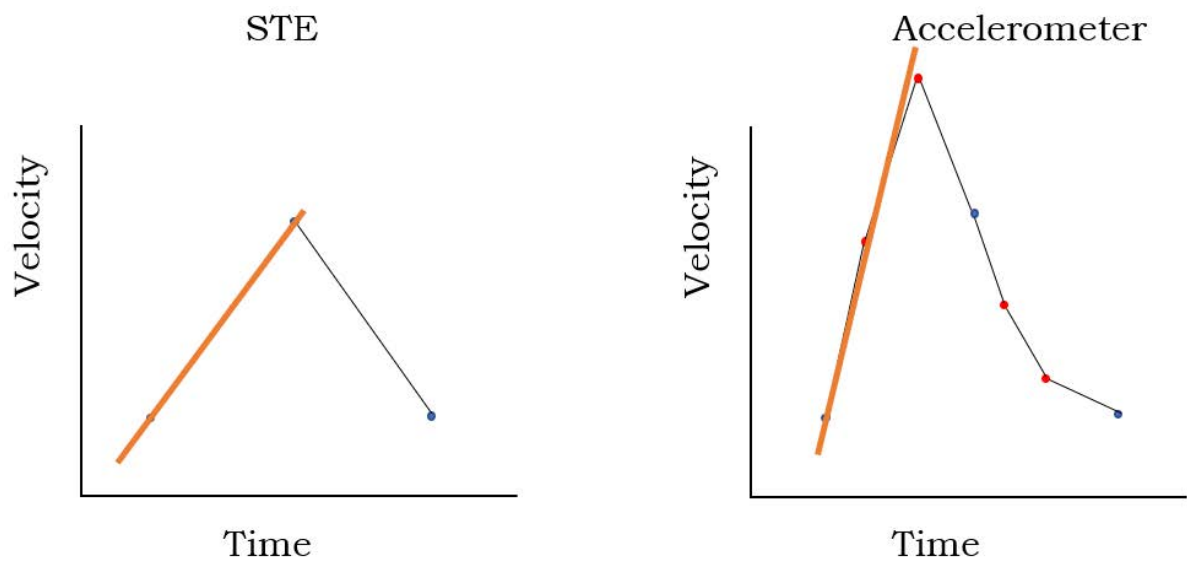


Figure D.9: The influence of a low temporal resolution for the velocity signal and acceleration signal.

Table D.2: Comparison of the heart measurement methods.

	TDI	STE	Accelerometer
Source	Echo	Echo	3D Sensor
Quantity	Displacement	Displacement	Acceleration
Temporal Resolution	180 fps	62 fps	500 Hz
Spatial Resolution	0.25 mm	0.24 mm	35 $\mu g/\sqrt{Hz}$ (x and y) [179] 65 $\mu g/\sqrt{Hz}$ (z)
Usability	Bedside	Bedside	Open Heart Operation

D.4.2. Overestimation

Having compared the measurement resolution, accelerometer measurements seem more accurate than ultrasound measurements. A second point of comparison between ultrasound measurements and accelerometer measurements is overestimation. This section discusses overestimation due to gravity and the difference between open or closed-chest measurements.

Gravity

A well-known problem in measurements with an accelerometer is overestimation in the obtained signals due to gravity. The heart motion has translational and rotational motion. When attaching an accelerometer, or in other words adding a mass on the heart wall, the gravity component will add an overestimation of the amplitude in the measured signals. The high pass filter at 0.5 Hz, described earlier, only removes the static component of gravity in the signal, the offset. The dynamic gravity component is still present in the signal. This dynamic component changes with the orientation of the accelerometer on the heart wall. So in order to remove this dynamic component the rotation angles are needed. This phenomenon is researched extensively by Remme et al. [180] and Krogh et al. [110] for the circumferential axis. Here, the overestimation due to gravity in the displacement signal depends on the heart rate. For a heart rate of 60 bpm the displacement was overestimated three to four times [180], as for a heart rate of 90 bpm the displacement had an overestimation of two [110]. The overestimation for the longitudinal and radial axes are unknown. However, since there is an overestimation in the circumferential displacement and because the heart makes rotational movements, it is assumed that there is also an overestimation in the two other axes.

The orientation of the accelerometer on the heart wall changes during the cardiac cycle. This means that the influence of the gravity on the X-, Y- and Z-axis also changes during the measurements. The best method to separate the gravity component from the heart signal is to measure the rotation angles of the heart movement with a gyroscope. These angles can be used to calculate the gravity component per axis which can then be subtracted from the axes separately. With only static filtering the motion of the heart can be overestimated. This should be kept in mind during the analysis of the signals [22, 56, 181].

Open- versus Closed-Chest

Besides the gravity component, the measurement conditions also influence the height of the amplitudes measured. The pig heart measurements are open-chest measurements, where the accelerometer is attached on the heart with the chest opened during measurements. The difference between open- and closed-chest measurements are analysed by Grymyr et al. [109]. Here an accelerometer is placed at the same position as in Figure D.1a, namely in the left ventricular apical region. Where after the accelerometer placement the chest is closed. Comparing the amplitudes from both measurements shows that the peak systolic velocity in the open-chest measurements is approximately two times larger than the peak systolic velocity in the closed-chest.

In conclusion, there is an amplitude overestimation in the signal due to gravity and the measurement conditions. This should be kept in mind when the pig signals are used for further analysis.

D.5. Trajectory Analysis

As stated above the amplitudes seen in the pig signals are an overestimation of the reality and do not give a good estimation of the amplitude of the human heart acceleration. However, the temporal and spatial resolution of the pig signals are better than the ultrasound measurements. Based on these observations, the assumption can be made that the shape seen in the pig signals is a good representation of the acceleration present in the heart cycle. This section will first discuss the trajectory of the acceleration signal. The same heart cycle moments as discussed in Appendix C are described, followed by a comparison of the trajectories found with different measurements methods and on different animals, in order to validate the shape trajectory of these pig acceleration signals.

The acceleration signal of a pig and the corresponding ECG signal can be seen in Figure D.10. Characteristic moments for ventricle motion in the ECG are the R-peak and the end of the T-wave. The R-peak stands for the ventricle depolarization, or in other words the beginning of the ventricle contraction. The R-peak is marked in the figure with a red triangle. Due to the depolarization an inward and twisting motion starts in the heart wall [182]. The T-wave stands for the ventricle repolarization (marked by a green square in the figure). When the T-wave is finished, the ventricle starts to relax. Since the leadless pacemaker with the energy harvester is placed in the right ventricle, the ventricle motions are the motions of interest. The ventricle has four events that are repeated every heartbeat,

namely: isovolumic contraction, ventricular ejection, isovolumic relaxation and ventricular filling [183].

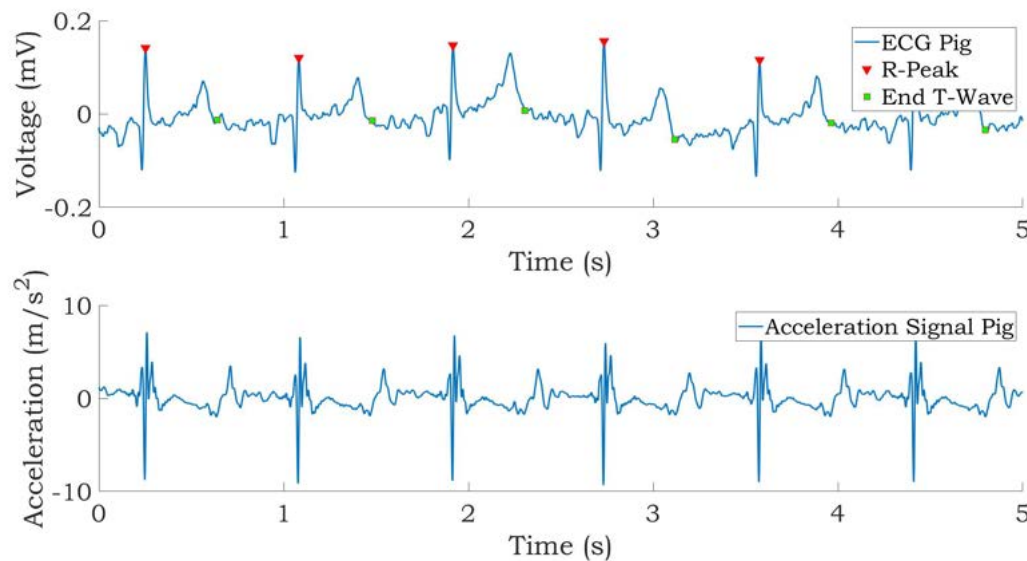


Figure D.10: The ECG and the heart wall acceleration signal measured simultaneously on the same pig. The moments of the R-peaks and the end of the T-waves are indicated.

The acceleration peaks present in the acceleration signal can be linked to the two ventricle motions, the contraction and relaxation. The acceleration signal in Figure D.10 is in sync with the ECG signal. It can be seen that the larger acceleration peaks are simultaneous with the R-peaks, the ventricle contraction. The smaller acceleration peaks are simultaneous with the end of the T-waves, the ventricle relaxation. The contraction peaks starts with a lower peak, followed by a higher peak. The lower peak is the isovolumic myocardial acceleration (IVA) and is the first contraction of the ventricle, the isovolumic contraction. This IVA-peak corresponds to the IVV-peak in the velocity. Due to this motion the pressure in the ventricle starts to rise. When a certain pressure is reached the ventricle starts to eject the blood, the late systole. This results in the higher acceleration peaks, since the ventricle motion is larger when compared to the first contraction motion, corresponding to the s-wave in the velocity. The relaxation consist of the early and late diastole and has a longer duration in the heart cycle than the contraction.

It can be concluded that the acceleration signals must contain two moments of motion where acceleration peaks can be seen, the contraction and relaxation. In Figure D.10 the contraction peaks are larger than the relaxation peaks, but this is not always the case. When analysing the five different pig signals, Figure D.11, it can be seen that for some pigs the relaxation has almost an amplitude as high as the amplitude of the contraction. Furthermore, it can also be seen that the five pigs have a different shape of the contraction and relaxation trajectories. All pigs are different and this also applies to humans.

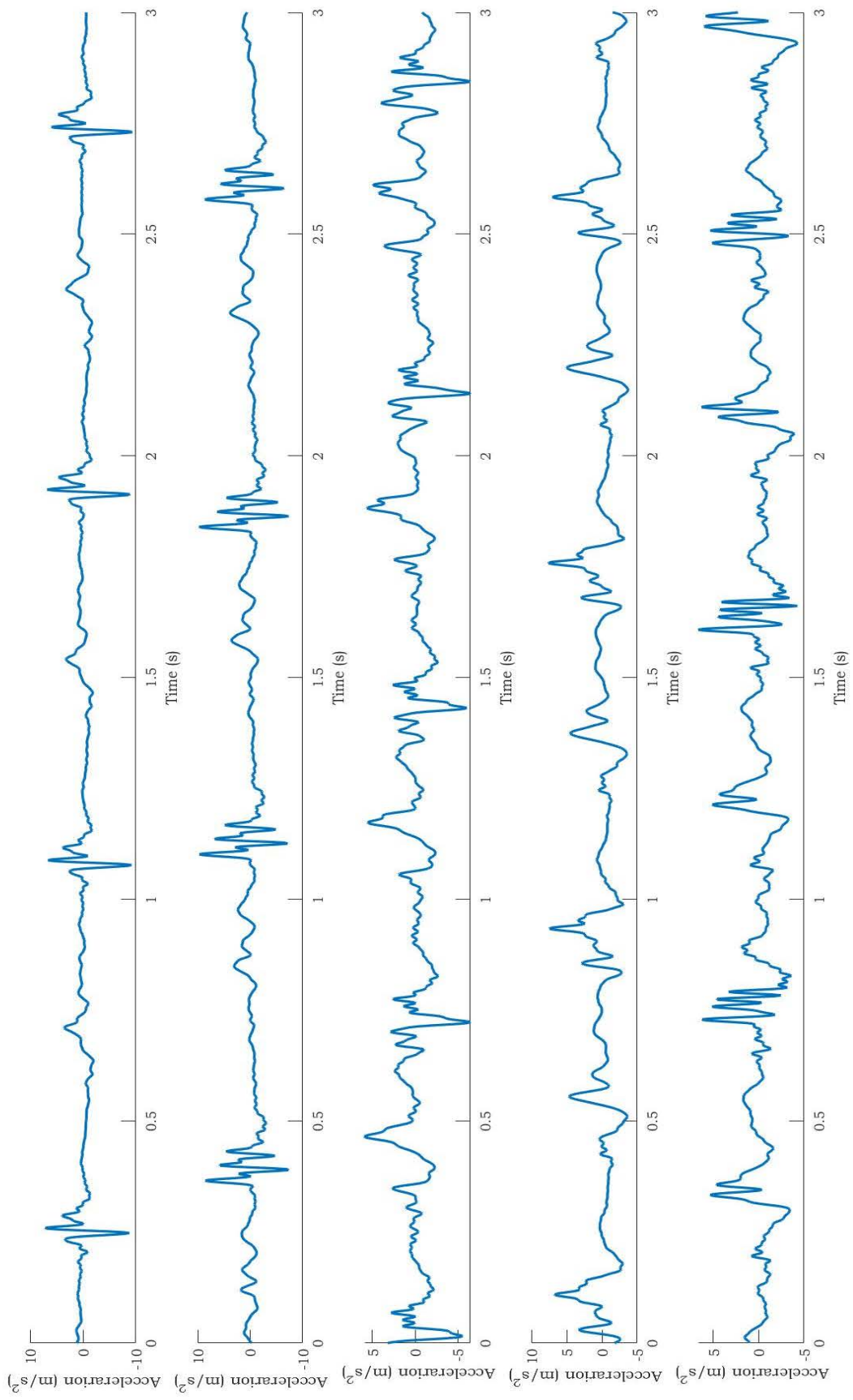


Figure D.11: All longitudinal pig heart acceleration signals.

D.5.1. Trajectory Overview

The shape of the heart acceleration signal is validated in two ways. The first manner is a visual comparison of the human acceleration measurements where the accelerometer is attached to the chest. Second, the shape of the pig heart acceleration signals are compared to different acceleration signals found in literature in which measurements were performed on different animals and humans with varying measurement methods. This comparison is done in order to validate if the trajectory of the pig heart signals is sufficient to use for the further research.

Visual Comparison Human Acceleration Signal

Here the shape of the pig acceleration signals is visually compared to the human acceleration signals measured with an accelerometer attached to the chest. Such a measurement is called a seismocardiogram (SCG). A zoom of the longitudinal acceleration signal of one of the testing persons is shown in Figure D.12. SCG measurements are analysed in detail in literature and consecutive events in the cardiac cycle are described in the signal. The peak represents the aortic valve opening (AO). As described earlier the pressure rises in the ventricle due to the start of the inward and twisting of the heart wall after the depolarization. When the pressure is high enough, the blood is ejected and the aortic valve is opened. Such a peak also occurs when the aortic valve is closed (AC), which can be classified as the relaxation peak. In the contraction peak also the mitral valve closure (MC) and rapid ejection (RE) can be observed [182].

When comparing the shape of the human acceleration signal measured on the chest, Figure D.12, with the shape of the pig heart wall motion measured epicardial, Figure D.7, it becomes evident that that the two signals have similarities. In both signals a contraction peak can be seen and a relaxation peak. The signals can not be compared one-to-one, but it should be noted that this would also not be possible when comparing two human measurements because everyone's heartbeat differs.

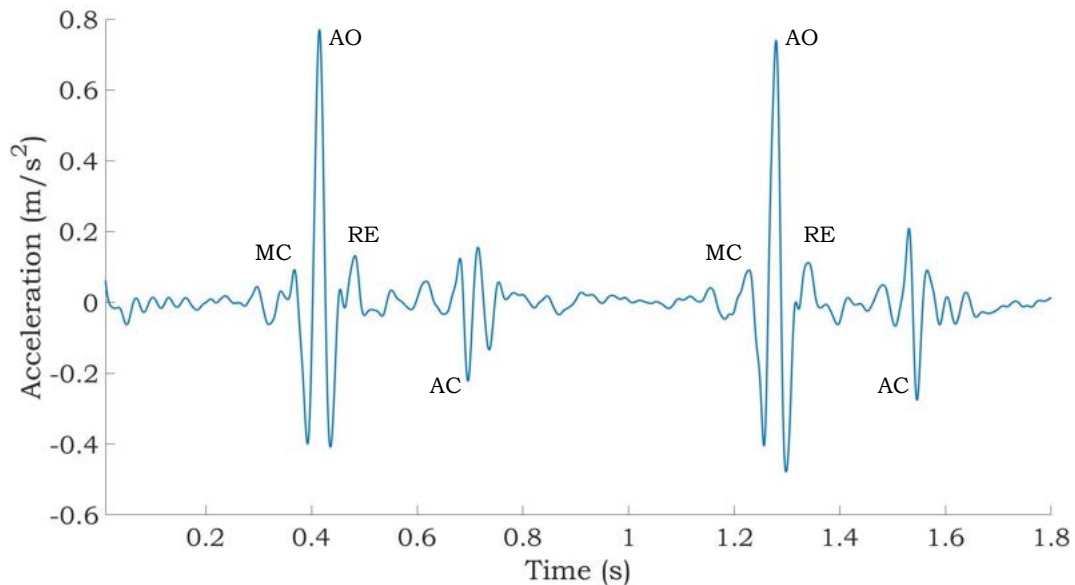


Figure D.12: A zoom of the human longitudinal acceleration signal measured with the accelerometer attached on the chest. With the AO aortic valve opening, AC aortic valve closing, MC mitral valve closure and RE rapid ejection indicated.

Literature

In literature various research is done where the heart wall acceleration signal is obtained. These signals show the same trajectory as seen in the pig heart measurements signals. An overview of these research outcomes is given in Table D.3. Here the species, measurement method, a figure of the signal and its source are shown. In the figures, a red area indicates the contraction peak and the green area indicates the relaxation peak. The contraction peak and relaxation peak are linked to the R-peak and T-wave of the corresponding ECG signal in the article. It can be seen that for different species

and different measurement methods, the signals consist of a contraction peak and relaxation peak. Differences are seen in the details of these peaks, such as the amount of peaks it consists of and the amplitude of these peaks. This could be due to the different measuring methods used, the fact that different species are compared or because everyone has a different heart rate and therefore a different signal.

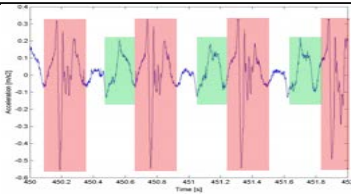
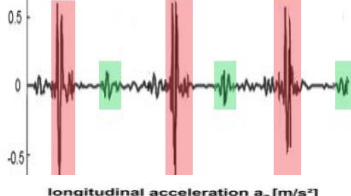
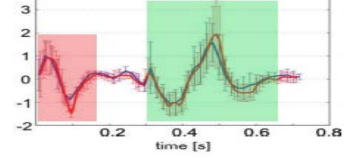
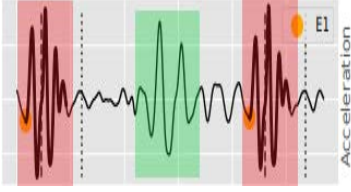
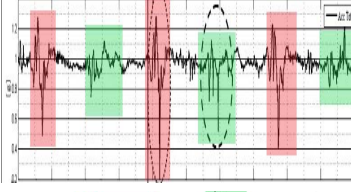
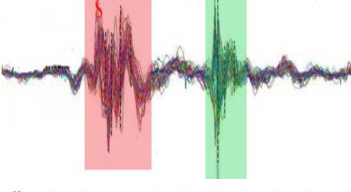
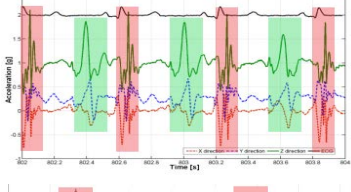
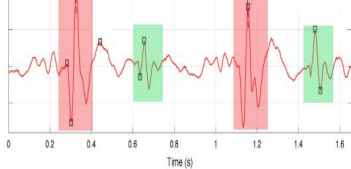
From the visual comparison of the measurements performed in the lab, Figure D.12, and the literature research, Table D.3, it can be concluded that the pig signals can be used for further analysis. The shape of the pig signals, Figure D.11, matches the shape of the acceleration signals measured at various species with various measurement methods.

Table D.3: Overview heart wall acceleration measurements for different species and different measurement methods.

Specie	Measurement Method	Figure	Reference
Human	Accelerometer epicardial attached to heart		[105]
Sheep	TDI of heart wall motion		[106]
Sheep	TDI of heart wall motion		[184]
Human	Accelerometer attached to chest		[185]
Sheep	Accelerometer placed inside leadless pacemaker		[108]
Dogs	Sonomicrometry (crystals attached epicardial)		[107]

Continued on next page

Table D.3 – continued from previous page

Specie	Measurement Method	Figure	Reference
Pigs	Accelerometer epicardial attached to heart		[186]
Human	Accelerometer in lead tip of pacemaker placed in ventricle		[187]
Human	MRI of heart wall motion		[188]
Pigs	Accelerometer epicardial attached to heart		[104]
Pigs	Accelerometer in lead tip of pacemaker placed in ventricle		[189]
Human	Chest wall vibration measurements		[190]
Pig	Accelerometer subepicardial attached to heart		[120]
Human	Accelerometer attached to chest		[182]

D.5.2. Building Block

As described the temporal resolution of an accelerometer is sufficient to reproduce the detailed trajectory of the acceleration motion of the heart wall. This is validated for humans with accelerometer measurements on the chest and other acceleration signals found in literature. In the pig signals two peak moments can be seen, one being the contraction and one being the relaxation. As stated, five pig heart acceleration signals are obtained from Grymyr et al. [103]. The longitudinal axis of the five pig heart measurements can be seen in Figure D.11. Analysing the five pig measurements, it becomes evident that in the amplitude height and the detailed shape of both peak moments differences are observed. The five different contraction signals and relaxation signals are isolated and used as building blocks for the heart signal generator, so the shape of the contraction and relaxation of the generated signals are based on the pig signals. In Table D.3, when analysing only the signals obtained from humans, it can be seen that different measurement methods give different values for the amplitude. It is also known that the pig signals overestimate the amplitude because of the dynamical gravity component and the open-chest measurements. The question is what the correct value for the amplitude of the contraction and relaxation acceleration of the heart wall at the apical septal or mid septal segment is.

To use the correct order of magnitude the IVA values found in Appendix C are used to specify the amplitude of the contraction and relaxation peaks. The five contraction and relaxation signal parts are used as building blocks in the heart signal generator. These signals are randomly selected and combined. When selected, the contraction and relaxation peaks are adjusted differently each time with a scaling value from a range, explained in Appendix C, in order to obtain a different signal every time. In this manner the fact that every person has a different heartbeat is simulated and the energy harvester can be tested on many different signals.

What should be kept in mind is that these signals are measured epicardial and the leadless pacemaker is placed endocardial. It is known that the motion of the heart wall is different when analysing epicardial and endocardial motion. In literature the acceleration of the heart wall is measured endocardial and epicardial [174]. In these measurements, differences appear in the longitudinal, radial and circumferential acceleration signals when comparing the two locations, that can be explained by differences in rotational motion and radial thickening of the heart wall. The question is how much these detailed motions ultimately affect the motion of the leadless pacemaker, which is attached to the heart wall of the right ventricle in the apex. Eggen et al. [108] placed an accelerometer in a leadless pacemaker, which is placed in the right ventricle of the heart of a sheep. The resulting acceleration signal, shown in D.3, has approximately the same shape as the acceleration signals from the pig hearts. Because of this similarity, it is assumed that for a first approximation of the generation of a human acceleration signal the pig signals can be used, but further research is needed.

D.6. Influence Heart Rate

The human measurements with the accelerometer are also used to analyse the influence of the heart rate on the acceleration amplitude. Measurements are performed on three persons with no known heart condition (men, age 23-28). Measurements are performed in rest and during exercise. For one person the measurements can be seen in rest and during exercise in Figure D.13. Here it can be seen that the heart rate influences the peak height and the duration of the signal. In other words, there is a positive force-frequency relation. The amplitude of the acceleration increases by a certain factor per beat per minute that the heart rate increases, which means the slope changes. The amplitudes measured in the chest motion setup are not representative for the acceleration present in the heart wall, since the signals are measured on the chest and not directly on the heart wall, so these measurements can not be used to determine this increasing acceleration slope.

To determine this slope for the contraction and the relaxation literature is used. In research by Roche et al. [118] and Cifra et al. [119] it is seen that for an increasing heart rate, the acceleration amplitude for the contraction increases exponentially. To determine the slope two tangents are used, one between 70-100 bpm and one between 100-180 bpm. In both studies the values are obtained from the basal region instead of apical region, resulting in the reduction of the two slope numbers in Table D.4 to avoid an overestimation of the peak acceleration. Pauliks et al. [121] shows that for a lower region the difference

between the acceleration values for a heart rate in rest and a heart rate in exercise are smaller than for a higher heart region. The slope numbers can be seen in Table D.4. For the contraction velocity, Cifra et al. [119] observed a linear increase for increasing heart rates. For the heart signal generator, where acceleration signals are generated, only the slopes of the acceleration increase are used. It should be validated whether the velocity signals have a linear increase. This is validated in Appendix F.

Little research has been performed on the slope of the influence of the heart rate on relaxation acceleration amplitude. The relaxation velocity has also a linear increase when the heart rate increases [119]. Since in the contraction a linear increase in the velocity is also seen in reaction to a increasing heart rate, it is assumed that the relaxation has also an exponential increase in the relaxation acceleration amplitude when the heart rate increases. The slope of the relaxation velocity is higher than the slope of the contraction velocity. Because of this the acceleration slope between 70-100 bpm and 100-180 bpm is estimated higher than the acceleration slope for the contraction, see Table D.4. For a heart rate during exercise, Nguyen et al. [120] observed also a higher relaxation peak than the contraction peak, for the lower heart rate the contraction peak is higher. This could be explained by the fact that during the relaxation of the heart there is active and passive motion. Active from the heart wall, where muscle fibrils become actively longer by the absorption of calcium, and passive from the blood that flows into the ventricle. This combination of active and passive motion makes that for a higher heart rate the acceleration of the relaxation could be higher than the contraction, where only active motion is present and the blood resists the motion (E.R. Holman, personal communication, November 5, 2020).

Table D.4: The slope numbers of the tangents to the graphs of the exponential growth of the heart acceleration due to the rise of the heart rate. The slope numbers are shown for the contraction and relaxation.

	HR <70 bpm	70 bpm <HR <100 bpm	HR >100 bpm
Contraction	0	0.014	0.054
Relaxation	0	0.017	0.060

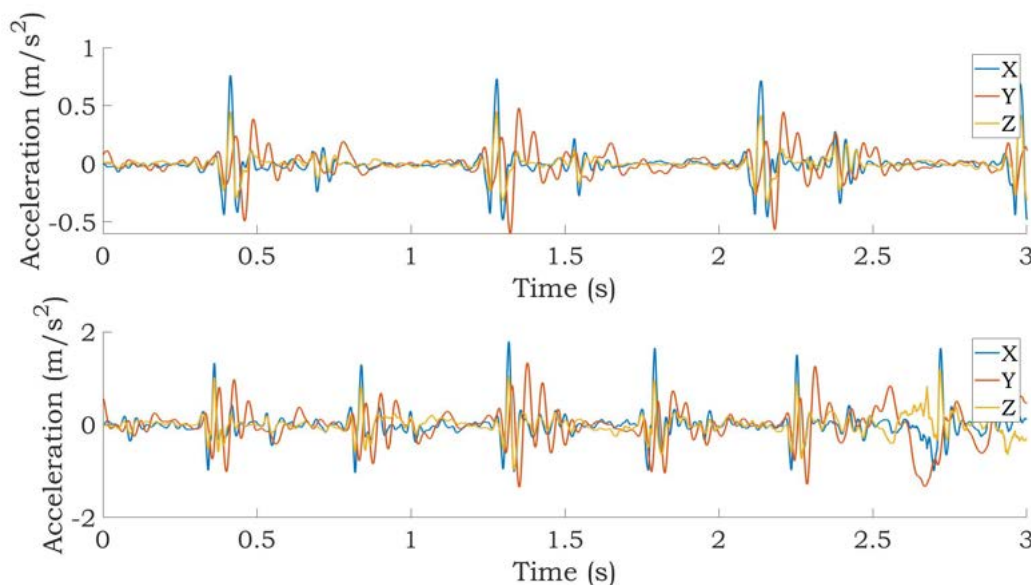


Figure D.13: The human acceleration measurements during rest and exercise visual presented.

Besides increasing the amplitude height, the duration of the heart cycle is also influenced by an increase in the heart rate. The influence of the heart rate on the cycle duration is investigated by Bombardini et al. [123]. A force sensor is attached to the chest of patients and measured the duration of the systole and diastole for different heart rates. Furthermore, the time duration for different heart

rates is also investigated by Bombardini et al. [122], where measurements are performed with a micro electromechanical system sensor that measures the motion. The systolic and diastolic time during rest and exercise shows the slope at which the percentage of the systole and diastole duration per total time is influenced due to the heart rate. In Figure D.14 this influence is shown, where the percentages are an average of the values found in both studies [122, 123]. In percentage terms, the duration of the diastole decreases for an increasing heart rate, while the percentage of the systole increases for an increasing heart rate. This means that for a heart in rest the duration of the diastole is larger than the duration of the systole. An increasing heart rate, however, decreases the diastolic time more than the systolic time of the total heart cycle.

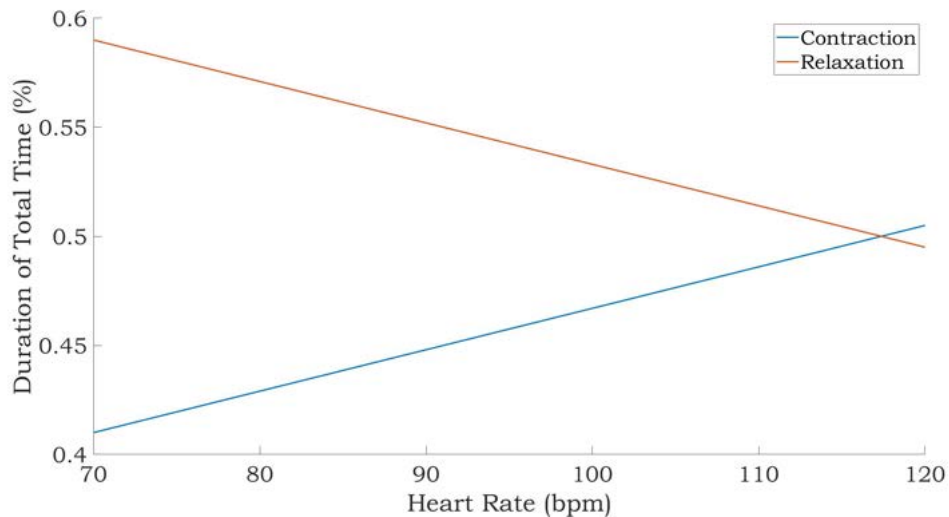
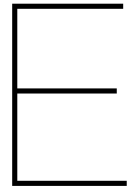


Figure D.14: The influence of the heart rate on the duration of the contraction and relaxation.

The influence of the heart rate on the acceleration peak and the contraction and relaxation time changes the surface below the acceleration signal, meaning that the velocity signal is also changed. As stated, the velocity values for the contraction and relaxation increases linearly, with a higher slope for the relaxation [119]. It should be validated that the surface change in the acceleration signal has a linear increasing influence on the velocity values generated.



Orientation

Besides the longitudinal axis measured with ultrasound in the four chamber view, also the circumferential and radial displacements are obtained via the ultrasound measurements. The pig heart acceleration signals also contain the information of all three axes. In this appendix it is analysed which axis should be used as input for the testing of the energy harvester.

E.1. PCA Pig Heart

First, a Principle Component Analysis (PCA) is performed. With a PCA it is calculated whether a dataset can be described by less variables but retain as much statistical information as possible [191]. Using PCA the principle axis of motion is determined, this results in a selection of the main axes used as input for the energy harvester. With PCA orthogonal components are calculated that describe, in this case, the acceleration data. Each principle component contains a certain statistical information, or in other words, a variance. The first principle component contains the most variance and the last principle component the least variance. It is normal to select the number of components for describing the data that covers 70% of the variance. The acceleration data, a three dimensional data set, gives three principle components. When the first principle component covers more than 70%, the acceleration signals multiplied by this principle component give one vector that describes the data. The magnitude of the components in the principle component display the contribution of a direction in the total motion.

The PCA analysis is performed for the pig heart acceleration signals, both at apical and basal location. Here it is analysed, for both locations, if one of the three axes has a larger contribution in the heart wall motion or not. This is analysed for the acceleration and velocity. If the variance of the first principle component is smaller than 70%, the second principle component is shown, in order to meet the 70% criteria. In Table E.1 and Table E.2 the PCA for the apical and basal velocity and acceleration signals can be seen, respectively. Here it can be seen how much an axis contributes to the first and, if needed, the second principle component. A contribution larger than 0.4 is taken as a sufficient influence of the axis in the principle component.

When first analysing Table E.1, the velocity signals, and comparing the principle components from the apical and basal segments, it can be seen that for the principle components of the apical segment the influence of the axes is more widely distributed. Only for pig 5 one axis has the largest contribution to the principle component. For the other pigs the influence of the axis is spread. When analysing the principle components from the basal segment, it can be seen that for two pigs one axis is the main contribution to the principle component, for two pigs it is two components, and one pig has a contribution of three axes to form the principle component. From the velocity signals it can be said that the velocity in the apical segment consist of a combination in the longitudinal, circumferential and radial motion, varying per pig. Since we don't know precisely how the accelerometer is placed during each separate measurement, it is unknown which direction has the largest contribution. But it is seen that the contribution is a combination of motions.

Table E.1: PCA of the apical and basal velocity signals.

	Apical			Basal		
	Total Variance (%)	PC1	PC2	Total Variance (%)	PC1	PC2
Pig 1	82.45	0.6057 0.7957 -0.002		73.17	0.8929 -0.2656 0.3637	
Pig 2	87.54	-0.1172 0.9914 -0.059	0.8774 0.1312 0.4615	83.91	-0.5618 0.5582 0.6105	
Pig 3	93.33	-0.1904 0.9316 -0.3096	0.9436 -0.0867 -0.3195	73.09	0.928 -0.2492 0.277	
Pig 4	87.47	0.4925 0.6994 0.5179		75.54	0.8429 -0.3218 0.4313	
Pig 5	87.43	0.2856 0.9429 0.1712		92.1	-0.3359 0.9401 -0.0583	0.8685 0.3331 0.367

For the acceleration signals the same observation is seen in Table E.2 as in the velocity analysis. Meaning that for the principle components of the apical segment the influence of the axes is more widely distributed. Neither one of the five pigs has a dominant axis in the apical segment determining the direction of the principle component. For the basal segment, two pigs have one dominant component in the principle component, two pigs have two dominant components and one pig has more dominant components in the principle components.

Table E.2: PCA of the apical and basal acceleration signals.

		Apical			Basal		
	Total Variance (%)	PC1	PC2	Total Variance (%)	PC1	PC2	
Pig 1	84.23	0.7885	-0.3189	80.57	0.9837		
		0.3378	-0.49		-0.1166		
		0.514	0.8113		-0.1366		
Pig 2	84.26	0.1564	0.6083	92.86	0.8667	-0.051	
		0.0304	0.7845		-0.4953	0.0306	
		0.9872	-0.1205		0.0594	0.9982	
Pig 3	89.09	-0.2082	0.4984	72.62	0.9853		
		-0.6692	0.5549		-0.0902		
		0.7133	0.6661		-0.1453		
Pig 4	82.27	0.5177	0.7566	88.39	0.9721	-0.2137	
		0.7505	-0.6257		0.1876	0.9557	
		0.4107	0.1898		-0.1407	-0.2023	
Pig 5	87.01	-0.2766	0.4938	82.34	0.976	0.2157	
		-0.5798	0.5984		-0.2176	0.9672	
		0.7664	0.631		0.0004	-0.1342	

In this analysis it can be seen that for the motion at the apical segment of the heart not one axis is the dominant motion axis. The contribution of the longitudinal, radial and circumferential axis is varying per pig. This could be due to the fact that the accelerometers are not placed in the same orientation on the pigs. However, this cannot be verified as the researcher was not present at the measurements. Regardless whether the accelerometer is always positioned exactly the same, the movement in the apical zone is a mix of the three axes. This should be kept in mind for the testing of an energy harvester intended for powering pacemakers. Since this can influence the reliability of the energy harvester and the amount of power harvested.

E.2. Comparison Three Dimensions

With the contribution per axis analysed for the motion, in this section the human velocity and acceleration amplitude are analysed for the longitudinal, radial and circumferential axes. For this analysis the STE measurements are used, since the TDI measurements only obtain the longitudinal direction. The longitudinal direction is measured in the four heart chamber view and the radial and circumferential direction is measured in the apical short axis view. Because of this only the apical septal segments are compared, since the basal and mid radial and circumferential are not measured in the apical short axis view. The velocity signals of the three axes from one patient can be seen in Figure E.1. In the figure it can be seen that there are differences between the velocity signals. However, in the three directions the same trajectory can be seen. The trajectory of the described IVV-peak, s-wave, e-wave and a-wave. As stated earlier, every person has a different heartbeat. This applies also to the radial and circumferential direction. The mean contraction and relaxation velocity and acceleration of the nine patients is shown in Table E.3. Here it can be observed that for the acceleration and velocity, the contraction and relaxation has a larger amplitude than for the radial and circumferential direction.

For the calculation of the circumferential velocity it should be kept in mind that the tangent of the angular velocity is used. To be able to perform the calculations, the radius of the ventricle at apical

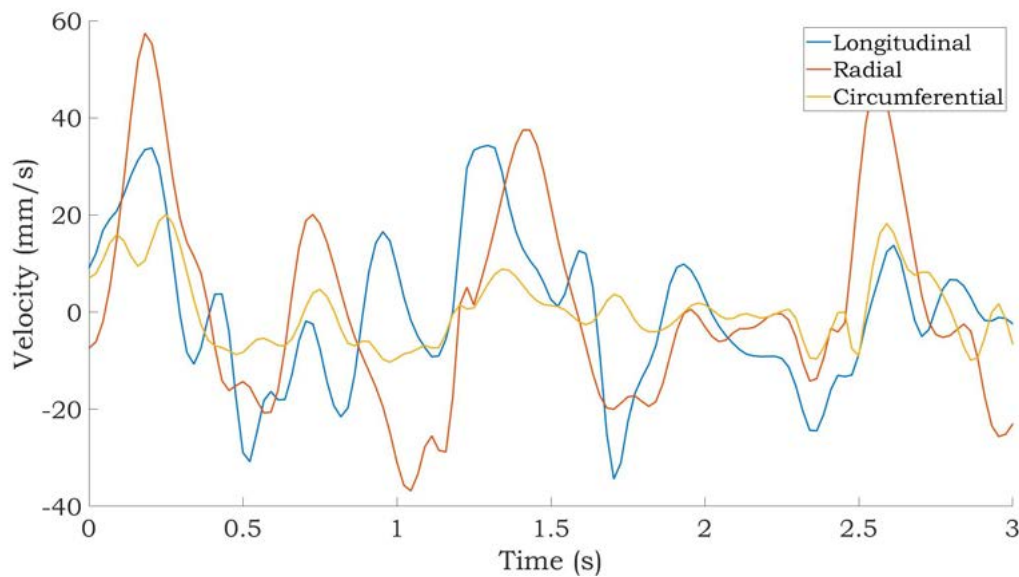


Figure E.1: The apical septal heart wall velocity of a human in the three directions.

Table E.3: The measured mean velocity and acceleration of the longitudinal, radial and circumferential apical septal position of the nine patients.

	Velocity		Acceleration	
	Contraction (mm/s)	Relaxation (mm/s)	Contraction (m/s ²)	Relaxation (m/s ²)
Longitudinal	38.74	-43.05	0.63	-0.67
Radial	30.34	-27.79	0.44	-0.43
Circumferential	14.90	-15.35	0.32	-0.33

height is obtained in EchoPAC. The found acceleration and velocity are thus an approximation of which it is not certain that this represents the reality. For now, it is assumed that the circumferential velocity and acceleration are lower than the longitudinal velocity and acceleration, but this should be investigated more thoroughly. Furthermore, the ultrasound measurements are performed by different laboratory technicians. This can result in different measurement values, as the measurement technique can differ per laboratory technician [112]. For future research it is advised to obtain measurements by the same laboratory technician.

E.3. Generator Orientation

In the first analysis it was seen that for the apical segment the contribution of the motion from the longitudinal, circumferential and radial direction is not dominated by one direction. The contribution of the directions is varying. This could be due to the fact that the accelerometer was not placed in the same position during each measurement or because the differences in the heartbeat per specie. In the second analysis, it was seen that in the human STE measurements the peak amplitude of the apical velocity and acceleration is higher than the two other directions. A traditional energy harvester can only harvest energy from one dimension. For the apical segment not one motion is dominant and on top of that was in the human measurements seen that the amplitudes are higher in the longitudinal direction. This results in that it is decided to use the longitudinal direction as input for the heart signal generator.

When harvesting in only one direction an amount of energy that can be harvested, present in the motion, is lost. How much energy is lost should be investigated and the energy harvesting direction should be optimized. However, the final orientation of the energy harvester design depends on the positioning of the leadless pacemaker, which is different for each person during surgery. Because

of this, during the design process it must be taken into account that the harvester does not end up in the optimal position. In a non-optimal position the energy harvester should also generate enough power to recharge the battery of the pacemaker. Furthermore, another challenge is the heart wall rotation and the fact that the leadless pacemaker is fixated in soft tissue. In [94] it is stated that for an energy harvester it is a challenge to guide the movement in the desired direction, while the undesired directions are constrained. The rotational movement of the heart wall and because of the fixation in soft tissue, making a wobbly movement of the leadless pacemaker, can influence the reliability of the energy harvester and the amount of power harvested. Zurbuchen et al. [2] stated that their model should be validated for rotational components, in order to investigate the impact of Coriolis-, Euler-, and outer centrifugal force on the device. A next step, after testing the energy harvester on a shaker, is to test the energy harvester with the heart wall environment imitated. The energy harvester should be fixated in a material just as soft as the heart wall and be tested on the three dimensional motion. Via this, the influence of the wobbly motion can be investigated. It is also a good idea to place an energy harvester in a environment, where the heart cycle is simulated and realistic heart wall movement is obtained. For instance, the LifeTec Group in Eindhoven is specialized in this.



Heart Signal Generator

The characteristics discussed in previous appendices are used to design a heart signal generator to approximate the acceleration signal of a human. The output of this generator can be used to test energy harvesters for the purpose of powering a pacemaker. The code is explained step by step and the results are presented.

F.1. Code

In this section the heart signal generator code is explained. Before running the generator code the user must enter the desired heart rate value and the number of cycles. The number of cycles determines the length of the signal, in combination with the heart rate. The generator first ensures that heartbeat has the correct trajectory and that it is slightly different for each run. How this is done is explained in the Section *Trajectory*. Then in Section *Scaling and Heart Rate Influence*, it elaborated how the scaling and the influence of the heart rate are performed in the code. Section *Signal between Contraction and Relaxation* explains the final touches to obtain a correct acceleration signal.

F.1.1. Trajectory

First, it is explained how it is ensured that the signal is slightly different every run, using the pig heart acceleration signals. As stated in Appendix D, the contraction and relaxation parts are isolated from the five pig heart acceleration signals. The heart signal generator uses the pig signals as building blocks, where a simulated time response of the dynamic model of the contraction and relaxation peaks is obtained. The dynamic systems are obtained from a transfer function estimation. This estimation is found from an input vector and the original data using a nonlinear least-squares search method. These input vectors are obtained by trial and error in order to maximise the agreement between the original signal and the signal obtained with the transfer function, see Figure F.1. The specified number of poles in the transfer function is nine. In Equation F.1 it can be seen how the transfer functions are constructed. The goodness of the fit obtained is 83.05% for the contraction and 92.32% for the relaxation. This is determined with a normalized root mean square error between the simulated response and measurement data. The dynamic systems are loaded into the heart signal generator.

$$H(s) = \frac{Y(s)}{X(s)} = \frac{b_0 + b_1s + \dots + b_8s^8}{a_0 + a_1s + \dots + a_9s^9} \quad (\text{F.1})$$

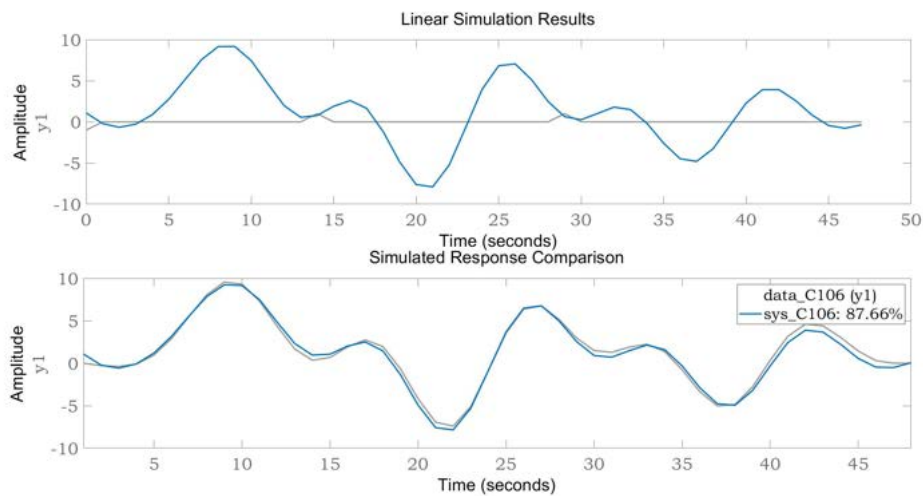


Figure F.1: System identification for the contraction peak of a pig signal. In the first figure the input vector corresponding to the contraction data is shown. In the second figure the simulated response of the dynamic system can be seen, compared to the measured data.

The heart signal generator starts with a random selection of one of the five contractions and relaxations of the pig signals. The corresponding identified dynamic system and initial conditions are selected. The `lsim` function gives a simulated time response of the dynamic system model to the input history. Every run a new input vector is generated for both the contraction and relaxation, varying in impulse locations and peak heights, causing a different simulated time response. The fact that every person has a different heartbeat is imitated. To obtain this input vector, first the number of impulses are specified. Then the locations and height of the impulses are randomly determined in a for loop, with a specified distance between the pulses. A validation is added in this loop, to check whether the new input vector does not give a totally random time response. As said, the contraction and relaxation are

used as building block. While a variation is desired, a totally different signal unrelated to a heartbeat is undesired. For the input vector for the contraction, a second validation is added. Here, it is validated whether the positive acceleration peak is larger than the negative peak. This in order to make sure that a plausible acceleration signal is obtained. In the second part of the code a matrix is formed where the newly produced input factor is multiplied with the number of specified cycles. Here a randomness factor is added. The impulse heights in the new input matrix are multiplied with a factor between 0.6 and 1.4, in order to obtain small differences in the yet to be produced contraction and relaxation peaks. With the new input vectors formed, the simulated time response of the contraction and relaxation is estimated. For this, as stated, the `lsim` function is used. The input is the dynamic system identified for the pig heart acceleration signals, the new input vectors, the time vector and the initial condition corresponding to the pig heart signals.

F.1.2. Scaling and Heart Rate Influence

Both the contraction- and the relaxation-signal of the pig heart are adjusted to add more variation, and are scaled to remove overestimation. The peaks are scaled to the amplitudes in human signals, as discussed in Appendix C.

The contraction is scaled to a value between 0.26 m/s^2 and 1.82 m/s^2 , and each cycle in the new signal it is varied with a scale-factor between 0.8 and 1.2, as the human heart contracts with a slightly different acceleration each time. In the measurements performed at the LUMC, it is seen that the relaxation peak is lower than the contraction peak. In the generator, the relaxation peak is linked to the contraction. The peak is scaled to a random factor times the contraction peak. This factor is randomly chosen each new cycle, and lies between 0.3 and 0.7.

The influence of the heart rate on the acceleration is included, as explained in Appendix D. With an increasing heart rate, the peak of the relaxation increases faster compared to the peak of the contraction. Also, the influence of the heart rate on the contraction and relaxation time duration is added to the acceleration signal. The duration of the contraction parts and relaxation parts are scaled with the heart rate, as explained in Appendix D. The time between the two peaks is determined by the duration of a heart cycle and the combined duration of a contraction and relaxation for a specific heart rate, as determined in Appendix D.6.

Furthermore, it is assured that the integral of the positive acceleration equals the integral of the negative acceleration, to prevent random trends in the velocity signal. Finally, another visual validation check is added to make sure that the positive peak of the relaxation does not exceed the bounds of common-sense. For example for a heart rate at rest, the peak of the relaxation should be smaller than the peak of the contraction.

F.1.3. Signal between Contraction and Relaxation

The next part of the generator is to generate the parts between the contraction and relaxation. The parts are a sum of cosine and sine with varying amplitudes and frequencies. These parts have a low acceleration of almost zero, and will not affect the movement of the energy harvester and the amount of generated power.

The contraction peak, relaxation peak and the parts in between the peaks, are pasted one behind the other combined sequentially, and repeated for the number of heart cycles entered by the user. A filter is added in order to smooth the transition points from the different signal parts. The detection of these locations can be seen in Figure F.2. The signals are connected with a forward and backward auto regressive fit, and smoothed with a moving median filter to ensure a smooth transition. Finally, the signal is prepared for the shaker. The sampling frequency of the signal is adjusted to the frequency needed for the shaker and the signal is scaled from m/s^2 to g , where $1g = 9.81\text{m/s}^2$. The generated acceleration signal is saved and ready to be used for the testing of an energy harvester intended for powering a leadless pacemaker.

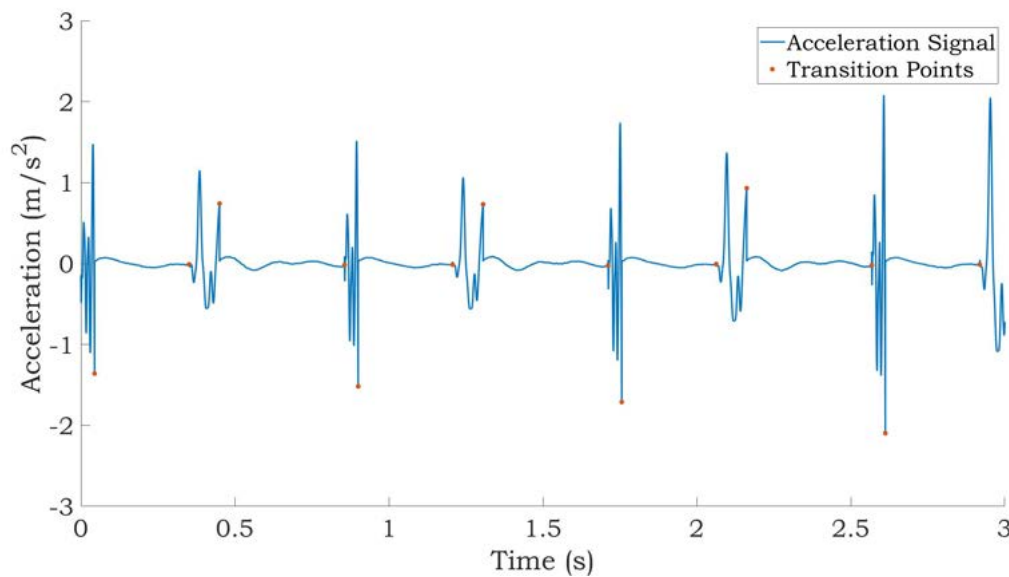


Figure F.2: Detection of the transition points that are smoothed by the filter.

F.2. Results

This section shows examples of acceleration signals generated by the heart signal generator. In Figure F.3 two acceleration signals with their corresponding velocity signals can be observed, generated for a heart rate of 70 bpm. When comparing the two signals generated for the same heart rate, differences can be seen in the peak height and the trajectory of the contraction and relaxation peaks. This is due to the random selection of one of the five pig heart contractions and relaxations, in combination with the new input vector generated for the dynamic system. When analysing the velocity signals the same shape as described in Appendix C can be seen. The IVV-peak followed by the s-wave, e-wave and a-wave. Also, differences between the two velocity signals can be seen. These differences imitate the fact that every person has a different heartbeat, and thus a different heart acceleration and velocity signal. In rest, the relaxation has a longer time duration in the total heart cycle than the contraction. Because of this longer duration, is in the acceleration signal the surface under the relaxation peak larger than under the contraction peak. This explains the higher velocity for the relaxation.

In Figure F.3, also a heart signal generated at 130 bpm can be seen. When comparing this signal to the signals generated for 70 bpm, a difference in the amplitude and the duration of the heart cycle is observed. The same holds when the velocity signals are compared. Increasing the heart rate, increases the peak height in the acceleration and velocity signals and the heart cycle duration decreases, as described in Appendix D. The shape of the velocity, with the IVV-peak, s-wave, e-wave and a-wave persists for higher heart rates. Figure F.4b shows the FFT corresponding to the acceleration signal in Figure F.4a. Comparing this FFT to the FFT of the pig heart acceleration signal in Figure D.5a, similarities can be observed, since both FFT's show a higher power level at the lower frequencies, followed by a dip around 50 Hz, followed by a small increment around 60 and 70 Hz.

In Appendix D was stated that it has to be validated whether the velocity amplitude of the s-wave and e-wave increases linearly and the contraction and relaxation acceleration increases exponentially. In Figure F.5a and Figure F.5b the influence of the heart rate on the velocity and acceleration is presented. The points in both figures represent the average amplitude of ten heart signals on that specific heart rate for the contraction and relaxation. The lines fitted in both figures show the trend. In Figure F.5a, a linear increase for the contraction and relaxation can be seen, with $R = 0.8173$ and $R = 0.9050$. In Figure F.5b an exponential increase for both the contraction and relaxation can be seen with $R = 0.9903$ and $R = 0.9827$. It can be concluded that the velocity has indeed a linear increase and the acceleration increases with an approximated exponential function for an increasing heart rate. The exponential trend and the linear trend are related, since the acceleration is the differentiation of the

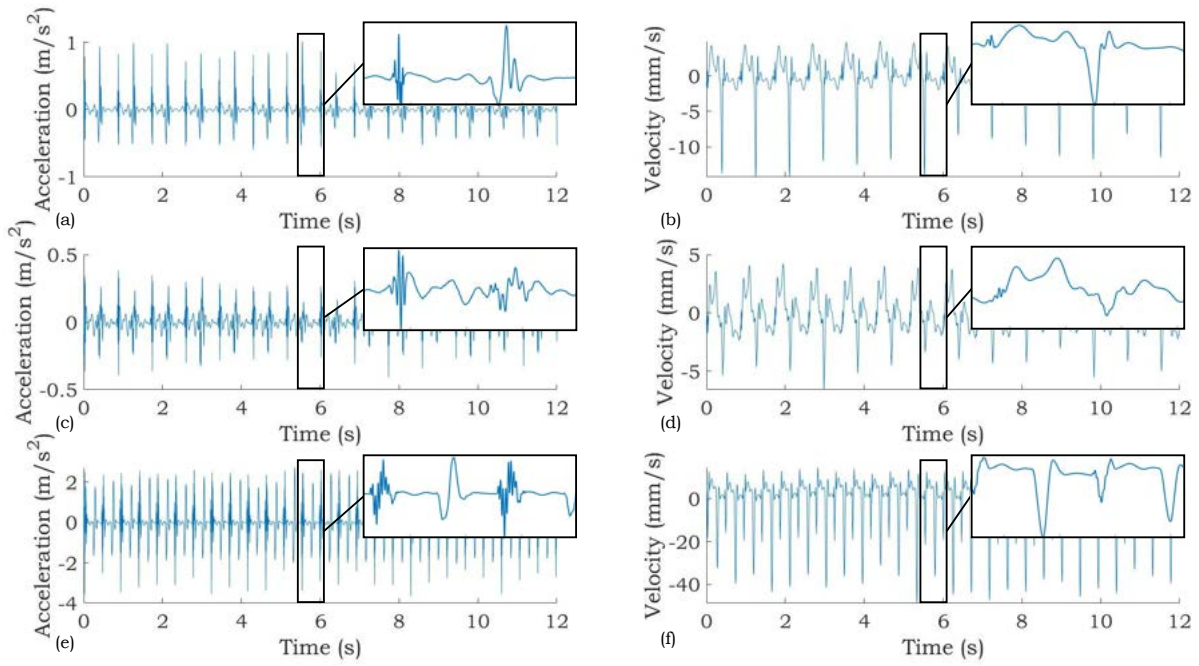


Figure F.3: Three examples of signals generated by the heart signal generator for a heart rate of 70 bpm and 130 bpm. (a,b) The acceleration and velocity profile of a heart signal of 70 bpm. (c,d) The second acceleration and velocity profile of a heart signal of 70 bpm. (e,f) The acceleration and velocity profile of a heart signal of 130 bpm.

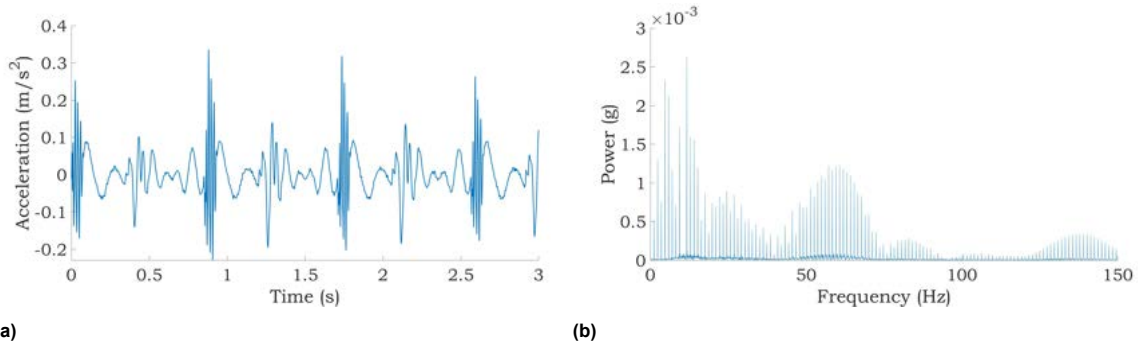


Figure F.4: Signal generated by the generator. (a) A generated acceleration signal at 70 bpm. (b) The corresponding FFT of the acceleration signal.

velocity. The slope of the linear increasing e-wave velocity is higher than the IVV-peak slope, as in [119].

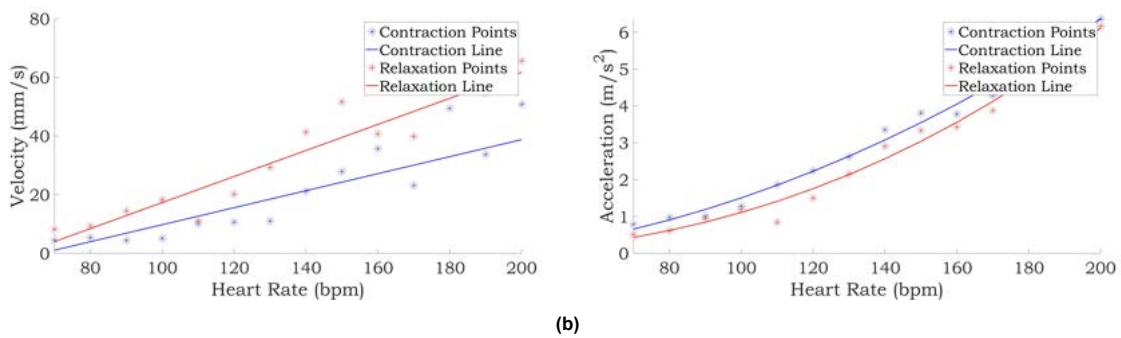


Figure F.5: The influence of the heart rate on the (a) Velocity in the heart signal generator and (b) The acceleration signals generated by the heart signal generator.

When analysing the velocity signals obtained from the ultrasound measurements at the LUMC, the peak height of the s-wave generated in this heart signal generator is relatively low. In Appendix C where the longitudinal velocity is shown of all the six segments, it is seen that the s-wave amplitude of the apical and mid segment is higher than in Figure F.3. The peak height of the s-wave in Figure F.3 has more similarities with the velocity signal measured at the apical lateral region. The similarities can also be observed in literature, where the heart wall velocity is measured for the base, mid and between the apical segment and the apex [192]. Here, it can be seen that for the apical-apex segment the velocity at the s-wave is much lower than for the mid region and basal region. The shape of the s-wave is also different, the IVV-peak is lower and the s-wave is higher and wider. This observation is also found by Lotfi-Tokaldany et al. [116], where the velocity is analysed for the three regions. For the apex is the s-wave velocity 0.32 cm/s, which corresponds to the velocities generated in the heart signal generator. When analysing the location of the accelerometer placed during the pig heart measurements, the location of this sensor is between apical septal and apical lateral region. This could explain the fact that the velocity signal has more similarities with this location, than with the motion at the mid septal segment. As explained, the heart has different motions at different heart locations. It differs for endocardial and epicardial, in rotational and translation motion and from base to the apex. It is thought, that this difference from base to apex shows the difference in the peak height of the s-wave. The heart motion differs for each segment, which can be seen in the velocity and acceleration signal. The amplitude can be scaled for the apical septal and mid septal segments, where a leadless pacemaker is placed, but the pig heart acceleration signal used for the heart signal generator are measured between the apical septal and apical lateral region. Scaling the signals with the peak amplitudes from the apical septal and mid septal segments does not change the trajectory of the velocity signal. The trajectory of the velocity signal only changes when the specific segments are measured separately, or in other words, when the heart motion is measured for the different segments.



Energy Harvester

For the lab experiments, an electromagnetic energy harvester with moving mid magnets, a static coil and repulsive magnets at the top and bottom was designed. The heart signals have a small acceleration amplitude, resulting in the fact that the stiffness of the energy harvester must be low to obtain motion in the mid magnets to harvest some energy. For the designed energy harvester a problem arose, since the shaker must be held vertical for the controller to function properly, so the energy harvester was also placed in a vertical position. The stiffness of the energy harvester was low. Due to the influence of the gravity did the magnets not float in the middle, but had a lower equilibrium outside the coil. Motion of the magnets outside the coil does not result in any power generation, so this energy harvester could not be used for the experiment. The energy harvester used during experiments was already present in the lab. The specifications of the used energy harvester are shown, followed by the design process of the unused energy harvester.

G.1. Energy Harvester for Experiments

The energy harvester used during the experiments is an energy harvester consisting of a stack of eight moving magnets and a static coil. This energy harvester was designed by M. de Jong, K. van Puffelen, J. Roos, E. van de Wetering during their Bachelor thesis and was available in the lab. In this section the specifications of this energy harvester are shown. The energy harvester with moving mid magnets and a static coil has spring magnets on both sides of the moving magnet, giving a nonlinear restoring force. These repulsive magnets are clamped in the end caps made of 3D printed PLA. The tube is made of transparent PVC and ferrofluid is added around the magnets as lubrication. In Figure G.1a the dimensions of the energy harvester are shown. In order to reduce the local air damping in the tube, ring magnets have been used for the moving mid magnets. The characteristics of the magnets used can be seen in Table G.1. Table G.2 presents the specifications of the energy harvester.

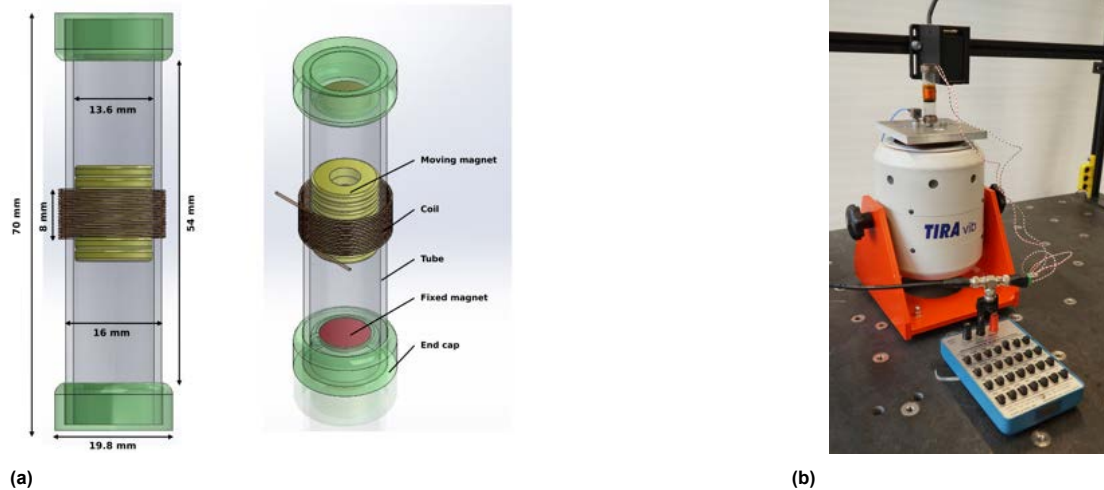


Figure G.1: The energy harvester. (a) A schematic image of the energy harvester with dimensions specified. (b) The energy harvester attached on the shaker.

Table G.1: Characteristics of the two magnets used

	Diameter [mm]	Thickness [mm]	Flux density [T]	Mass [g]
NdFeB-N40	13 (6*)	2	1.25	1.56
NdFeB-N42	10	1	1.22	0.59

* Inner diameter of the ring magnet

Table G.2: Specifications of the energy harvester

Coil resistance [Ω]	160.9
Inductance [mH]	8.49
Coil windings	680
Wire diameter [μm]	71
Moving mass [g]	12.47

The energy harvester is modelled as a mass, spring and damper system. The equation of motion for this energy harvester is Equation G.1. The corresponding nonlinear restoring force in Equation G.2, determined via an axisymmetric model in COMSOL and fitted in Matlab. A total damping of 5% was estimated, resulting in $\zeta = 0.05$ [193].

$$m \cdot \frac{d^2z}{dt^2} + c \cdot \frac{dz}{dt} + k \cdot z(t) = -m \cdot \frac{d^2y}{dt^2} = -F \quad (\text{G.1})$$

$$k \cdot z(t) = 396 \cdot 10^3 \cdot z(t)^3 + 32.51 \cdot z(t) \quad (\text{G.2})$$

They analysed the influence of the ferrofluid used in a finite element model in COMSOL. The Coulomb friction will change into viscous friction, which was in this case lower than the Coulomb friction. The stick slip effect of the Coulomb friction will also disappear.

G.2. Design Process of the unused Energy Harvester

This section will first introduce the COMSOL Multiphysics model, followed by the dynamical analysis and the prototyping of the energy harvester.

G.2.1. COMSOL Multiphysics

In COMSOL Multiphysics a model of the desired energy harvester was made, in order to obtain the force-displacement graph to determine the stiffness. To reduce calculation time, an axisymmetric 2D model was chosen. The model geometry can be seen in Figure G.2a. In the middle (the half of) the two moving magnets can be seen, with on the top and bottom the repulsive magnets. Around the magnets a large area of air is simulated, in order to mimic the environment. In Figure G.2b the moving mid magnets during a parametric sweep and the magnetic flux density (T) can be seen. A parametric sweep is performed, where the moving mid magnets are swept from the bottom to the top of the harvester by which and the force-displacement data is obtained, which can be loaded into Matlab.

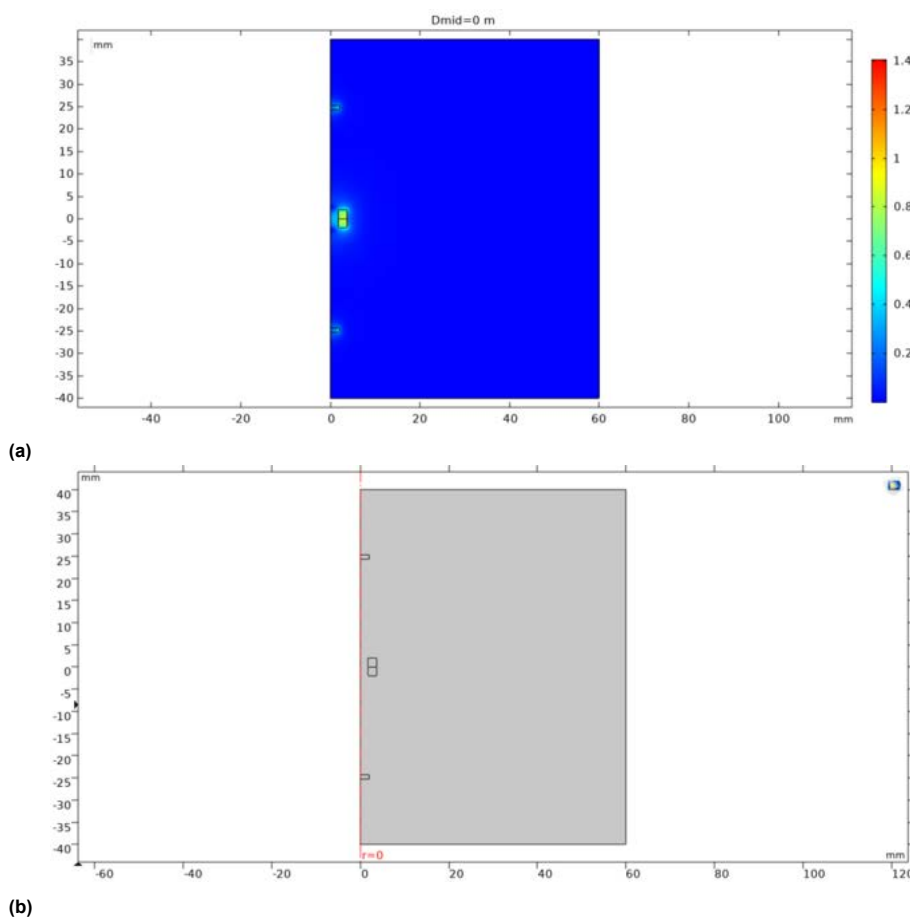


Figure G.2: Analysis performed in COMSOL. (a) The magnet design in COMSOL, with two moving magnets in the middle, spring magnets (one on the top and one on the bottom), surrounded by air. (b) The magnetic flux density (T) with a displacement of 38 mm.

G.2.2. Dynamical Analysis

The force-displacement data was loaded into Matlab and a function was fitted onto the data point with `cftool`, Figure G.3. It can be seen that the function does not fit the entire force-displacement data. However, the region of interest, between -5 mm and 5 mm has a good fit, which is sufficient for the analysis. The slope numbers of the fitted line on the force-displacement data points represent the stiffness coefficients of the moving magnet configuration. The energy harvester was modeled as a Duffing oscillator, Equation G.3, a combination of G.1 and G.2. Where m is the mass of the moving magnets, c is the damping coefficient, k_1 the linear stiffness term and k_3 the nonlinear stiffness term.

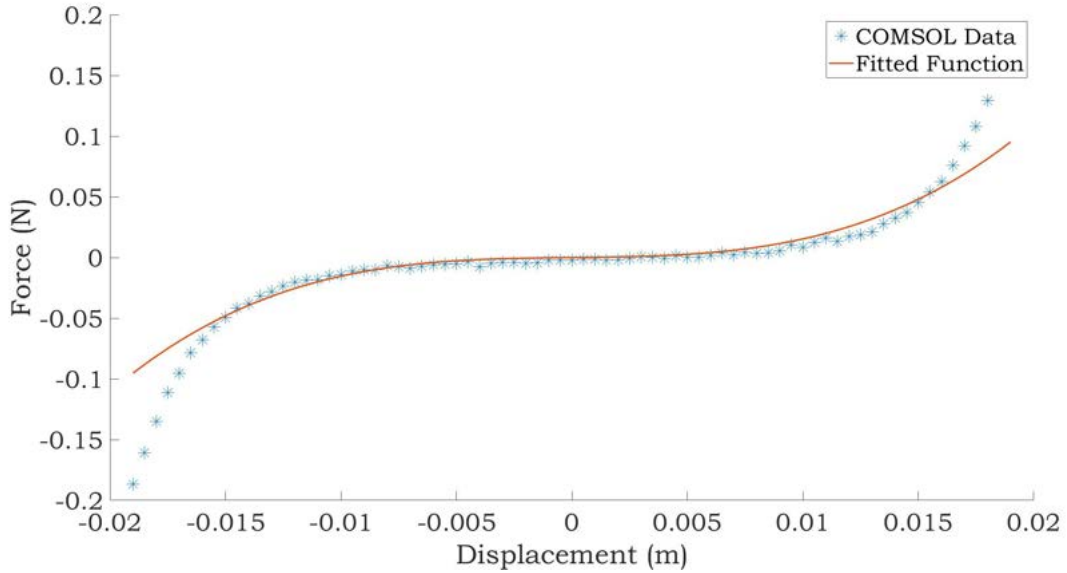


Figure G.3: The force-displacement data obtained from the COMSOL model on the fitted function in Matlab.

$$F = m\ddot{x} + c\dot{x} + k_1x + k_3x^3 \quad (\text{G.3})$$

The linear and nonlinear stiffness found in the simulation are: $0.2x + 13330x^3$. The mass of the moving magnet is 1 gram. The damping coefficient is calculated with Equation G.4, where the damping factor ζ was estimated at 3%.

$$c = 2 \cdot m \cdot \zeta \cdot \sqrt{\frac{k_1}{m}} \quad (\text{G.4})$$

These values were used in the ordinary differential equation (ODE) solver, where a heart signal generated at 160 bpm was used as input, since lower heart rates showed a small displacement of the moving mid magnets. The simulated displacement and velocity of the energy harvester can be seen in Figure G.4a and Figure G.4b, respectively. A peak to peak amplitude of 8 mm was the largest amplitude found for this configuration with different magnet combinations, so it was decided to make a prototype of this.

G.2.3. Prototyping

After the dynamical simulation, the energy harvester was build. The length and inner diameter of the Acrylic tube are 50 mm and 8 mm, respectively. The end caps for the magnets were 3D printed and for the copper coil 500 windings were made. The dimensions and properties of the magnets used can be seen in Table G.3. With the energy harvester placed in vertical position and observing the mid magnet position, it was seen that the magnets are not floating in the middle, but at a lower point outside the coil. Making the energy harvester not usable for testing.

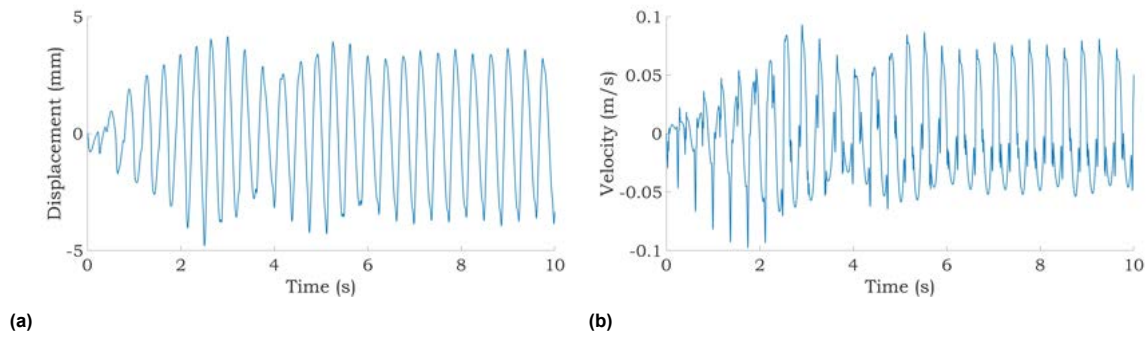


Figure G.4: The results of the ODE solver. **(a)** The displacement of the moving magnet on the generated heart signal of 160 bpm. **(b)** The velocity of the moving magnet by the motion of the generated heart signals of 160 bpm.

Table G.3: The dimensions and properties of the magnets used in the energy harvester design.

	Diameter [mm]	Height [mm]	Mass [g]	Flux Density [T]
NdFeB-N35	7.4(3.5*)	2	0.498	1.17
Sm2Co5-YX20	4	1	0.094	0.9

*Inner diameter of the magnet



Heart Wall Imitation

During the graduation project, it was also investigated how the heart wall could be imitated. This could be used in further research on the effects of soft tissue on the power generation of the motion energy harvester. Although it has been investigated, it was not used during experiments in this research, because it was out of scope of the research question.

H.1. Material

In order to investigate whether the pacemaker obtains a wobbly motion due to the heart wall motion, the heart wall itself must be simulated. For the experiment the mechanical properties of the heart wall are important. The material used during the experiment should have the same Young's modulus and thickness as the heart wall. In this way it can be investigated which motion a pacemaker makes in the heart, during the heart contraction and relaxation. The Young's modulus of the cardiac muscle lies between 10-15 kPa and the Shear modulus between 5-50 kPa [194, 195]. In literature, materials used to reproduce the mechanical properties of the human skin are silicone elastomers or gelatinous substances [196]. The human skin has other mechanical properties than the human heart wall. However, it is a good start in order to mimic soft human tissue. Another material that can be used to reproduce the heart wall is agarose. Agarose is a hydrogel, just as gelatin, and is a polysaccharide extracted from seaweed. It becomes a gel in response to temperature reduction [197]. The difference between gelatin and agarose is, however, that the melting temperature of gelatin lies around the body temperature [198]. Due to this, and the fact that gelatin can be kept only one to two weeks in the refrigerator, gelatin will not be used as material in this experiment.

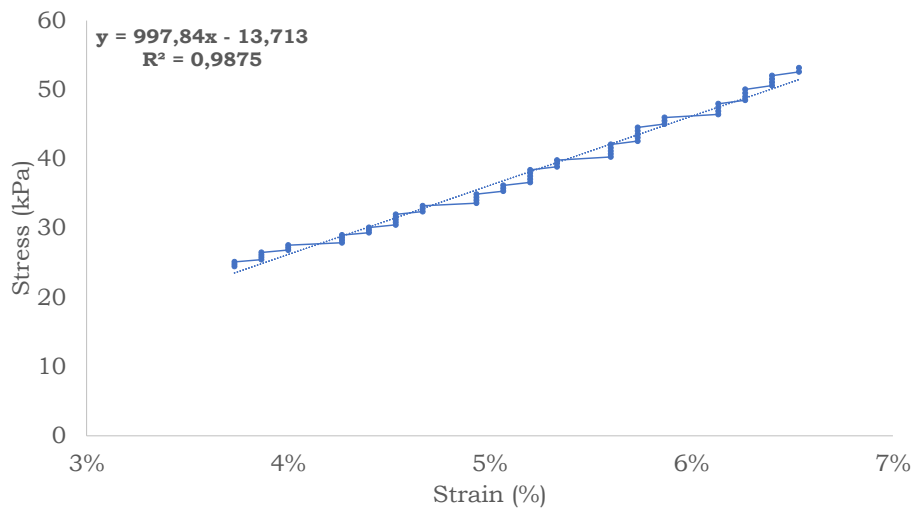
To find the right material for the experiment, several mixtures are made to test if they meet the heart wall properties. Three of these mixtures are made from silicone. For silicone two components are needed namely, a *A* component, which is the filler, and a *B* component, which is the basis. The silicone used is Poly-Sil PS 8530 SET and the mixing concentration for component *A* and *B* is 1:1. However, from literature it is known that by reducing the filler concentration, the stiffness from the silicone decreases, it increases its flexibility [199]. In other words, the filler can tune the properties of the silicone elastomers [196]. The first mixture consists of 1:1 of *A*:*B*, the second mixture of 1:3 and the third mixture of 1:7. A fourth mixture is made, this mixture is made from agarose, consisting of 3% agarose. The four mixtures can be seen in Figure H.1.



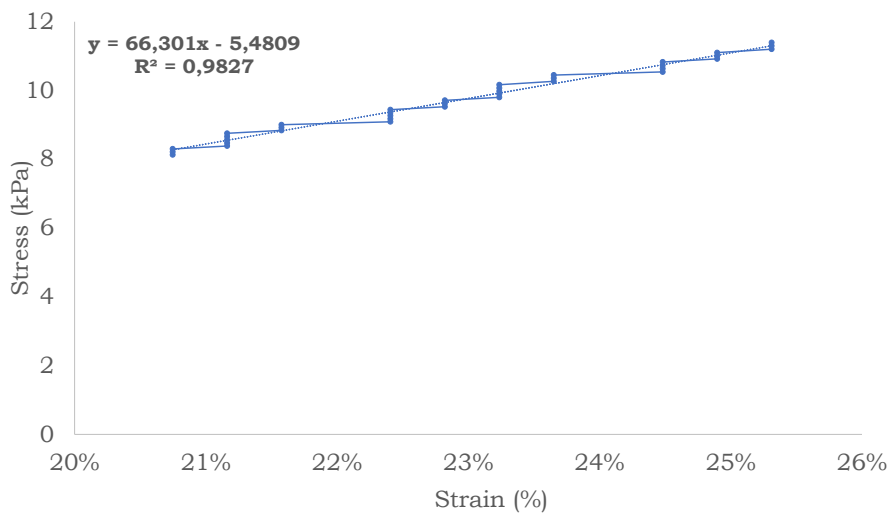
Figure H.1: The four samples obtained for the mechanical tests.

With the three silicone mixtures, mechanical tests are performed to measure the Young's modulus, in order to compare this to the Young's modulus of the heart wall. It was decided not to use the agarose mixture, since it was felt by hand that the Young's modulus was too high in order to imitate the heart wall tissue. Besides this, agarose is also maintainable for two weeks. For experiments something that lasts longer is desired. The mechanical tests are performed on a Mark 10, where the force-displacement of the material is measured. With the force and corresponding displacement, the strain and stress can be calculated when the surface is known. Using the strain and stress, the Young's modulus can be calculated. The stress-strain graphs for the silicone 1:1, 1:3 and 1:7 mixtures can be seen in Figure H.2a, Figure H.2b and Figure H.2c, respectively.

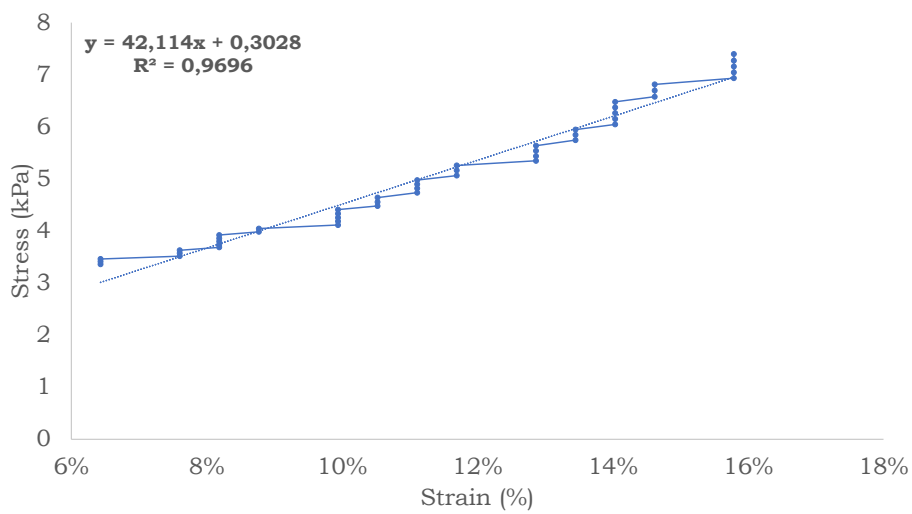
In the three figures it can be seen that the Young's Modulus of the three mixtures are 997.84 kPa, 66.30 kPa and 42.14 kPa, respectively. As expected, reducing the concentration of the filler component decreases the Young's modulus. In literature, the influence of the filler concentrations used differs. Since Markert et al. [200] found that a concentration of 4% of the filler component gives a Young's modulus of 13.1 kPa, but Saleem et al. [199] found that a filler concentration of 4% gives a Young's modulus of 21 MPa. This difference may be due to a difference in molecular structure [201]. However, in this case for a filler concentration of 12.5% the Young's modulus is 42.14 kPa. This Young's modulus imitates the



(a)



(b)



(c)

Figure H.2: The stress-strain graphs. (a) The 1:1 silicone mixture. (b) The 1:3 silicone mixture (c) The 1:7 silicone mixture.

properties of the skin, but the Young's modulus of the heart wall is lower [202]. It can be investigated whether different types of silicone approach the Young's modulus of the heart wall more closely. At least, this analysis show that the Young's modulus can be approximated by reducing the filler.

With silicone, the mechanical characteristics of the heart wall can be imitated. However, the influence of connective tissue formation, scar tissue and the blood flow in the heart ventricle is not included. The influence of these phenomena on the leadless pacemaker motion and thus the energy harvester motion is unknown. It should be investigated whether these things should be included in the testing of an energy harvester intended for powering pacemaker or not. Furthermore, the thickness of the material should match the thickness of the heart wall. In order to fixate this imitated heart wall material to the shaker, the material can be clamped between two plates. One with a hole in the middle, so that the energy harvester can be fixated in the soft tissue. The bottom plate can be screwed to the shaker.

Bibliography

- [1] Mark A. Wood and Kenneth A. Ellenbogen. Cardiac pacemakers from the patient's perspective, 5 2002. ISSN 00097322.
- [2] A. Zurbuchen, A. Pfenniger, A. Stahel, C. T. Stoeck, S. Vandenberghe, V. M. Koch, and Rolf Vogel. Energy harvesting from the beating heart by a mass imbalance oscillation generator. *Annals of Biomedical Engineering*, 41(1):131–141, 1 2013. ISSN 00906964. doi: 10.1007/s10439-012-0623-3.
- [3] Ning Li, Zhiran Yi, Ye Ma, Feng Xie, Yue Huang, Yingwei Tian, Xiaoxue Dong, Yang Liu, Xin Shao, Yang Li, Lei Jin, Jingquan Liu, Zhiyun Xu, Bin Yang, and Hao Zhang. Direct Powering a Real Cardiac Pacemaker by Natural Energy of a Heartbeat. *ACS Nano*, 13(3):2822–2830, 3 2019. ISSN 1936086X. doi: 10.1021/acsnano.8b08567.
- [4] D Briand, E Yeatman, and S Roundy. *Micro Energy Harvesting*. ProQuest Ebook Central, Berlin, 2015. URL <https://ebookcentral-proquest-com.tudelft.idm.oclc.org/lib/delft/detail.action?docID=1896062>.
- [5] Shaofan Qi, Roger Shuttleworth, S. Olutunde Oyadiji, and Jan Wright. Design of a multiresonant beam for broadband piezoelectric energy harvesting. *Smart Materials and Structures*, 19(9), 9 2010. ISSN 09641726. doi: 10.1088/0964-1726/19/9/094009.
- [6] Kjartan Bjarni Kristjánsson and Steinar Þorvaldsson. *Test System to Evaluate Energy-Harvesting Technologies for Wireless Sensors*. PhD thesis, University of Gothenburg, Gothenburg, 2016.
- [7] Igor Neri, Flavio Travasso, Riccardo Mincigrucci, Helios Vocca, Francesco Orfei, and Luca Gammaitoni. A real vibration database for kinetic energy harvesting application. *Journal of Intelligent Material Systems and Structures*, 23(18):2095–2101, 12 2012. ISSN 1045389X. doi: 10.1177/1045389X12444488.
- [8] Hiroshi Kanai, Michie Sato, Yoshiro Koiwa, and Noriyoshi Chubachi. Transcutaneous Measurement and Spectrum Analysis of Heart Wall Vibrations. Technical Report 5, 1996.
- [9] Hiroshi Kanai, Hideyuki Hasegawa, Noriyoshi Chubachi, Yoshiro Koiwa, and Motonao Tanaka. Noninvasive valuation of Local Myocardial Thickening and Its Color-Coded Imaging. Technical Report 4, 1997.
- [10] Food and Drug Administration. CFR - Code of Federal Regulations Title 21. 8, 2019. doi: 21CFR870.
- [11] B Chittester. Medical Device Clinical Trials – How Do They Compare with Drug Trials?, 2014. URL <https://www.mastercontrol.com/gxp-lifeline/medical-device-clinical-trials-how-do-they-compare-with-drug-trials-/>.
- [12] Walter F. Boron and Emile L. Boulpaep. *Medical Physiology A Cellular and Molecular Approach*. 2012. ISBN 978-1-4377-1753-2.
- [13] Cleveland Clinic. Heart Valves, 2018. URL <https://my.clevelandclinic.org/health/articles/17067-heart-valves>.
- [14] Chien Jung Lin, Chieh Yu Lin, Chen Hao Chen, Bin Zhou, and Ching Pin Chang. Partitioning the heart: Mechanisms of cardiac septation and valve development, 9 2012. ISSN 09501991.
- [15] Satoshi Nakatani. Left Ventricular Rotation and Twist: Why Should We Learn? *Journal of Cardiovascular Ultrasound*, 19(1):1, 2011. ISSN 1975-4612. doi: 10.4250/jcu.2011.19.1.1.

- [16] Jana Vasković. Layers of the heart, 2020. URL <https://www.kenhub.com/en/library/anatomy/layers-of-the-heart>.
- [17] Ruta Jasaityte and Jan D'Hooge. Strain rate imaging: Fundamental principles and progress so far, 10 2010. ISSN 17555191.
- [18] Spyretta Golemati and Konstantina S Nikita. *Cardiovascular Computing-Methodologies and Clinical Applications*. 2019. ISBN 978-981-10-5092-3. URL <http://www.springer.com/series/10358>.
- [19] Kevin Beck. Phases of the Cardiac Action Potential, 10 2018. URL <https://sciencing.com/phases-cardiac-action-potential-6523692.html>.
- [20] Melanie Humphreys, Celia Warlow, and John McGowan. Arrhythmias and their Management. In *Nursing the Cardiac Patient*, pages 132–155. Wiley Blackwell, 8 2013. ISBN 9781118785331. doi: 10.1002/9781118785331.ch10.
- [21] R. E. Klabunde. Cardiac Cycle - Isovolumetric Contraction (Phase 2), 9 2016. URL <https://www.cvphysiology.com/Heart%20Disease/HD002b>.
- [22] Espen W. Remme, Lars Hoff, Per Steinar Halvorsen, Edvard Naerum, Helge Skulstad, Lars A. Fleischer, Ole Jakob Elle, and Erik Fosse. Validation of cardiac accelerometer sensor measurements. *Physiological measurement*, 30(12):1429–1444, 2009. ISSN 13616579. doi: 10.1088/0967-3334/30/12/010.
- [23] Ole-Johannes H.N. Grymyr. *Myocardial function and 3D motion analysis using a three-axis accelerometer during cardiac surgery*. PhD thesis, Faculty of Medicine, Oslo, 2017.
- [24] Manish Bansal and Ravi R. Kasliwal. How do i do it? Speckle-tracking echocardiography, 2013. ISSN 00194832.
- [25] St. Jude Medical. Living with your Pacemaker A Patient's Guide to Understanding Cardiac Pacemakers. Technical report, 2015.
- [26] Jamie Eske. Sinus tachycardia: Everything you need to know, 11 2019. URL <https://www.medicalnewstoday.com/articles/327091>.
- [27] Oklahoma Heart Hospital. Heart block: symptoms, diagnosis, and treatment, 10 2017. URL <https://www.okheart.com/about-us/ohh-news/heart-block-symptoms-diagnosis-and-treatment>.
- [28] Valentin Tsibulko, Ivo Iliev, and Irena Jekova. A Review on Pacemakers: Device Types, }Operating Modes and Pacing Pulses. }Problems Related to the Pacing Pulses Detection. *Int. J. BIO Automation*, 18(2):89–100, 2014. URL <https://www.researchgate.net/publication/284181619>.
- [29] M.A. Bernabei. The Micra Transcatheter Pacing Study: }The Making of a Revolution in Pacemaking. *The Journal of Lancaster General Hospital*, 9(3): 75–79, 2014.
- [30] Neal Bhatia and Mikhael El-Chami. Leadless pacemakers: A contemporary review, 2018. ISSN 16715411.
- [31] Medtronic. Micra AV. 1 2020. URL <https://www.medtronic.com/us-en/about/news/micra-av-fda-approval.html>.
- [32] Aetna. Leadless Cardiac Pacemaker, 2015. URL www.aetna.com/cpb/medical/data/800_899/0893.html.
- [33] Medtronic. REVO MRI SURESCAN RVDRO1. Technical report, .
- [34] Medtronic. Micra™ MC1VR01. Technical report, .

- [35] Paul D. Mitcheson, Eric M. Yeatman, G. Kondala Rao, Andrew S. Holmes, and Tim C. Green. Energy harvesting from human and machine motion for wireless electronic devices. *Proceedings of the IEEE*, 96(9):1457–1486, 9 2008. ISSN 00189219. doi: 10.1109/JPROC.2008.927494.
- [36] Adrian Zurbuchen, Andreas Haeberlin, Lukas Bereuter, Alois Pfenniger, Simon Bosshard, Micha Kernen, Paul Philipp Heinisch, Juerg Fuhrer, and Rolf Vogel. Endocardial energy harvesting by electromagnetic induction. *IEEE Transactions on Biomedical Engineering*, 65(2):424–430, 2 2018. ISSN 15582531. doi: 10.1109/TBME.2017.2773568.
- [37] Bogdan Vysotskyi, Fabien Parrain, Denis Aubry, Philippe Gaucher, and Elie Lefevre. Innovative Energy Harvester Design Using Bistable Mechanism with Compensational Springs in Gravity Field. In *Journal of Physics: Conference Series*, volume 773. Institute of Physics Publishing, 12 2016. doi: 10.1088/1742-6596/773/1/012064.
- [38] Bogdan Vysotskyi, Denis Aubry, Philippe Gaucher, Xavier Le Roux, Fabien Parrain, and Elie Lefevre. Nonlinear electrostatic energy harvester using compensational springs in gravity field. *Journal of Micromechanics and Microengineering*, 28(7), 5 2018. ISSN 13616439. doi: 10.1088/1361-6439/aabc90.
- [39] M Deterre, B Boutaud, and et. al. Energy Harvesting System for Cardiac Implant Applications. In *2011 Symposium on Design, Test, Integration & Packaging of MEMS/MOEMS (DTIP)*, pages 387–391, Aix-en-Provence, 2011. IEEE. ISBN 9782355000133.
- [40] Jens Twiefel and Henrik Westermann. Survey on broadband techniques for vibration energy harvesting. In *Journal of Intelligent Material Systems and Structures*, volume 24, pages 1291–1302, 7 2013. doi: 10.1177/1045389X13476149.
- [41] Hiroshi Toshiyoshi, Suna Ju, Hiroaki Honma, Chang Hyeon Ji, and Hiroyuki Fujita. MEMS vibrational energy harvesters. *Science and Technology of Advanced Materials*, 20(1):124–143, 1 2019. doi: 10.1080/14686996.2019.1569828.
- [42] Maria Teresa Todaro, Francesco Guido, Vincenzo Mastronardi, Denis Desmaele, Gianmichele Epifani, Luciana Algeri, and Massimo De Vittorio. Piezoelectric MEMS vibrational energy harvesters: Advances and outlook, 11 2017. ISSN 01679317.
- [43] Mohammed F. Daqaq, Ravindra Masana, Alper Erturk, and D. Dane Quinn. On the role of nonlinearities in vibratory energy harvesting: A critical review and discussion, 2014. ISSN 00036900.
- [44] Ngan Tran, Mergen H. Ghayesh, and Maziar Arjomandi. Ambient vibration energy harvesters: A review on nonlinear techniques for performance enhancement, 6 2018. ISSN 00207225.
- [45] Robert Rantz and Shad Roundy. Characterization of Real-world Vibration Sources and Application to Nonlinear Vibration Energy Harvesters. *Energy Harvesting and Systems*, 4(2):67–76, 4 2017. ISSN 2329-8774. doi: 10.1515/ehs-2016-0021.
- [46] Galayko D, Karami A, and et. al. Kinetic Energy Harvesting for the IoT: Perspectives and Challenges for the Next Decade. In *2018 25th IEEE International Conference on Electronics, Circuits and Systems (ICECS)*, pages 593–596, Bordeaux, 2018. IEEE. ISBN 9781538695623. doi: 10.1109/ICECS.2018.8617991.
- [47] M. H. Ansari and M. Amin Karami. Piezoelectric energy harvesting from heartbeat vibrations for leadless pacemakers. In *Journal of Physics: Conference Series*, volume 660. Institute of Physics Publishing, 12 2015. doi: 10.1088/1742-6596/660/1/012121.
- [48] M. Amin Karami and Daniel J. Inman. Powering pacemakers from heartbeat vibrations using linear and nonlinear energy harvesters. *Applied Physics Letters*, 100(4), 1 2012. ISSN 00036951. doi: 10.1063/1.3679102.
- [49] M. H. Ansari and M. Amin Karami. Experimental investigation of fan-folded piezoelectric energy harvesters for powering pacemakers. *Smart Materials and Structures*, 26(6), 5 2017. ISSN 1361665X. doi: 10.1088/1361-665X/aa6cfd.

- [50] B Vysotskyi, P Gaucher, and D Aubry. Electrostatic vibration energy harvester using Multimodal-shaped springs for pacemaker application. In *2018 Symposium on Design, Test, Integration & Packaging of MEMS and MOEMS (DTIP)*, pages 1–6, Roma, 2018. IEEE. ISBN 9781538661994. doi: 10.1109/DTIP.2018.8394216.
- [51] K Pandia, S Ravindran, R Cole, Kovacs G, and Giovangrandi L. Motion artifact cancellation to obtain heart sounds from a single chest-worn accelerometer. In *International Conference on Acoustics, Speech and Signal Processing*, pages 590–593, Dallas, 2010. IEEE. ISBN 9781424442966.
- [52] A Khorovets. What Is An Electrocardiogram (ECG)? *The Internet Journal of Health*, 1(2):832, 1990.
- [53] Wansuree Massagram, Victor M. Lubecke, Anders Høst-Madsen, and Olga Boric-Lubecke. Assessment of heart rate variability and respiratory sinus arrhythmia via doppler radar. *IEEE Transactions on Microwave Theory and Techniques*, 57(10):2542–2549, 10 2009. ISSN 00189480. doi: 10.1109/TMTT.2009.2029716.
- [54] Hyoung Jong Kim, Ki Ho Kim, Yun Seok Hong, and Jin Joo Choi. Measurement of human heartbeat and respiration signals using phase detection radar. *Review of Scientific Instruments*, 78(10), 2007. ISSN 00346748. doi: 10.1063/1.2798937.
- [55] T Horiuchi, E.E. Tuna, K Masamune, and M. C. Çavuşoğlu. Heart motion measurement with three dimensional sonomicrometry and acceleration sensing. In *IEEE/RSJ International Conference on Intelligent Robots and Systems*, pages 4143–4149, Vilamoura, 2012. ISBN 9781467317368. doi: 10.1109/IROS.2012.6386095.
- [56] L Hoff, O J Elle, M J Grimnes, S Halvorsen, H J Alker, and E Fosse. Measurements of Heart Motion using Accelerometers. In *The 26th Annual International Conference of the IEEE Engineering in Medicine and Biology Society*, pages 2049–2051, San Francisco, 2004. IEEE. doi: 10.1109/IEMBS.2004.1403602.
- [57] Elliot R McVeigh. MRI OF MYOCARDIAL FUNCTION: MOTION TRACKING TECHNIQUES. Technical Report 2, 1996.
- [58] K. Yamamoto, T. Fujita, A. Badel, F. Formosa, K. Kanda, and K. Maenaka. Energy Estimation for Electret Harvester with Nonlinear Spring. *Proceedings*, 1(10):585, 8 2017. ISSN 2504-3900. doi: 10.3390/proceedings1040585.
- [59] S G Burrow and L R Clare. A Resonant Generator with Non-Linear Compliance for Energy Harvesting in High Vibrational Environments. In *2007 IEEE International Electric Machines & Drives Conference*, pages 715–720, Antalya, 2007. IEEE. doi: 10.1109/IEMDC.2007.382755.
- [60] R. Ramlan, M. J. Brennan, B. R. MacE, and I. Kovacic. Potential benefits of a non-linear stiffness in an energy harvesting device. *Nonlinear Dynamics*, 59(4):545–558, 3 2010. ISSN 0924090X. doi: 10.1007/s11071-009-9561-5.
- [61] F. Cottone, H. Vocca, and L. Gammaitoni. Nonlinear energy harvesting. *Physical Review Letters*, 102(8), 2 2009. ISSN 00319007. doi: 10.1103/PhysRevLett.102.080601.
- [62] Peter L. Green, Evangelos Papatheou, and Neil D. Sims. Energy harvesting from human motion and bridge vibrations: An evaluation of current nonlinear energy harvesting solutions. *Journal of Intelligent Material Systems and Structures*, 24(12):1494–1505, 8 2013. ISSN 1045389X. doi: 10.1177/1045389X12473379.
- [63] Gael Sebald, Hiroki Kuwano, Daniel Guyomar, and Benjamin Ducharme. Experimental Duffing oscillator for broadband piezoelectric energy harvesting. *Smart Materials and Structures*, 20(10), 2011. ISSN 1361665X. doi: 10.1088/0964-1726/20/10/102001.
- [64] M. I Younis. *MEMS Linear and Nonlinear Statics and Dynamics*. Springer, 2011. ISBN 978-1-4419-6019-1. doi: 10.1007/978-1-4419-6020-7. URL <http://www.springer.com/series/6289>.

- [65] F. Cottone, L. Gammaitoni, H. Vocca, M. Ferrari, and V. Ferrari. Piezoelectric buckled beams for random vibration energy harvesting. *Smart Materials and Structures*, 21(3), 3 2012. ISSN 09641726. doi: 10.1088/0964-1726/21/3/035021.
- [66] Stephen W. Tsai and H. Thomas. Hahn. *Introduction to composite materials*. Technomic Pub, 1980. ISBN 0877622884.
- [67] Seyed N. Mahmoodi, Nadei Jalili, and Mohammed F. Daqaq. Modeling, nonlinear dynamics, and identification of a piezoelectrically actuated microcantilever sensor. *IEEE/ASME Transactions on Mechatronics*, 13(1):58–65, 2 2008. ISSN 10834435. doi: 10.1109/TMECH.2008.915823.
- [68] D. Dane Quinn, Angela L. Triplett, Lawrence A. Bergman, and Alexander F. Vakakis. Comparing linear and essentially nonlinear vibration-based energy harvesting. *Journal of Vibration and Acoustics, Transactions of the ASME*, 133(1), 2011. ISSN 10489002. doi: 10.1115/1.4002782.
- [69] Son D. Nguyen, Einar Halvorsen, and Igor Paprotny. Bistable springs for wideband microelectromechanical energy harvesters. *Applied Physics Letters*, 102(2), 1 2013. ISSN 00036951. doi: 10.1063/1.4775687.
- [70] Huicong Liu, Chengkuo Lee, Takeshi Kobayashi, Cho Jui Tay, and Chenggen Quan. A new S-shaped MEMS PZT cantilever for energy harvesting from low frequency vibrations below 30 Hz. *Microsystem Technologies*, 18(4):497–506, 4 2012. ISSN 09467076. doi: 10.1007/s00542-012-1424-1.
- [71] W. Q. Liu, A. Badel, F. Formosa, and Y. P. Wu. A new figure of merit for wideband vibration energy harvesters. *Smart Materials and Structures*, 24(12), 10 2015. ISSN 1361665X. doi: 10.1088/0964-1726/24/12/125012.
- [72] Christopher Lee, David Stamp, Nitin R. Kapania, and José Oscar Mur-Miranda. Harvesting vibration energy using nonlinear oscillations of an electromagnetic inductor. In *Energy Harvesting and Storage: Materials, Devices, and Applications*, volume 7683, page 76830Y. SPIE, 4 2010. ISBN 9780819481474. doi: 10.1117/12.849895.
- [73] Kai Tao, Sun Who Lye, Jianmin Miao, Lihua Tang, and Xiao Hu. Out-of-plane electret-based MEMS energy harvester with the combined nonlinear effect from electrostatic force and a mechanical elastic stopper. *Journal of Micromechanics and Microengineering*, 25(10), 9 2015. ISSN 13616439. doi: 10.1088/0960-1317/25/10/104014.
- [74] Y. Lu, F. Cottone, S. Boisseau, F. Marty, D. Galayko, and P. Basset. A nonlinear MEMS electrostatic kinetic energy harvester for human-powered biomedical devices. *Applied Physics Letters*, 107(25), 12 2015. ISSN 00036951. doi: 10.1063/1.4937587.
- [75] Mohammed F. Daqaq. Transduction of a bistable inductive generator driven by white and exponentially correlated Gaussian noise. *Journal of Sound and Vibration*, 330(11):2554–2564, 5 2011. ISSN 0022460X. doi: 10.1016/j.jsv.2010.12.005.
- [76] Lars Cyril Julin Blystad and Einar Halvorsen. An energy harvester driven by colored noise. *Smart Materials and Structures*, 20(2), 2 2011. ISSN 09641726. doi: 10.1088/0964-1726/20/2/025011.
- [77] Einar Halvorsen, Lars-Cyril Julin Blystad, Svein Husa, and Eskild Westby. Simulation of Electromechanical Systems Driven by Large Random Vibrations. In *2007 International Conference on Perspective Technologies and Methods in MEMS Design*, pages 117–122, Lviv-Polyana, 2007. IEEE. doi: 10.1109/MEMSTECH.2007.4283441.
- [78] Gael Sebald, Hiroki Kuwano, Daniel Guyomar, and Benjamin Ducharme. Simulation of a Duffing oscillator for broadband piezoelectric energy harvesting. *Smart Materials and Structures*, 20(7), 2011. ISSN 1361665X. doi: 10.1088/0964-1726/20/7/075022.

- [79] Chunchuan Liu and Xingjian Jing. Nonlinear vibration energy harvesting with adjustable stiffness, damping and inertia. *Nonlinear Dynamics*, 88(1):79–95, 4 2017. ISSN 1573269X. doi: 10.1007/s11071-016-3231-1.
- [80] Samuel C. Stanton, Clark C. McGehee, and Brian P. Mann. Reversible hysteresis for broadband magnetopiezoelastic energy harvesting. *Applied Physics Letters*, 95(17), 2009. ISSN 00036951. doi: 10.1063/1.3253710.
- [81] Shengxi Zhou, Junyi Cao, Wei Wang, Shengsheng Liu, and Jing Lin. Modeling and experimental verification of doubly nonlinear magnet-coupled piezoelectric energy harvesting from ambient vibration. *Smart Materials and Structures*, 24(5), 5 2015. ISSN 1361665X. doi: 10.1088/0964-1726/24/5/055008.
- [82] Wen An Jiang and Li Qun Chen. Snap-through piezoelectric energy harvesting. *Journal of Sound and Vibration*, 333(18):4314–4325, 9 2014. ISSN 10958568. doi: 10.1016/j.jsv.2014.04.035.
- [83] P. L. Green, K. Worden, K. Atallah, and N. D. Sims. The benefits of Duffing-type nonlinearities and electrical optimisation of a mono-stable energy harvester under white Gaussian excitations. *Journal of Sound and Vibration*, 331(20):4504–4517, 9 2012. ISSN 0022460X. doi: 10.1016/j.jsv.2012.04.035.
- [84] Mohammed F. Daqaq. Response of uni-modal duffing-type harvesters to random forced excitations. *Journal of Sound and Vibration*, 329(18):3621–3631, 2010. ISSN 10958568. doi: 10.1016/j.jsv.2010.04.002.
- [85] Y. Lu, E. O’Riordan, F. Cottone, S. Boisseau, D. Galayko, E. Blokhina, F. Marty, and P. Basset. A batch-fabricated electret-biased wideband MEMS vibration energy harvester with frequency-up conversion behavior powering a UHF wireless sensor node. *Journal of Micromechanics and Microengineering*, 26(12), 9 2016. ISSN 13616439. doi: 10.1088/0960-1317/26/12/124004.
- [86] Stephen P. Beeby, Leran Wang, Dibin Zhu, Alex S. Weddell, Geoff V. Merrett, Bernard Stark, Gyorgy Szarka, and Bashir M. Al-Hashimi. A comparison of power output from linear and non-linear kinetic energy harvesters using real vibration data. *Smart Materials and Structures*, 22(7), 7 2013. ISSN 09641726. doi: 10.1088/0964-1726/22/7/075022.
- [87] Sebastien Boisseau, Ghislain Despesse, and Bouhadjar Ahmed Seddik. Adjustable Nonlinear Springs to Improve Efficiency of Vibration Energy Harvesters. *Applied Mechanics*, 80(6):13–20, 2012. doi: 10.1115/1.4023961.
- [88] Luca Gammaitoni, Helios Vocca, Igor Neri, Flavio Travasso, and Francesco Orfei. Vibration Energy Harvesting: Linear and Nonlinear Oscillator Approaches. Technical report. URL www.intechopen.com.
- [89] Hiroki Takahashi, Hideyuki Hasegawa, and Hiroshi Kanai. Automated identification of the heart wall throughout the entire cardiac cycle using optimal cardiac phase for extracted features. *Japanese Journal of Applied Physics*, 50(7 PART 2), 7 2011. ISSN 00214922. doi: 10.1143/JJAP.50.07HF16.
- [90] Bojing Shi, Zhou Li, and Yubo Fan. Implantable Energy-Harvesting Devices, 11 2018. ISSN 15214095.
- [91] H Goto, T Sugiura, Y Harada, and T Kazui. Feasibility of using the automatic generating system for quartz watches as a leadless pacemaker power source. Technical report, 1999.
- [92] Edward N Shen, Cory H Ishihara, and Dwayne R Uehara. Leadless Pacemaker: Report of the First Experience in Hawai’i. 77(4), 2018.
- [93] M. H. Ansari and M. Amin Karami. Modeling and experimental verification of a fan-folded vibration energy harvester for leadless pacemakers. *Journal of Applied Physics*, 119(9), 3 2016. ISSN 10897550. doi: 10.1063/1.4942882.

- [94] Martin Deterre. Toward an energy harvester for leadless pacemakers. Technical report, 2013. URL <https://tel.archives-ouvertes.fr/tel-00868838>.
- [95] Libor Rufer, Mikael Colin, and Skandar Basrou. Application driven design, fabrication and characterization of piezoelectric energy scavenger for cardiac pacemakers. In *2013 Joint IEEE International Symposium on Applications of Ferroelectric and Workshop on Piezoresponse Force Microscopy, ISAF/PFM 2013*, pages 340–343. IEEE Computer Society, 2013. doi: 10.1109/ISAF.2013.6748687.
- [96] Nathan Jackson, Oskar Olszewski, Cian O’Murchu, and Alan Mathewson. Powering a leadless pacemaker using a PiezoMEMS energy harvester. In *Smart Sensors, Actuators, and MEMS VIII*, volume 10246, page 102460V. SPIE, 6 2017. ISBN 9781510609938. doi: 10.1117/12.2264437.
- [97] Alois Pfenniger, Magnus Jonsson, Adrian Zurbuchen, Volker M. Koch, and Rolf Vogel. Energy harvesting from the cardiovascular system, or how to get a little help from yourself, 2013. ISSN 00906964.
- [98] A Zurbuchen, A Haeberlin, J Schaerer, A Pfenniger, and R Vogel. Harvesting energy from the heart wall motion – Device weight considerations. In *Biomedizinische Technik*, volume 59, pages S259–S262. Walter de Gruyter GmbH, 10 2014. doi: 10.1515/bmt-2014-5002.
- [99] Bas M. van Dalen, Johan G. Bosch, Floris Kauer, Osama I.I. Soliman, Wim B. Vletter, Folkert J. ten Cate, and Marcel L. Geleijnse. Assessment of Mitral Annular Velocities by Speckle Tracking Echocardiography versus Tissue Doppler Imaging: Validation, Feasibility, and Reproducibility. *Journal of the American Society of Echocardiography*, 22(11):1302–1308, 11 2009. ISSN 08947317. doi: 10.1016/j.echo.2009.08.004.
- [100] Eugene Lin and Adam Alessio. What are the basic concepts of temporal, contrast, and spatial resolution in cardiac CT? *Journal of Cardiovascular Computed Tomography*, 3(6):403–408, 11 2009. ISSN 19345925. doi: 10.1016/j.jcct.2009.07.003.
- [101] Radomir Chabiniok, Vicky Y. Wang, Myrianthi Hadjicharalambous, Liya Asner, Jack Lee, Maxime Sermesant, Ellen Kuhl, Alistair A. Young, Philippe Moireau, Martyn P. Nash, Dominique Chapelle, and David A. Nordsletten. Multiphysics and multiscale modelling, data–model fusion and integration of organ physiology in the clinic: Ventricular cardiac mechanics. *Interface Focus*, 6(2), 4 2016. ISSN 20428901. doi: 10.1098/rsfs.2015.0083.
- [102] Gianni Pedrizzetti, Piet Claus, Philip J. Kilner, and Eike Nagel. Principles of cardiovascular magnetic resonance feature tracking and echocardiographic speckle tracking for informed clinical use, 8 2016. ISSN 1532429X.
- [103] Ole Johannes H.N. Grymyr, Espen W. Remme, Andreas Espinoza, Helge Skulstad, Ole J. Elle, Erik Fosse, and Per S. Halvorsen. Assessment of 3D motion increases the applicability of accelerometers for monitoring left ventricular function. *Interactive Cardiovascular and Thoracic Surgery*, 20(3):329–337, 2015. ISSN 15699285. doi: 10.1093/icvts/ivu404.
- [104] Ali Wajdan, Magnus Reinsfelt Krogh, Manuel Villegas-Martínez, Per Steinar Halvorsen, Ole-Johannes Grymyr, Ole Jakob Elle, and Espen W. Remme. Monitoring cardiac function by accelerometer – detecting start systole
}from the acceleration signal makes additional ECG recordings for
}R-peak detection redundant.
- [105] Per Steinar Halvorsen, Andreas Espinoza, Lars Albert Fleischer, Ole Jakob Elle, Lars Hoff, Runar Lundblad, Helge Skulstad, Thor Edvardsen, Halfdan Ihlen, and Erik Fosse. Feasibility of a three-axis epicardial accelerometer in detecting myocardial ischemia in cardiac surgical patients. *Journal of Thoracic and Cardiovascular Surgery*, 136(6):1496–1502, 12 2008. ISSN 00225223. doi: 10.1016/j.jtcvs.2008.08.043.

- [106] Ikuo Hashimoto, Aarti Hejmadi Bhat, Xiaokui Li, Michael Jones, Crispin H. Davies, Julia C. Swanson, Sebastian T. Schindera, and David J. Sahn. Tissue Doppler-derived myocardial acceleration for evaluation of left ventricular diastolic function. *Journal of the American College of Cardiology*, 44(7):1459–1466, 10 2004. ISSN 07351097. doi: 10.1016/j.jacc.2004.06.067.
- [107] Erik Lyseggen, Stein Inge Rabben, Helge Skulstad, Stig Urheim, Cecilie Risoe, and Otto A. Smiseth. Myocardial acceleration during isovolumic contraction: Relationship to contractility. *Circulation*, 111(11):1362–1369, 3 2005. ISSN 00097322. doi: 10.1161/01.CIR.0000158432.86860.A6.
- [108] Michael D. Eggen, Vladimir Grubac, and Matthew D. Bonner. Design and Evaluation of a Novel Fixation Mechanism for a Transcatheter Pacemaker. *IEEE Transactions on Biomedical Engineering*, 62(9):2316–2323, 9 2015. ISSN 15582531. doi: 10.1109/TBME.2015.2449320.
- [109] Ole Johannes H.N. Grymyr, Anh Tuan T. Nguyen, Fjodors Tjulkins, Andreas Espinoza, Espen W. Remme, Helge Skulstad, Erik Fosse, Kristin Imenes, and Per S. Halvorsen. Continuous monitoring of cardiac function by 3-dimensional accelerometers in a closed-chest pig model. *Interactive Cardiovascular and Thoracic Surgery*, 21(5):573–582, 2015. ISSN 15699285. doi: 10.1093/icvts/ivv191.
- [110] Magnus Reinsfelt Krogh, Giang M. Nghiem, Per Steinar Halvorsen, Ole Jakob Elle, Ole Johannes Grymyr, Lars Hoff, and Espen W. Remme. Gravity Compensation Method for Combined Accelerometer and Gyro Sensors Used in Cardiac Motion Measurements. *Annals of Biomedical Engineering*, 45(5):1292–1304, 5 2017. ISSN 15739686. doi: 10.1007/s10439-017-1798-4.
- [111] Andrei D. Margulescu, Dewi E. Thomas, Thomas E. Ingram, Vlad D. Vintila, Margaret A. Egan, Dragos Vinereanu, and Alan G. Fraser. Can Isovolumic Acceleration Be Used in Clinical Practice to Estimate Ventricular Contractile Function? Reproducibility and Regional Variation of a New Noninvasive Index. *Journal of the American Society of Echocardiography*, 23(4), 2010. ISSN 08947317. doi: 10.1016/j.echo.2010.01.008.
- [112] Suchita Joshi, Julie M. Edwards, Dirk G. Wilson, Joon K. Wong, Sailesh Kotecha, and Alan G. Fraser. Reproducibility of myocardial velocity and deformation imaging in term and preterm infants. *European Journal of Echocardiography*, 11(1):44–50, 1 2010. ISSN 15252167. doi: 10.1093/ejehocard/jep161.
- [113] Thor Edvardsen, Bernhard L. Gerber, Jérôme Garot, David A. Bluemke, João A.C. Lima, and Otto A. Smiseth. Quantitative assessment of intrinsic regional myocardial deformation by Doppler strain rate echocardiography in humans: Validation against three-dimensional tagged magnetic resonance imaging. *Circulation*, 106(1):50–56, 7 2002. ISSN 00097322. doi: 10.1161/01.CIR.0000019907.77526.75.
- [114] Theodore P. Abraham, Veronica L. Dimaano, and Hsin Yueh Liang. Role of tissue doppler and strain echocardiography in current clinical practice, 11 2007. ISSN 00097322.
- [115] Carlos Eduardo Suaide Silva, Luiz Darcy Cortez Ferreira, Luciana Braz Peixoto, Claudia Gianini Monaco, Manuel Adán Gil, Juarez Ortiz São Paulo, and SP Brazil. Study of the Myocardial Contraction and Relaxation Velocities through Doppler Tissue Imaging Echocardiography. A New Alternative in the Assessment of the Segmental Ventricular Function. Technical Report 2, 2002.
- [116] Masoumeh Lotfi-Tokaldany, Shala Majidi, Farahnaz Nikdoust, Savand Roomi, Mahmood Sheikhfathollahi, and Hakimeh Sadeghian. Normal Values for Longitudinal Tissue Velocity and Strain Rate Imaging in Individual Segments of the Left and Right Ventricles of Healthy Adult Hearts. Technical report, 2013. URL www.aium.org.
- [117] Antonella Fontana, Antonella Zambon, Francesca Cesana, Cristina Giannattasio, and Giuseppe Trocino. Tissue doppler, triplane echocardiography, and speckle tracking echocardiography: Different ways of measuring longitudinal myocardial velocity and deformation parameters. A comparative clinical study. *Echocardiography*, 29(4):428–437, 4 2012. ISSN 07422822. doi: 10.1111/j.1540-8175.2011.01618.x.

- [118] Susan Lucy Roche, Michael Vogel, Oli Pitknen, Brian Grant, Cameron Slorach, Cheryl Fackoury, Derek Stephens, Jeffrey Smallhorn, Lee N. Benson, Paul F. Kantor, and Andrew N. Redington. Isovolumic acceleration at rest and during exercise in children: Normal values for the left ventricle and first noninvasive demonstration of exercise-induced force-frequency relationships. *Journal of the American College of Cardiology*, 57(9):1100–1107, 3 2011. ISSN 07351097. doi: 10.1016/j.jacc.2010.09.063.
- [119] Barbara Cifra, Luc Mertens, Moniba Mirkhani, Cameron Slorach, Wei Hui, Cedric Manlhiot, Mark K. Friedberg, and Andreea Dragulescu. Systolic and Diastolic Myocardial Response to Exercise in a Healthy Pediatric Cohort. *Journal of the American Society of Echocardiography*, 29(7):648–654, 7 2016. ISSN 10976795. doi: 10.1016/j.echo.2016.02.015.
- [120] Anh Tuan T. Nguyen, Fjodors Tjulkins, E. Knut, Aasmundtveit, Nils Hoivik, Lars Hoff, Ole Johannes Grymyr, Per Steinar Halvorsen, and Kristin Imenes. Packaging of a multifunctional implantable heart monitoring device. In *DTIP 2014 - Symposium on Design, Test, Integration and Packaging of MEMS/MOEMS*. Institute of Electrical and Electronics Engineers Inc., 3 2014. ISBN 9782355000287. doi: 10.1109/DTIP.2014.7056657.
- [121] Linda B Pauliks, Michael Vogel, Christoph F M, R Ian Williams, Nicola Payne, Andrew N Redington, and Alan G Fraser. Regional Response of Myocardial Acceleration During Isovolumic Contraction During Dobutamine Stress Echocardiography: A Color Tissue Doppler Study and Comparison with Angiocardigraphic Findings. Technical report, 2005.
- [122] Tonino Bombardini, Rosa Sicari, Elisabetta Bianchini, and Eugenio Picano. Abnormal shortened diastolic time length at increasing heart rates in patients with abnormal exercise-induced increase in pulmonary artery pressure. *Cardiovascular Ultrasound*, 9(1), 2011. ISSN 14767120. doi: 10.1186/1476-7120-9-36.
- [123] Tonino Bombardini, Vincenzo Gemignani, Elisabetta Bianchini, Lucia Venneri, Christina Petersen, Emilio Pasanisi, Lorenza Pratali, David Alonso-Rodriguez, Mascia Pianelli, Francesco Faita, Massimo Giannoni, Giorgio Arpesella, and Eugenio Picano. Diastolic time - Frequency relation in the stress echo lab: Filling timing and flow at different heart rates. *Cardiovascular Ultrasound*, 6, 2008. ISSN 14767120. doi: 10.1186/1476-7120-6-15.
- [124] Luca Martini. *Real-time control of an electrodynamic shaker*. PhD thesis, Universit_a di Bologna, Bologna, 2015.
- [125] L. Della Flora and H. A. Gründling. Time domain sinusoidal acceleration controller for an electrodynamic shaker. *IET Control Theory and Applications*, 2(12):1044–1053, 2008. ISSN 17518644. doi: 10.1049/iet-cta:20080188.
- [126] Thijs W.A. Blad and Nima Tolou. On the efficiency of energy harvesters: A classification of dynamics in miniaturized generators under low-frequency excitation. *Journal of Intelligent Material Systems and Structures*, 30(16):2436–2446, 9 2019. ISSN 15308138. doi: 10.1177/1045389X19862621.
- [127] Lynette Gabriel. Guidance for Industry Guidance for the Submission of Research and Marketing Applications for Permanent Pacemaker Leads and for Pacemaker Lead Adaptor 510(k) Submissions Preface Public Comment Additional Copies. Technical report, 2000. URL <http://www.fda.gov/cdrh/ode/guidance/372.pdf>, or.
- [128] Owen Faris. Clinical trials for medical devices: FDA and the IDE process, 2006.
- [129] Mahesh Peddigari, Ga Yeon Kim, Chan Hee Park, Yuho Min, Jong Woo Kim, Cheol Woo Ahn, Jong Jin Choi, Byung Dong Hahn, Joon Hwan Choi, Dong Soo Park, Jae Keun Hong, Jong Taek Yeom, Kwi Il Park, Dae Yong Jeong, Woon Ha Yoon, Jungho Ryu, and Geon Tae Hwang. A comparison study of fatigue behavior of hard and soft piezoelectric single crystal macro-fiber composites for vibration energy harvesting. *Sensors (Switzerland)*, 19(9), 5 2019. ISSN 14248220. doi: 10.3390/s19092196.

- [130] Inki Jung, Youn Hwan Shin, Sangtae Kim, Ji young Choi, and Chong Yun Kang. Flexible piezoelectric polymer-based energy harvesting system for roadway applications. *Applied Energy*, 197: 222–229, 2017. ISSN 03062619. doi: 10.1016/j.apenergy.2017.04.020.
- [131] Monika Gall, Bärbel Thielicke, and Ingo Schmidt. Integrity of piezoceramic patch transducers under cyclic loading at different temperatures. *Smart Materials and Structures*, 18(10), 2009. ISSN 09641726. doi: 10.1088/0964-1726/18/10/104009.
- [132] Donald F Dahms. Implantable Pacemaker Testing Guidance. Technical report, 1990.
- [133] F Ponsaerts, M Op de Beeck, and F Horemans. GENEES Guideline Best Practices for Electronics in Medical Devices. Technical report, 2016. URL www.cedm.be.
- [134] Jens Uwe Voigt, Gianni Pedrizzetti, Peter Lysyansky, Tom H. Marwick, Helen Houle, Rolf Baumann, Stefano Pedri, Yasuhiro Ito, Yasuhiko Abe, Stephen Metz, Joo H.yun Song, Jamie Hamilton, Partho P. Sengupta, Theodore J. Kolias, Jan d’Hooge, Gerard P. Aurigemma, James D. Thomas, and Luigi P.aolo Badano. Definitions for a common standard for 2D speckle tracking echocardiography: consensus document of the EACVI/ASE/Industry Task Force to standardize deformation imaging. *European heart journal cardiovascular Imaging*, 16(1):1–11, 1 2015. ISSN 20472412. doi: 10.1093/ehjci/jeu184.
- [135] Idith Haber, Dimitris N Metaxas, Tal Geva, and Leon Axel. Three-dimensional systolic kinematics of the right ventricle. *Am J Physiol Heart Circ Physiol*, 289:1826–1833, 2005. doi: 10.1152/ajpheart.00442.2005.-The. URL www.ajpheart.org.
- [136] Thomas A. Holly, Brian G. Abbott, Mouaz Al-Mallah, Dennis A. Calnon, Mylan C. Cohen, Frank P. D’Filippo, Edward P. Ficaro, Michael R. Freeman, Robert C. Hendel, Diwakar Jain, Scott M. Leonard, Kenneth J. Nichols, Donna M. Polk, and Prem Soman. Single photon-emission computed tomography, 2010. ISSN 10713581.
- [137] David I. Hamilton. *Diagnostic Nuclear Medicine: A Physics Perspective*. Springer-Verlag Berlin Heidelberg, 2004. ISBN 978-3-662-06588-4. doi: 10.1007/978-3-662-06588-4.
- [138] National Institute of Biomedical Imaging and Bioengineering (NIBIB). Computed Tomography (CT). URL <https://www.nibib.nih.gov/science-education/science-topics/computed-tomography-ct>.
- [139] Harald Brodoefel, Ulrich Kramer, Anja Reimann, Christof Burgstahler, Stephen Schroeder, Andreas Kopp, and Martin Heuschmid. Dual-source CT with improved temporal resolution in assessment of left ventricular function: A pilot study. *American Journal of Roentgenology*, 189(5): 1064–1070, 11 2007. ISSN 0361803X. doi: 10.2214/AJR.07.2228.
- [140] Abi Berger. Magnetic Resonance Imaging. *BMJ*, 324, 2002.
- [141] S Mondillo and et al. Speckle-Tracking Echocardiography A New Technique for Assessing Myocardial Function. *Ultrasound Med*, 30:71–83, 2011. ISSN 0278-4297. URL www.aium.org.
- [142] Colin Deane. Doppler Ultrasound: principles and practice, 2002. URL https://sonoworld.com/Client/Fetus/html/doppler/capitulos-html/chapter_01.htm.
- [143] Livia Kapusta, Johan M Thijssen, Marinus H M Cuypers, Petronella G M Peer, and Otto Daniëls Daniëls. ASSESSMENT OF MYOCARDIAL VELOCITIES IN HEALTHY CHILDREN USING TISSUE DOPPLER IMAGING. Technical report, 2000.
- [144] Thomas Binder. M-Mode ultrasound imaging. URL <https://www.123sonography.com/ebook/m-mode-ultrasound-imaging#:~:text=M%2Dmode%20is%20defined%20as,displayed%20along%20the%20time%20axis.&text=The%20M%2Dmode%20can%20be,as%20color%20or%20tissue%20Doppler>.
- [145] Julie De Backer, D. Matthys, T. C. Gillebert, A. De Paepe, and J. De Sutter. The use of Tissue Doppler Imaging for the assessment of changes in myocardial structure and function in inherited cardiomyopathies. *European Journal of Echocardiography*, 6(4):243–250, 8 2005. ISSN 15252167. doi: 10.1016/j.euje.2004.09.010.

- [146] Gila Perk, Paul A. Tunick, and Itzhak Kronzon. Non-Doppler Two-dimensional Strain Imaging by Echocardiography-From Technical Considerations to Clinical Applications, 3 2007. ISSN 08947317.
- [147] Hanan Khamis, Sara Shimoni, Andreas Hagendorff, Nahum Smirin, Zvi Friedman, and Dan Adam. Optimization-based speckle tracking algorithm for left ventricle strain estimation: A feasibility study. *IEEE Transactions on Ultrasonics, Ferroelectrics, and Frequency Control*, 63(8): 1093–1106, 8 2016. ISSN 08853010. doi: 10.1109/TUFFC.2016.2569619.
- [148] Krishna K. Kadappu and Liza Thomas. Tissue doppler imaging in echocardiography: Value and limitations, 3 2015. ISSN 14442892.
- [149] A D Fleming, W N Mcdicken, G R Sutherland, and P R Hoskins. ASSESSMENT OF COLOUR DOPPLER TISSUE IMAGING USING TEST-PHANTOMS. Technical Report 9, 1994.
- [150] Harry Pavlopoulos and Petros Nihoyannopoulos. Strain and strain rate deformation parameters: From tissue Doppler to 2D speckle tracking. *International Journal of Cardiovascular Imaging*, 24 (5):479–491, 6 2008. ISSN 15695794. doi: 10.1007/s10554-007-9286-9.
- [151] Mundigler G and Zehetgruber M. Tissue Doppler Imaging: Myocardial Velocities and Strain-Are there Clinical Applications? Technical Report 2, 2002. URL www.kup.at/jcbc.
- [152] D Garcia, P Lantelme, and É Saloux. Introduction to speckle tracking in cardiac ultrasound imaging. In *Handbook of Speckle Filtering and Tracking in Cardiovascular Ultrasound Imaging and Video*, pages 571–598. Institution of Engineering and Technology, 3 2018. doi: 10.1049/pbhe013e{_}ch26.
- [153] FUJIFILM. Get High Resolution Anatomical Data with B-Mode Ultrasound! URL <https://www.visualsonics.com/product/software/b-mode-imaging>.
- [154] Hermann Blessberger and Thomas Binder. Two dimensional speckle tracking echocardiography: Basic principles. *Heart*, 96(9):716–722, 5 2010. ISSN 13556037. doi: 10.1136/hrt.2007.141002.
- [155] Jonas Johnson. *The Cardiac State Diagram : a new method for assessing cardiac mechanics*. PhD thesis, Stockholm, 2015.
- [156] Sigurd Gunnes, Camilla Storaas, Britta Lind, Jacek Nowak, and Lars Åke Brodin. Analysis of the effect of temporal filtering in myocardial tissue velocity imaging. *Journal of the American Society of Echocardiography*, 17(11):1138–1145, 11 2004. ISSN 08947317. doi: 10.1016/j.echo.2004.06.006.
- [157] Aristomenis Manouras, Kambiz Shahgaldi, Reidar Winter, Jacek Nowak, and Lars Åke Brodin. Comparison between colour-coded and spectral tissue Doppler measurements of systolic and diastolic myocardial velocities: Effect of temporal filtering and offline gain setting. *European Journal of Echocardiography*, 10(3):406–413, 5 2009. ISSN 15252167. doi: 10.1093/ejechocard/jen298.
- [158] Madalina Negoita, Massoud Zolgharni, Elham Dadkho, Matteo Pernigo, Michael Mielewczik, Graham D. Cole, Niti M. Dhutia, and Darrel P. Francis. Frame rate required for speckle tracking echocardiography: A quantitative clinical study with open-source, vendor-independent software. *International Journal of Cardiology*, 218:31–36, 9 2016. ISSN 18741754. doi: 10.1016/j.ijcard.2016.05.047.
- [159] Mayank M. Kansal, Prasad M. Panse, Haruhiko Abe, Giuseppe Caracciolo, Susan Wilansky, A. Jamil Tajik, Bijoy K. Khandheria, and Partho P. Sengupta. Relationship of contrast-enhanced magnetic resonance imaging-derived intramural scar distribution and speckle tracking echocardiography-derived left ventricular two-dimensional strains. *European Heart Journal Cardiovascular Imaging*, 13(2):152–158, 2 2012. ISSN 20472404. doi: 10.1093/ejechocard/jer163.

- [160] Patricia Reant, Louis Labrousse, Stephane Lafitte, Pierre Bordachar, Xavier Pillois, Liliane Tariosse, Simone Bonoron-Adele, Philippe Padois, Claude Deville, Raymond Roudaut, and Pierre Dos Santos. Experimental Validation of Circumferential, Longitudinal, and Radial 2-Dimensional Strain During Dobutamine Stress Echocardiography in Ischemic Conditions. *Journal of the American College of Cardiology*, 51(2):149–157, 1 2008. ISSN 07351097. doi: 10.1016/j.jacc.2007.07.088.
- [161] Gerhard Wess, Lisa J.M. Keller, Michael Klausnitzer, Markus Killich, and Katrin Hartmann. Comparison of longitudinal myocardial tissue velocity, strain, and strain rate measured by two-dimensional speckle tracking and by color tissue Doppler imaging in healthy dogs. *Journal of Veterinary Cardiology*, 13(1):31–43, 3 2011. ISSN 17602734. doi: 10.1016/j.jvc.2010.08.001.
- [162] Mehmet Ertürk, Ender Öner, Ali Kemal Kalkan, Hamdi Püşüroğlu, Sinem Özyılmaz, Özgür Akgül, Hale Ünal Aksu, İbrahim Faruk Aktürk, Ömer Çelik, and Nevzat Uslu. The role of isovolumic acceleration in predicting subclinical right and left ventricular systolic dysfunction in patient with metabolic syndrome. *Anadolu Kardiyoloji Dergisi*, 15(1):42–49, 1 2015. ISSN 13080032. doi: 10.5152/akd.2014.5143.
- [163] Wanda Lockwood. Electrocardiogram (EKG) Interpretation. Technical report, 2019.
- [164] M Rodrigues, A.C. Silva, A.P. Águas, and N.R. Grande. The coronary circulation of the pig heart: }comparison with the human heart. *Eur J Anat*, 9(2):67–87, 2005.
- [165] S Garg, P Singh, Sharma A, and Gupta G. Short Communication A gross comparative anatomical study of hearts in human cadavers and pigs. Technical Report 2, 2013. URL www.ijmds.org.
- [166] SIMON J. Crick, MARY N. Sheppard, Siew Yen Ho, Lior Gebstein, and Robert H. Anderson. Anatomy of the pig heart: comparisons with normal human cardiac structure. *Journal of Anatomy*, 193(1):105–119, 7 1998. ISSN 0021-8782. doi: 10.1046/j.1469-7580.1998.19310105.x.
- [167] Arash Kheradvar, Ramin Zareian, Shimako Kawauchi, Richard L. Goodwin, and Sandra Rugonyi. Animal models for heart valve research and development, 6 2017. ISSN 17406757.
- [168] Alexander J Hill and Paul A laizzo. Comparative Cardiac Anatomy. In *Handbook of Cardiac Anatomy, Physiology, and Devices*, pages 81–91. 2005.
- [169] Veronique M.F. Meijborg, Chantal E. Conrath, Tobias Opthof, Charly N.W. Belterman, Jacques M.T. De Bakker, and Ruben Coronel. Electrocardiographic T wave and its relation with ventricular repolarization along major anatomical axes. *Circulation: Arrhythmia and Electrophysiology*, 7(3):524–531, 2014. ISSN 19413084. doi: 10.1161/CIRCEP.113.001622.
- [170] Lior Gepstein, Gal Hayam, and Shlomo A. Ben-Haim. Activation-repolarization coupling in the normal swine endocardium. *Circulation*, 96(11):4036–4043, 1997. ISSN 00097322. doi: 10.1161/01.CIR.96.11.4036.
- [171] P. P. Lelovas, N. G. Kostomitsopoulos, and T. T. Xanthos. A Comparative Anatomic and Physiologic }Overview of the Porcine Heart. *Journal of the American Association for Laboratory Animal Science*, 53(5):432–438, 9 2014.
- [172] Nima Milani-Nejad and Paul M.L. Janssen. Small and large animal models in cardiac contraction research: Advantages and disadvantages, 3 2014. ISSN 1879016X.
- [173] Michael Vogel, Michael M.H. Cheung, Jia Li, Steen B. Kristiansen, Michael R. Schmidt, Paul A. White, Keld Sorensen, and Andrew N. Redington. Noninvasive assessment of left ventricular force-frequency relationships using tissue Doppler-derived isovolumic acceleration validation in an animal model. *Circulation*, 107(12):1647–1652, 4 2003. ISSN 00097322. doi: 10.1161/01.CIR.0000058171.62847.90.
- [174] Luigi Brancato, Tristan Weydts, Wouter Oosterlinck, Paul Herijgers, and Robert Puers. Packaging of implantable accelerometers to monitor epicardial and endocardial wall motion. *Biomedical Microdevices*, 19(3), 9 2017. ISSN 15728781. doi: 10.1007/s10544-017-0199-7.

- [175] Á. A. Pálsdóttir and D. H. Eiríksdóttir. *Analysis of a Cardiac Displacement Signal Recorded with an Ultrasound Vibrometer*. PhD thesis, School of Medicine and Health, Aalborg, 2018. URL <http://smh.aau.dk>.
- [176] M Brett. Gimbal lock, 2016. URL https://matthew-brett.github.io/transforms3d/gimbal_lock.html.
- [177] CHRobotics LLC. Understanding Euler Angles. URL <http://www.chrobotics.com/library/understanding-euler-angles>.
- [178] Freescale Semiconductor. Accelerometer Terminology Guide, 2007. URL www.freescale.com/support.
- [179] Kionix. KXM52 Series, 2005.
- [180] Espen W. Remme, Lars Hoff, Per Steinar Halvorsen, Anders Opdahl, Erik Fosse, and Ole Jakob Elle. Simulation model of cardiac three dimensional accelerometer measurements. *Medical Engineering and Physics*, 34(7):990–998, 9 2012. ISSN 13504533. doi: 10.1016/j.medengphy.2012.04.015.
- [181] Magnus Reinsfelt Krogh, Per Steinar Halvorsen, Ole Jakob Elle, Jacob Bergsland, and Espen Wattenberg Remme. Dynamic gravity compensation does not increase detection of myocardial ischemia in combined accelerometer and gyro sensor measurements. *Scientific Reports*, 9(1), 12 2019. ISSN 20452322. doi: 10.1038/s41598-018-35630-x.
- [182] Tilendra Choudhary, M. K. Bhuyan, and L. N. Sharma. Orthogonal subspace projection based framework to extract heart cycles from SCG signal. *Biomedical Signal Processing and Control*, 50:45–51, 4 2019. ISSN 17468108. doi: 10.1016/j.bspc.2019.01.005.
- [183] Andrew R Houghton. MAKING SENSE of Echocardiography A hands-on guide Second Edition. Technical report, 2014.
- [184] I. Hashimoto, X. K. Li, A. Hejmadi Bhat, M. Jones, and David J. Sahn. Quantitative assessment of regional peak myocardial acceleration during isovolumic contraction and relaxation times by tissue Doppler imaging. *Heart*, 91(6):811–816, 6 2005. ISSN 13556037. doi: 10.1136/hrt.2004.033845.
- [185] Rafael Cordero, Delphine Feuerstein, and Pierre Yves Joubert. The cardiac systolic mechanical axis: Optimizing multi-axial cardiac vibrations by projecting along a physiological reference frame. *Biomedical Signal Processing and Control*, 59, 5 2020. ISSN 17468108. doi: 10.1016/j.bspc.2020.101933.
- [186] Ole Jakob Elle, Steinar Halvorsen, Martin Gunnar Gulbrandsen, Lars Aurdal, Andre Bakken, Eigil Samset, Harald Dugstad, and Erik Fosse. Early recognition of regional cardiac ischemia using a 3-axis accelerometer sensor. *Physiological Measurement*, 26(4):429–440, 8 2005. ISSN 09673334. doi: 10.1088/0967-3334/26/4/009.
- [187] Aude Tassin, Adonis Kobeissi, Luca Vitali, Frédéric Rouleau, Philippe Ritter, Guido Gaggini, and Jean-Marc Dupuis. Relationship between Amplitude and Timing of Heart Sounds and Endocardial Acceleration. *PACE*, 32:101, 2009.
- [188] Felix Staehle, Bernd A. Jung, Simon Bauer, Jochen Leupold, Jelena Bock, Ramona Lorenz, Daniela Föll, and Michael Markl. Three-directional acceleration phase mapping of myocardial function. *Magnetic Resonance in Medicine*, 65(5):1335–1345, 2011. ISSN 15222594. doi: 10.1002/mrm.22744.
- [189] Guy Dori, Jorge E. Schliamser, Oscar Lichtenstein, Iliia Anshelevich, and Moshe Y. Flugelman. A novel system for continuous, real-time monitoring of heart motion signals. *European Journal of Medical Research*, 22(1), 3 2017. ISSN 2047783X. doi: 10.1186/s40001-017-0252-2.

- [190] Fumio Nogata, Yasunari Yokota, Yoko Kawamura, Hiroyuki Morita, and Yoshihiro Uno. Novel technique for visualizing heart motion without using ultrasonic cardiography. In *Proceedings - IEEE-EMBS International Conference on Biomedical and Health Informatics: Global Grand Challenge of Health Informatics, BHI 2012*, pages 249–252, 2012. ISBN 9781457721779. doi: 10.1109/BHI.2012.6211558.
- [191] Ian T. Jolliffe and Jorge Cadima. Principal component analysis: A review and recent developments, 4 2016. ISSN 1364503X.
- [192] Steven J Lester. Myocardial Imaging Tissue Doppler and Strain Imaging DISCLOSURE Relevant Financial Relationship(s) None Off Label Usage None, 2018.
- [193] Shuai Wu, P. C.K. Luk, Chunfang Li, Xiangyu Zhao, and Zongxia Jiao. Investigation of an Electromagnetic Wearable Resonance Kinetic Energy Harvester with Ferrofluid. *IEEE Transactions on Magnetics*, 53(9), 9 2017. ISSN 00189464. doi: 10.1109/TMAG.2017.2714621.
- [194] Andrew M. Handorf, Yaxian Zhou, Matthew A. Halanski, and Wan Ju Li. Tissue stiffness dictates development, homeostasis, and disease progression, 1 2015. ISSN 15558592.
- [195] Carlos F. Guimarães, Luca Gasperini, Alexandra P. Marques, and Rui L. Reis. The stiffness of living tissues and its implications for tissue engineering, 5 2020. ISSN 20588437.
- [196] A. K. Dabrowska, G. M. Rotaru, S. Derler, F. Spano, M. Camenzind, S. Annaheim, R. Stämpfli, M. Schmid, and R. M. Rossi. Materials used to simulate physical properties of human skin. *Skin Research and Technology*, 22(1):3–14, 2 2016. ISSN 16000846. doi: 10.1111/srt.12235.
- [197] Conor T. Buckley, Stephen D. Thorpe, Fergal J. O'Brien, Anthony J. Robinson, and Daniel J. Kelly. The effect of concentration, thermal history and cell seeding density on the initial mechanical properties of agarose hydrogels. *Journal of the Mechanical Behavior of Biomedical Materials*, 2(5):512–521, 10 2009. ISSN 17516161. doi: 10.1016/j.jmbbm.2008.12.007.
- [198] Y Toyama, R Sahara, Y Iino, and K Kubota. pH Dependence of Rheological Properties of Gelatin Gel Mixed with Agar or Agarose. *Transactions of the Materials Research Society of Japan*, 36(3):383–386, 2011.
- [199] Anjum Saleem, Lars Frommann, and Alexandru Soever. Fabrication of extrinsically conductive silicone rubbers with high elasticity and analysis of their mechanical and electrical characteristics. *Polymers*, 2(3):200–210, 9 2010. ISSN 20734360. doi: 10.3390/polym2030200.
- [200] Chad D. Markert, Xinyi Guo, Aleksander Skardal, Zhan Wang, Shantaram Bharadwaj, Yuanyuan Zhang, Keith Bonin, and Martin Guthold. Characterizing the micro-scale elastic modulus of hydrogels for use in regenerative medicine. *Journal of the Mechanical Behavior of Biomedical Materials*, 27:115–127, 11 2013. ISSN 17516161. doi: 10.1016/j.jmbbm.2013.07.008.
- [201] SpecialChem. Silicone Rubber: Complete Guide on Highly Durable Elastomer. URL <https://omnexus.specialchem.com/selection-guide/silicone-rubber-elastomer#>.
- [202] L Koene. Kinetic Non-Lethal Weapons Risk assessment of kinetic-energy non-lethal weapons View project Impact on Adobe Structures View project. Technical report, 2008. URL <https://www.researchgate.net/publication/306559973>.